Reprints

Relativity of Electron and Energy Transfer Contributions in Nanoparticle-Induced Fluorescence Quenching

Dewan S. Rahman, Sanhita Deb, and Sujit Kumar Ghosh*

Department of Chemistry, Assam University, Silchar-788011, India

✦ Supporting Information

ABSTRACT: Metallic nanostructures are known to drastically modify the spontaneous emission of molecular probes placed in their vicinity. The main critical parameters that modify the spontaneous rate of emission of organic fluoroprobes near metallic nanostructures are the location of the fluoroprobes around the particle, its separation from the metal surface, and the molecular dipole orientation with respect to the particle surface. Depending on its relative position and orientation with respect to the nanostructures, the fluoroprobe may experience an enhanced or suppressed electric field, leading to a higher or lower excitation rate, respectively, in comparison to a fluoroprobe in free space. The fluorescence of molecules in direct contact with the metal is completely quenched. Possible deactivation pathways of the photoexcited fluoroprobes near metal nanostructures could be enunciated as the intermolecular interactions, electron transfer, energy transfer, and the emission from the molecular probes near the metal surface. Under optimal conditions, both electron and energy transfer processes are considered to be major deactivation pathways for excited fluoroprobes on metal surface, and therefore it has remained difficult to separate their cumulative effects in nanoparticle-induced fluorescence quenching. On the basis of these perspectives, pyrene and its derivatives and four different sizes of silver nanoparticles have, judiciously, been selected in such a way that eventually paves a substantial avenue in realizing electron and energy transfer contributions in nanoparticle-induced fluorescence quenching.
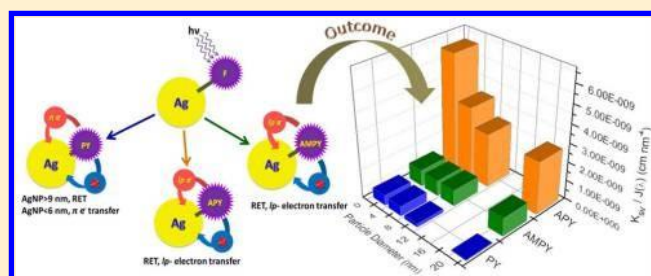
1. INTRODUCTION

In recent years, there has been a great deal of research endeavors to investigate the photophysical aspects of multicomponent nanostructured assemblies arising from the invasive integration of molecular probes and metallic nanostructures that mimics many ubiquitous processes in materials and life sciences.[1-4] The ability of metal nanostructures in manipulating and guiding light at the nanometer length scale and, therefore, to modulate the fluorescence emission of vicinal fluoroprobes has propelled their widespread interest in fluorescence-based sensing in biology and nanophotonics technologies.[5-7] Noble metal particles, copper, silver, and gold, in the nanometer size regime exhibit strong absorption in the visible region, and this is, indeed, a small particle effect because they are absent in the individual atom as well as in their bulk.[8] The time-varying electric field of the electromagnetic radiation causes collective oscillation of the conduction electrons in metal nanoparticles with a resonance frequency, often coined as localized surface plasmon resonance (LSPR).[9] These collective oscillations of the conduction band electrons enable strong optical absorption and scattering in the subwavelength structures, with spectral properties dependent upon size, shape, interparticle interactions, dielectric properties, and local environment around the nanoparticles.[10] The localized surface plasmon resonances of metallic nanostructures imbue significant influences on the photophysical properties of organic fluoroprobes in the close vicinity of the conducting metal surfaces, and therefore the field

of plasmonics imparts a considerable impact in biophotonics through radiative decay engineering.[11-13] To meet the challenges that lie ahead, the understanding of plausible interactions in nanoparticle–fluoroprobe hybrid assemblies is essential before miniaturizing them into devices.[14]

Because fluorescence spectroscopy is a very sensitive technique, there is a growing recognition in understanding the physicochemical aspects of the molecule–surface interactions of fluorescent probes attached onto the surface of noble metal nanoparticles.[15] For these studies, silver nanoparticles have been of interest as, compared to gold, the silver plasmon band is more sensitive to chemical modifications of the surface upon adsorption of nucleophile or electron donors.[16] Moreover, the plasma frequency of silver nanoparticles in the visible region overlaps with the emission wavelength of usual energy donors.[17] Therefore, fluorophore-bound silver nanoparticles provide a convenient way to examine the mechanistic details of various de-excitation pathways of the photoexcited fluoroprobes, such as energy and electron transfer to the bound nanoparticles. Photoinduced electron transfer (PET), in which a charge transfer complex is formed between an electron donor and an electron acceptor that can return to the ground state without emission of a photon, is one of the pathways of

deactivation of the excited probe molecules leading to quenching of fluorescence intensity of the molecular probes. Förster resonance energy transfer (FRET), where the donor molecule absorbs a photon and there is an acceptor molecule close to the donor molecule, can occur from the donor to the acceptor, resulting in a decrease of the fluorescence intensity and lifetime of the donor molecule.

Although the photophysical aspects of molecular probes near metallic nanostructures have extensively been investigated, there have been fewer experimental investigations on spectroscopic properties of pyrene moieties attached onto the surface of metallic nanoparticles. Rotello and colleague[18] have reported the fabrication of multivalent colloid-based receptors as well as dynamic systems based on nanoparticle scaffolds in which the migration of alkanethioate ligands with pyrene units has been suggested upon the addition of guest molecules. George Thomas and Kamat[19] have reported the engineering of thiol-capped gold nanocluster surfaces with 1-aminoethylpyrene and demonstrated that fluorescence intensity can be enhanced an order of magnitude due to transfer of lone pair of electrons from the molecular probes to the gold nanoparticles when the organic dyes are placed in the vicinity of the metallic particles. Zhu and coauthors[20] have reported the synthesis and photophysical properties of 10-(1-pyrenyl)-6-oxo-decanethiol and 17-(1-pyrenyl)-1-oxo-heptadecanethiol capped gold nanoparticles, and unusual fluorescence enhancement was observed upon aging dichloromethane dispersions of these colloidal particles. The findings of this experiment elucidated the role of the chain density gradient and the motion of termini groups of alkanethiolates adsorbed onto the surface of gold nanoparticles for the fluorescence enhancement. Kamat's group[21] has demonstrated the spectroscopic investigation of direct electron transfer between gold nanoparticles and surface bound (1-pyrenyl)-6-oxaheptanethiol molecules induced by pulsed laser irradiation. It has been observed that binding of pyrene-thiol directly to the gold nanoparticles results in quenching of singlet excited state, and the charge separation is sustained for a microsecond before undergoing recombination. Pal and co-workers[22] have studied the fluorescence quenching behavior of aminomethylpyrene near gold nanoparticles in the size range of 8–73 nm; it was elucidated that the quenching efficiency of the metallic nanostructures is not a linear function of the particle size but rather different in the two different size regimes of the particles. It was observed that the smaller particles of gold are more efficient quenchers of molecular fluorescence than the larger ones, which is due to a higher surface-to-volume ratio of the small metallic particulates. Therefore, it is now well-established that fluorescence of pyrene moieties could be either enhanced or quenched depending on its relative position in the vicinity of noble metal nanostructures. While the fluorescence of molecular probes is quenched, indeed, although the physics behind possible deactivation pathways of the photoexcited fluoroprobe near metal nanostructures is established, the relative contributions of electron and energy transfer processes are worth investigation.

In this Article, pyrene and its two amine derivatives have elegantly been employed as fluorescent probes, and four different sizes of silver nanoparticles have, judiciously, been selected to study the interactions in metal–fluoroprobe hybrid assemblies. Size-selective silver nanoparticles have been synthesized using sodium borohydride as the reducing agent and trisodium citrate as the reducing as well as capping agent.

a strong correlation is observed between the observed fluo- rescence intensity and the photophysical properties of the metal–fluoroprobe hybrid assemblies. It is observed that fluorophore-bound silver nanoparticles provide a convenient way to examine the mechanistic details of various deactivation pathways of photoexcited fluoroprobes, such as electron and energy transfer to the bound nanoparticles, and eventually pave a substantial avenue in realizing the relativity of electron and energy transfer contributions in nanoparticle-induced fluores- cence quenching.

2. EXPERIMENTAL SECTION

Reagents and Instruments. All of the reagents used were of analytical reagent grade. Silver nitrate ($AgNO_3$), sodium borohydride ($NaBH_4$), trisodium citrate, and molecular probes, pyrene (PY), aminopyrene (APY), and aminomethylpyrene (AMPY), were purchased from Sigma-Aldrich and were used without further purification. As it is difficult to dissolve pyrene and its derivatives in water but readily in methanol, the stock solutions of the fluoroprobes were prepared in a 95/5 (v/v) water–methanol mixture at a concentration of 0.1 mM. Double distilled water was used throughout the course of this investigation. The temperature was 298 ± 1 K for all mea- surements.

Absorption spectra were measured in a PerkinElmer Lambda 750 UV–vis–NIR spectrophotometer using a 1 cm quartz cuvette. Fluorescence spectra were recorded with a PerkinElmer LS-45 spectrofluorimeter equipped with a pulsed xenon lamp and a photomultiplier tube with R-928 spectral response. The spectrofluorimeter was linked to a personal computer and utilized the FL WinLab software package for data collection and processing. Transmission electron microscopy (TEM) was carried out on a JEOL JEM-2100 microscope with a magni- fication of 200 kV. Samples were prepared by placing a drop of solution on a carbon-coated copper grid and dried overnight under vacuum. High-resolution transmission electron micro- graph (HRTEM) and selected area electron diffraction (SAED) pattern were obtained using the same instrument. Cyclic voltammetry measurements were performed by a CHI-660C electrochemical workstation. Data have been collected using Pt electrode as working as well as counter electrode, and Ag/AgCl electrode (in 3.0 M KCl) was used as the reference electrode at temperature 298 K. The concentration of the fluoroprobes (4.5 μM) and silver nanoparticles (11.9 μM) was kept constant in the pure state and during the formation of metal (11.9 μM)– fluoroprobe (4.5 μM) hybrid assemblies. The solutions were prepared in aqueous 0.1 M tetrabutylammonium perchlorate (TBAP) as supporting electrolyte at pH ≈ 7.0.

Synthesis of Size-Selective Silver Nanoparticles. Silver nanoparticles of four different sizes have been synthesized by wet chemical reduction of silver nitrate using sodium boro- hydride as the reducing agent and trisodium citrate as the reducing agent as well as the capping agent. A detailed descri- ption of the synthesis of silver nanoparticles has been described in the Supporting Information. However, a lexicon of the synthetic conditions for the preparation of four different sizes of silver nanoparticles has been enunciated in Table 1.

Making Metal–Probe Hybrid Assembly. In a typical set, an aliquot of Ag NPs (0.75–10 μM) from different sets was added to a solution of pyrene or its derivatives (0.03–0.3 μM), and the final volume of the solution was maintained at 5 mL. The pH of all of the solutions was adjusted to ∼7.0. The solution was allowed to incubate for 12 h to complete the

Table 1. Synthetic Conditions for the Four Different Sets of Silver Nanoparticles[a]

set	vol of AgNO$_3$ (0.1 M) (mL)	vol of citrate (1%) (mL)	condition (°C)	AgNO$_3$:NaBH$_4$	color	λ_{max} (nm)	diameter (nm)
A	0.125	2.5	0	1:20	yellow	379	2 ± 0.5
B	0.125	2.5	25	1:9	yellow	392	6 ± 1
C	0.125	2.5	25	1:6	yellow	399	9 ± 2
D	0.125	1.0	100		greenish yellow	409	21 ± 3

[a]For silver nanoparticle synthesis, the total volume of the solution was 50 mL.

surface complexation process, and the fluorescence of each solution was measured in the spectrofluorimeter.

3. RESULTS AND DISCUSSION

The as-synthesized colloidal dispersions of the silver particles have been characterized by absorption spectroscopy and transmission electron microscopic studies. Figure 1 shows the
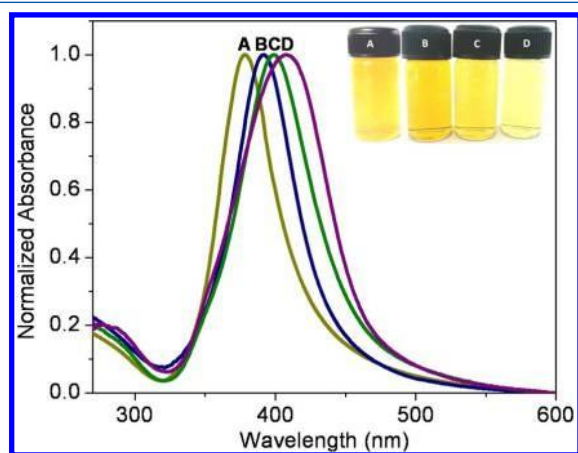

Figure 1. (A–D) Normalized UV–visible spectra of silver nano-particles (50 μM) of variable sizes of sets A–D, respectively. Inset shows the digital photograph of the corresponding silver particles.

normalized absorption spectra of four different sets of silver colloids. The inset shows the digital camera photograph exhibiting the characteristic colors of four different sets of silver nanoparticles. In the UV–vis spectrum, it is seen that the absorption maximum appears at 379, 392, 399, and 408 nm for silver particles of sets A, B, C, and D, respectively. This absorption band arises due to the localized surface plasmon band of spherical silver nanoparticles; for nanoparticles much smaller than the wavelength of light, the electromagnetic field is uniform across a particle such that all of the conduction electrons move in-phase producing only dipole-type oscillations that are manifested by a single narrow peak in the LSPR spectrum.[23] Moreover, the shape of the LSPR spectrum is determined by the relative dimension of the particles to that of the incident electromagnetic radiation. It is apparent that the absorption spectrum is red-shifted and broadened from sets A to D, indicating the gradual increase in size of the silver nanoparticles. This is due to the fact that the observed spectral shift results from the "spreading" of particle's surface charge over a larger surface area so that the surrounding medium better compensates the restoring force, thus showing the electron oscillations.[23]

The morphology, composition, and crystallinity of the as-synthesized silver particles are presented in Figure 2. Transmission electron micrographs of the representative silver particles (panels a–d) show that the particles are spherical or

nearly spherical with average diameter in the range of 2 ± 0.5, 6 ± 1, 9 ± 2, and 21 ± 3 nm for sets A, B, C, and D, respectively. The number concentration (number of particles per milliliter of the solution, N) of silver particles can be calculated by taking the ratio of total volume of the atoms to the effective volume of each particle taken in average.[24] The approximate numbers of silver nanoparticles per milliliter of the solution have been calculated using the formula, $N = (N_0C/1000f)(r/R)^3$, where N_0 is the Avogadro number, C is the concentration of the silver precursor, f is the packing fraction of the atoms in the nanostructures, r is the radius of silver atoms, and R is the average radii of the particles. Assuming the packing fraction as 0.74 for fcc silver[25] and a precursor concentration of 0.25 mM, the number concentration of silver particles has been ca. 8.33 × 10^{14}, 3.09 × 10^{13}, 9.14 × 10^{12}, and 7.19 × 10^{11} mL^{-1} for sizes 2, 6, 9, and 21 nm, respectively. High-resolution TEM image (panel e) of the silver particles of set D exhibits the lattice fringes with an interplanner spacing of ~0.232 nm consistent with (111) plane of silver; the continuous fringe pattern observed in the HRTEM image demonstrates the single crystalline nature of the silver nanoparticles.[26] Selected area electron diffraction (panel f) of the silver particles of set D illustrates four sets of lattice planes with d spacings of 2.32, 2.04, 1.44, and 1.22 Å that correspond to the (111), (200), (220), and (311) planes of the face-centered cubic silver particles.[27]

Pyrene is a polycyclic aromatic hydrocarbon consisting of four fused benzene rings, resulting in a flat aromatic system, and is used commercially to make dyes and dye precursors. There have been extensive studies on the photophysics of pyrene: its electronic spectrum and state assignments, kinetic details of excimer formation, spectral pressure effects, photoionization, delayed luminescence, and quasilinear spectra, etc.[28] Because of their numerous well-characterized photophysical and photochemical properties, pyrene[29] and its amine derivatives[30,31] have been widely used as fluorescent probes to study their emission behavior in varieties of microenvironments. The absorption and emission spectra of pyrene moieties, pyrene, aminopyrene, and aminomethylpyrene, are shown in Figure 3. The molecular structures of the fluorescent probes are shown in the inset. It is seen that the aqueous solution of pyrene and its derivatives possesses well-defined absorption and emission bands ($\lambda_{ex} \approx 274$ nm) in the visible region, which can be attributed to the monomeric form of the fluoroprobes.[22,32] The excitation of the fluoroprobes in any absorption maximum produces the identical emission spectrum. Moreover, the fluorescence intensity increases linearly with increasing concentration for all three dye molecules, indicating no significant perturbation or higher order aggregation in the experimental concentration range. The absorption and emission spectral features of the pyrene moieties are summarized in Table 2.

Now, we have studied the emission behavior of pyrene and its derivatives ($\lambda_{ex} \approx 274$ nm) in the presence of silver nanoparticles of four different sizes. The representative fluorescence

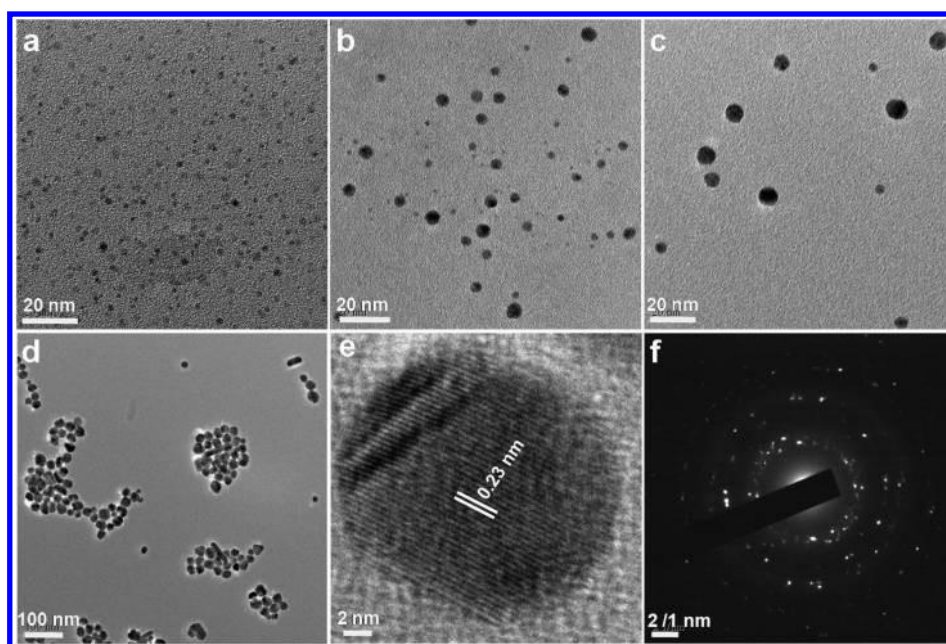spectrum of PY, APY, and AMPY in the presence of 6 nm silver

Figure 2. (a–d) Transmission electron micrographs of silver nanoparticles of sets A–D, respectively; and (e) high-resolution transmission electron micrograph and (f) selected area electron diffraction pattern of set D silver particles.
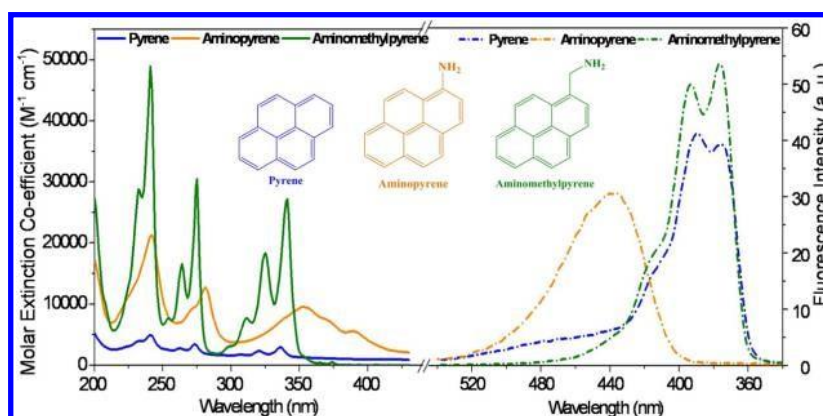

Figure 3. Absorption (25, 25, and 25 µM) and emission (0.3, 0.04, and 0.03 µM) spectra of pyrene, aminopyrene, and aminomethylpyrene. Inset shows the molecular structures of the fluorescent probes.

Table 2. Absorption and Emission Spectral Characteristics of the Molecular Probes

probes	absorption max (nm)	emission max (nm)	quantum yield
pyrene	241, 262, 273, 320, 336	375, 389	0.35 in ethanol
aminopyrene	242, 281, 353, 389	438	0.58 in water
aminomethylpyrene	240, 264, 274, 311, 325, 340	377, 394	

particles (set B) is shown in Figure 4. In these experiments, quite dilute solutions (0.03–0.3 µM) have been used so as to minimize the effects of excitation attenuation and solution self-absorption (so-called "trivial effects"). It is seen that the emission of pyrene moieties showed a distinctly different profile in the presence of different concentrations of silver nano-particles. The quenching of molecular fluorescence in the vicinity of metallic nanostructures could be treated by the

of a metallic nanostructure may be influenced by radiative and the nonradiative de-excitation rates involved in the fluorescence emission in a manner similar to the effect of a nearby macroscopic metallic surface.[7,34] Depending on its relative position and orientation with respect to the nanostructure, the fluoroprobe may experience an enhanced or suppressed electric field, leading to a higher or lower excitation rate, respectively, in comparison to a fluorophore in free space. In metal–fluoroprobe hybrid assemblies, the excitation of the electronic plasma resonance leads to an increase in the absorption rate. In addition, the emission intensity is strongly frequency depen-model proposed by Weitz et al.[33] A fluoroprobe in the vicinity

dent: not only can the metal altered local photonic mode density lead to changes in the radiative decay rate of the fluorophores, but the presence of the metal also opens new nonradiative decay pathways via energy transfer to metal surface plasmon modes.[35] In the present experiment, it is observed that metallic nanostructures are efficient quenchers of molecular fluorescence, while it is noted that the silver nanoparticles are, themselves, nonfluorescent. When the fluoroprobes are allowed to interact with the nanoparticles, a
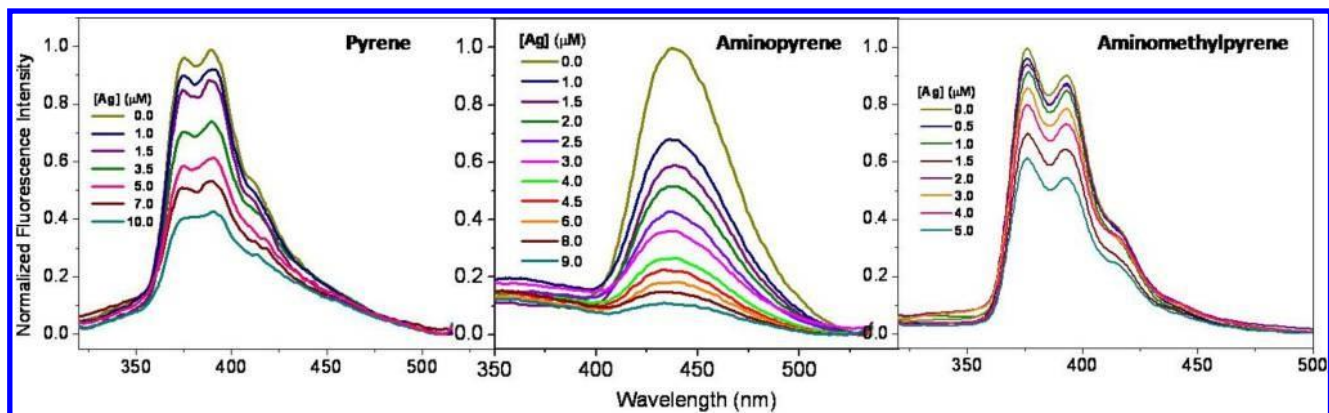
Figure 4. Fluorescence spectra of pyrene (0.3 μM), aminopyrene (0.04 μM), and aminomethylpyrene (0.03 μM) in the presence of variable concentrations of 6 nm silver nanoparticles.
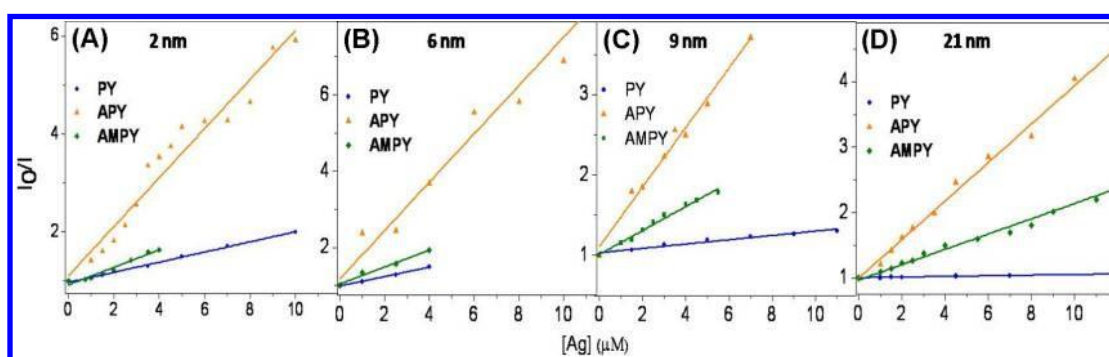

Figure 5. Stern–Volmer plots showing the quenching efficiency of pyrene (0.3 μM), aminopyrene (0.04 μM), and aminomethylpyrene (0.03 μM) in the presence of (A) 2, (B) 6, (C) 9, and (D) 21 nm silver nanoparticles.

part of the fluoroprobes is adsorbed onto the metallic surface while the rests remain free in solution, and thus the only fluorescing components are the free pyrene moieties in the solution. The Stern–Volmer constant, K_{SV}, is related to the photoluminescence efficiency via the relationship of the Stern–Volmer equation[36] accounting for both static and dynamic (collisional) quenching as:

$$\frac{I_0}{I} = 1 + K_{SV}[Q] \tag{1}$$

where I_0 and I are the intensities of the emission spectra of the pyrene moieties in the absence and presence of the nanostructures, $K_{SV} = K_S + K_D$, where K_S and K_D are the static and dynamic quenching constants, respectively, and $[Q]$ is the quencher concentration. Both static and dynamic quenching requires molecular contact between the fluorophore and quencher.[11] Figure 5 shows the profiles with the relative efficiency, I_0/I, as a function of silver concentration for all sets of the metallic nanostructures. It is also noted that the relative efficiency increases linearly with an increase in the concentration of silver nanostructures. However, the salient feature of physical significance is that the extent of quenching is the least in case of pyrene, moderate for aminomethylpyrene, and highest for the aminopyrene for all sets of particles. Moreover, smaller silver particles are efficient quenchers of molecular fluorescence than the larger ones as has been observed in previous investigations.[22]

Now, we have tried to elucidate the mechanism of quenching of molecular fluorescence upon interaction with the silver nanostructures. When using fluorescing molecules as local

probes for measuring surface plasmon fields, we have to recall the particularities of molecular fluorescence near a metal sur- face. Both radiative and nonradiative decay rates are expected to depend, critically, on the size and shape of the nanoparticle, the distance between the probe molecule and the nano- particle, the orientation of the molecular dipole with respect to the fluoroprobe–nanoparticle axis, and the overlap of the molecule's emission with the nanoparticle's absorption spectrum.[37] In the vicinity of a metal, the fluorescence rate of molecules becomes a function of the distance between the molecule and the metal surface.[38] In direct contact with the metal, the fluorescence of molecules is completely quenched. While pyrene and its amine derivatives are added into the citrate-stabilized silver nanoparticles dispersion, one can speculate on the point of binding of the molecular probes to the metallic surface. Silver atoms at the surface of the particle are coordinately unsaturated; that is, unoccupied orbitals are available for nucleophiles to donate electrons.[39] While the pyrene moieties are chemisorbed onto the surface of ultrasmall particles, the distance between the probe molecule and the nanoparticle, and the orientation of the molecular dipole with respect to the fluoroprobe–nanoparticle axis could be assumed to remain constant, and therefore both electron and energy transfer processes are likely to contribute to the major deactivation pathways for excited fluoroprobes on the metal surface. Silver nanoparticles, themselves, show limited photo- activity under UV–visible irradiation, although photoinduced fusion and fragmentation have been observed under laser irradiation.[40] To examine the effect of addition of pyrene and its two derivatives containing amine functional groups of the
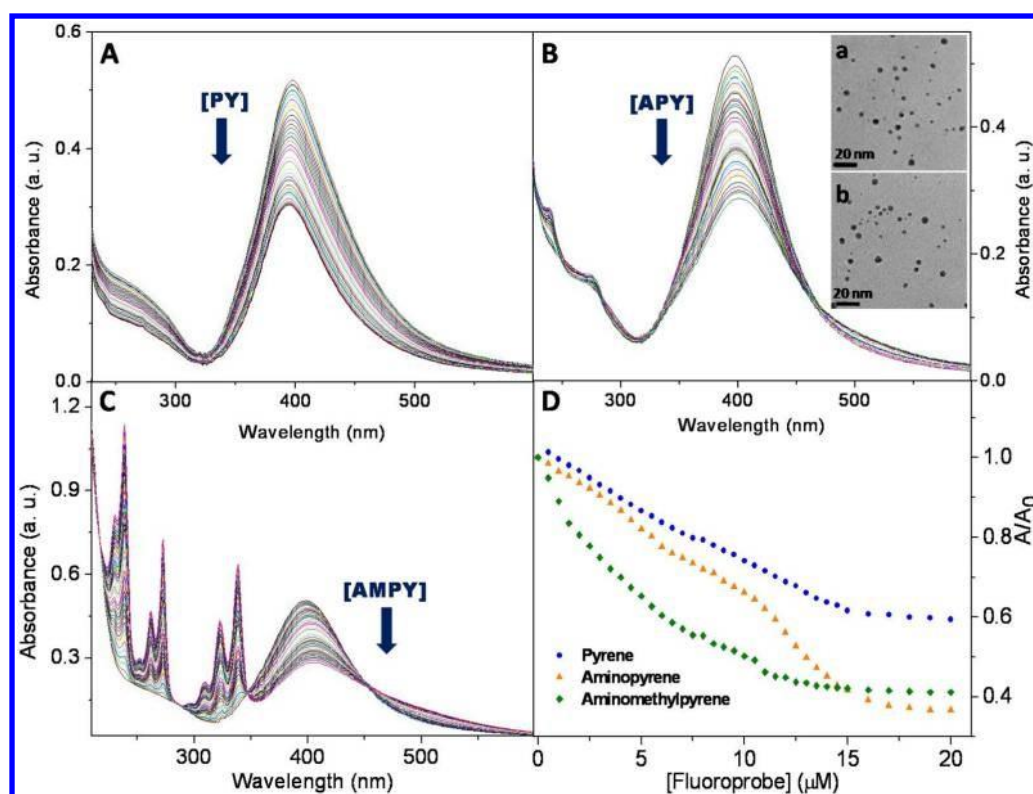
Figure 6. (A–C) Change in the surface plasmon band of 6 nm silver nanoparticles (50 μM) upon addition of pyrene (0.4–20 μM), aminopyrene (0.4–20 μM), and aminomethylpyrene (0.4–20 μM), respectively, and (D) relative dampening of absorbance of the silver nanoparticles upon addition of fluoroprobes in different concentrations. Inset in profile B shows the transmission electron micrographs of the silver particles (set B) (a) before and (b) after addition of aminopyrene molecules.

same homologous series on the surface plasmon absorption of the small metallic particulates, we have added the fluoroprobes to a particular concentration of the silver nanoparticles. Figure 6 shows the changes in the absorption spectral features of 6 nm silver nanoparticles (set B) (20 μM) upon successive addition of pyrene, aminopyrene, and aminomethylpyrene molecules. It is seen that when pyrene moieties are added to the silver nanoparticles, the localized surface plasmon band of silver gradually dampens with increase in concentration of fluoroprobes (panel A–C); these results imply a different extent of electron transfer from the fluoroprobes to the silver nanostructures.[39] Upon careful observation, it is observed that the LSPR maximum of the silver particles becomes blue-shifted upon addition of PY, remains almost unchanged for APY, and becomes red-shifted for AMPY molecules. The inset in profile B shows the transmission electron micrographs of the silver particles (set B) before (panel a) and after (panel b) addition of aminopyrene, which authenticate that the particle size remains nearly unchanged upon interaction with the probe molecules. A plot of A/A_0 as a function of fluoroprobe concentration (panel D) shows that the dampening of the silver surface plasmon band is the slowest for PY, intermediate for APY, and the highest for AMPY. It is noted that after a critical concentration (15 μM), APY dampens the LSPR more effectively than AMPY; however, after an incubation period of 12 h, APY more actively dampens the LSPR of the silver particles than AMPY at any concentration.

The position and intensity of the silver surface plasmon absorption band depend strongly on particle size, and the optical and electronic properties of the medium surrounding

the particles. This strong electronic interaction between pyrene

moieties and silver particles causes the change in the surface plasmon band of the silver nanoparticles. The pyrene derivatives, aminopyrene and aminomethylpyrene containing amine functionality, possess lone pair electrons capable of inter- acting with metal surface in competition with the stabilizing ligand shell, such as citrate, and therefore can, in principle, displace the labile ligand, citrate, on the surface of nano- particles.[41] Donation of a lone pair of electrons from the molecular probes to the nanoparticles causes a large reduction in absorption intensity of the silver particles. It is also possible that the fluoroprobes can displace citrate due to interaction of the π-system of the molecule with the surface as well;[42] therefore, pyrene being an aromatic hydrocarbon and devoid of any functionality also dampens the plasmon oscillation of the metallic nanoparticles. The system of π-orbitals adjacent to the metal particles could have a weak interaction with the particle surface[43] and thus shows little change in the absorption spectrum of the nanoparticles.[44] Another interesting feature is the high surface-to-volume ratio of the nanoparticles; the higher is the surface-to-volume ratio, the stronger is the interaction with electron-donating agents due to the coordinatively unsaturated surface atoms of the metals. The electron exchange from the PY to the Ag NPs or nucleophilic addition of APY and AMPY to Ag NPs leads to changes in the optical properties of the silver nanoparticles. Henglein and colleagues have shown that chemisorption of various nucleophiles has two opposing effects on the absorption spectra of colloidal silver.[45] When the electron transfer occurs to the metallic silver nanoparticles, the Fermi potential shifts to the more negative values correspond- ing to the blue shift of the surface plasmon absorption band;[45] this has been observed when PY donates electrons to the

surface of Ag NPs as seen in Figure 6A. The red shifting of the surface plasmon band of the Ag NPs is observed upon the nucleophilic addition of APY and AMPY to the Ag NPs as seen in Figure 6B and C. This may be explained by considering two opposing effects:[45] the number of charge increases in the particles, which yield blue shift of the band, and, on the other hand, $\delta+\delta-$ dipolar structure on the surface causes a red shift; when the later effect was prevailing, the red shift of the surface plasmon band is observed as has been seen for various silver–organic molecule systems.[46] However, because the lone pair of electrons on APY participates in resonance with its π-electrons in the pyrene ring, the extent of donation of the lone pair of electrons is low as compared to AMPY, and there is no significant shifting of the absorption maximum of the silver surface plasmon band.

Cyclic voltammograms of pure fluoroprobes, silver nanoparticles (set B), and metal–fluoroprobe hybrid assemblies are shown in Figure 7. The potential window has been selected
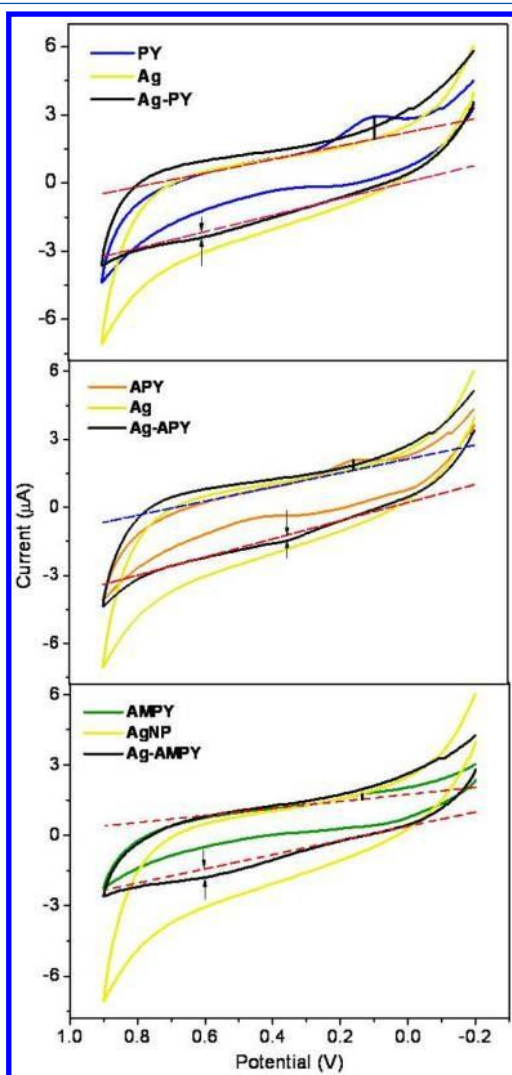

Figure 7. Cyclic voltammograms of the pure fluoroprobes (4.5 μM), silver nanoparticles (11.9 μM), and silver (11.9 μM)–fluoroprobe (4.5 μM) hybrid assemblies at pH ≈ 7.0.

anywhere between 0.0 and 0.5 V, with increasing the potential by 0.1 V on the anodic side until just before the oxygen evolution begins, and same for the cathodic side until hydrogen

evolution starts to take place. The observed anodic potentials (E_{pa}) are 100, 155, and 115 mV for PY, APY, and AMPY, respectively, while the corresponding cathodic potentials (E_{pc}) for metal–fluoroprobe hybrid assemblies are 600, 356, and 594 mV for Ag–PY, Ag–APY, and Ag–AMPY, respectively. Therefore, the potential differences between the anodic peak of the pure fluoroprobes and the cathodic peak of silver–fluoroprobe hybrid assemblies (ΔE_P) are 503, 201, and 469 mV for PY, APY, and AMPY molecules. This indicates that charge transfer takes place from the fluoroprobes to the silver nanoparticles, which reduces the potential differences between the fluoroprobes and silver–fluoroprobe hybrid assemblies.[47] Therefore, the less potential difference value in case of APY indicates the facile electron transfer in Ag–APY hybrid systems as compared to Ag–PY and Ag–AMPY and follows the order Ag–APY > Ag–AMPY > Ag–PY. In addition, the current in the anodic and cathodic peaks of the probe molecules and the silver–fluoroprobe hybrids also signify the charge transfer from the fluoroprobes to the silver nanoparticles. In case of PY molecules, the anodic positive current ($i_{pa} = 0.96$ μA) decreases upon addition of Ag NPs and almost vanishes in Ag–PY hybrid systems, but develops a signature of negative current ($i_{pa} = -0.25$ μA). Similar results have also been observed for Ag–APY ($i_{pa} = 0.42$ and -0.25 μA) and Ag–AMPY ($i_{pa} = 0.24$ and -0.38 μA) systems with peak shifting, that is, at different potential with a different current value. Therefore, from this observation, it is clear that anodic peak current is higher with the absence of cathodic peak current in pure fluoroprobes. Yet, upon addition of silver nanoparticles to form the silver–fluoroprobe hybrid assemblies, the anodic peak current is completely diminished with a signature of cathodic peak current ($i_{pc} = -0.25$, -0.25, and -0.38 μA). These phenomena also support the transfer of electrons from the fluoroprobes to the silver nanoparticles in the hybrid assemblies.[48]

In addition, if the donor molecule is placed in the vicinity of a conductive metal surface, resonance energy transfer takes place in which energy is transferred by a nonradiative, long-range dipole–dipole coupling from a fluorophore in an excited state serving as a donor to another proximal ground-state acceptor.[49,50] Förster resonance energy transfer (FRET) involves the nonradiative transfer of excitation energy from an excited donor to a ground-state acceptor via resonance when brought in close proximity, which can radiatively emit a lower energy photon.[51] FRET processes are driven by dipole–dipole interactions and depend on the degree of spectral overlap between donor fluorescence and acceptor absorption, and on the sixth power of the separation distance between the donor and acceptor pair.[50] In the present experiment, the resonance energy transfer is believed to be through the dipole–dipole near-field interaction, where the fluorophores act as dipolar donors and the plasmonic silver nanostructures act as dipolar acceptors.[51] According to this formalism, the Förster distance, R_0, was calculated in which the best distance resolution was exhibited below ~70 Å.[52] In the present experiment, the Förster distance, R_0, has been calculated as approximately 29–33 Å for different nanoparticle–fluoroprobe assemblies. Therefore, Förster formalism could, exclusively, be employed to explain the observed results. The probability of this Förster resonance energy transfer is proportional to the spectral overlap

between the absorption of the metallic nanostructures and the fluorescence emission of the probe molecules.[53] The overlap integral, $J(\lambda)$, expresses the degree of spectral overlap between

the donor emission and the acceptor absorption and can be written in terms of the following equation:[51]

$$J(\lambda) = \int_0^\infty F_D(\lambda)\varepsilon_A(\lambda)\lambda^4 \, d\lambda = \frac{\int_0^\infty F_D(\lambda)\varepsilon_A(\lambda)\lambda^4 \, d\lambda}{\int_0^\infty F_D(\lambda) \, d\lambda}$$

(2)

where $F_D(\lambda)$ is the corrected fluorescence intensity of the donor in the wavelength range λ to $\lambda + \Delta\lambda$ with the total intensity (area under the curve) normalized to unity, $\varepsilon_A(\lambda)$, the extinction coefficient of the acceptor at λ, which is typically in units of M^{-1} cm^{-1}, and $F_D(\lambda)$ is dimensionless. If $\varepsilon_A(\lambda)$ is expressed in units of M^{-1} cm^{-1} and λ is in nanometers, then $J(\lambda)$ is in units of M^{-1} cm^{-1} nm^4. In calculating $J(\lambda)$, we could use the corrected emission spectrum with its area normalized to unity or normalize the calculated value of $J(\lambda)$ by the area; in this experiment, we have calculated the overlap integral by correcting the emission spectrum with its area normalized to unity. Figure 8 shows the spectral overlap between the
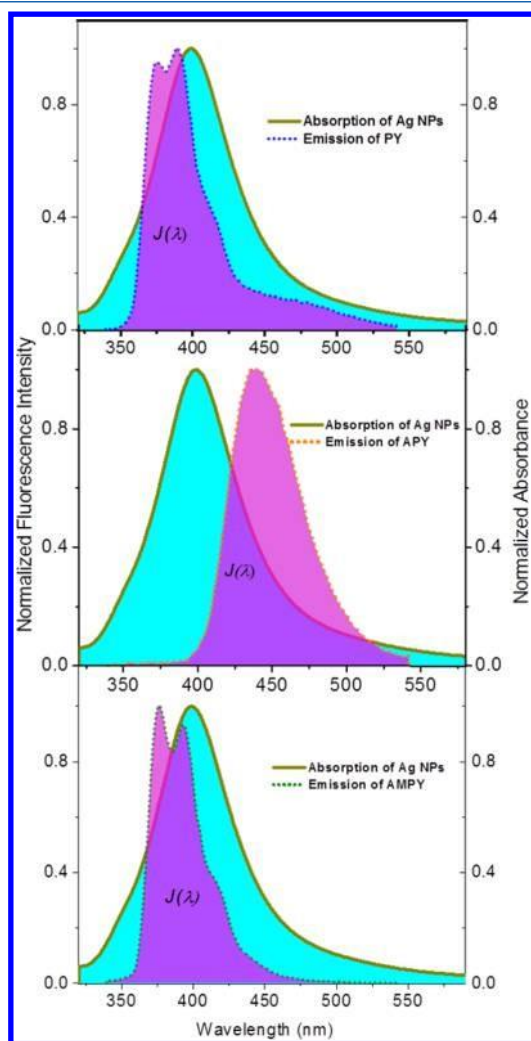

Figure 8. Overlap spectra of the emission spectrum of pyrene (0.3 μM), aminopyrene (0.04 μM), and aminomethylpyrene (0.03 μM) with the absorption spectrum of 6 nm silver nanoparticles (50 μM).

absorption spectrum of 6 nm silver nanoparticles (set B) and the emission spectrum of PY, APY, and AMPY ensuring

the silver nanoparticles has the maximum overlap with AMPY, lesser with PY, and the least with APY, which indicates AMPY could transfer energy more effectively than PY and APY molecules. In the present experiment, silver nanoparticles have been selected as the model nanostructures because the LSPR of the silver particles possesses maximum absorption in the emission range of pyrene and its derivatives.[8] Therefore, there is significant overlap between the absorption spectrum of silver nanoparticles with the emission spectrum of pyrene or its derivatives. Thus, energy transfer contributes considerably in the fluorescence quenching of silver–fluoroprobe hybrid assemblies. Therefore, the relative contributions of both electron and energy transfer could be realized. Other noble metal nanoparticles, for example, Au, Pd, and Pt, do not absorb, appreciably, in the emission range of the pyrene and its derivatives.[9,10] Therefore, energy transfer contribution toward the quenching of fluorescence of the pyrene derivatives should be very small as compared to electron transfer contribution. Under such situation, the separation of electron and energy transfer contributions would not be reasonable. Furthermore, quantum dots are, themselves, fluorescent. The fluorescence of the molecular probes on the surface of the quantum dots would be complicated by the electronic transitions of the particulates, and mere separation of electron and energy transfer contributions would be exaggerated due to also many simultaneous events in the quantum dot–fluoroprobe hybrid assemblies.

The rate of Förster resonance energy transfer for a donor and acceptor separated by a distance r is given by[51]

$$k_T(r) = \frac{Q_D \kappa^2}{\tau_D r^6} \left(\frac{9000(\ln 10)}{128\pi^5 N \eta_A^4} \right) J(\lambda)$$

(3)

efficient resonant energy transfer. It is seen that the LSPR of

where Q_D is the quantum yield of the donor in the absence of acceptor, η is the refractive index of the medium, N_A is Avogadro's number, r is the distance between the donor and acceptor, and τ_D is the lifetime of the donor in the absence of acceptor. The term κ^2 is a factor describing the relative orientation in space of the transition dipoles of the donor and acceptor; the value of κ^2 is usually assumed to be 2/3, which is appropriate for dynamic random averaging of the donor and acceptor. Except for the overlap integral, because all of the parameters are constants for a particular probe molecule, therefore it is plausible to express all of the values in terms of overlap integral rather than the rate of energy transfer. To elucidate an explicit correlation between the fluorescence spectra of the molecular probes and the localized surface plasmon resonance spectra of the metallic nanoparticles, overlap spectra consisting of emission spectrum of PY or APY or AMPY and absorption spectra of four different sizes of silver nanoparticles are presented in Figure 9. An account of related parameters in size-selective silver nanoparticle-induced fluorescence quenching of pyrene moieties is enunciated in Table 3. It is seen that the overlap integral at first increases and then decreases with increase in particle size with APY mole- cules that results from the cumulative effect of gradual red shift ($\lambda_{max} \approx 379$–409) of the absorption maximum and decrease in extinction coefficient, $\varepsilon(\lambda)$, with increase in size of the particles. Moreover, it is noted that the overlap integral decreases for PY or AMPY molecules as the spectral overlap does not increase consequently with the red shift of the absorption maximum, while the extinction coefficient $\varepsilon(\lambda)$ decreases with increase in size of the particles. The Stern–Volmer plots show that the K_{SV} value decreases with increase in size of the Ag NPs. Yet, it is
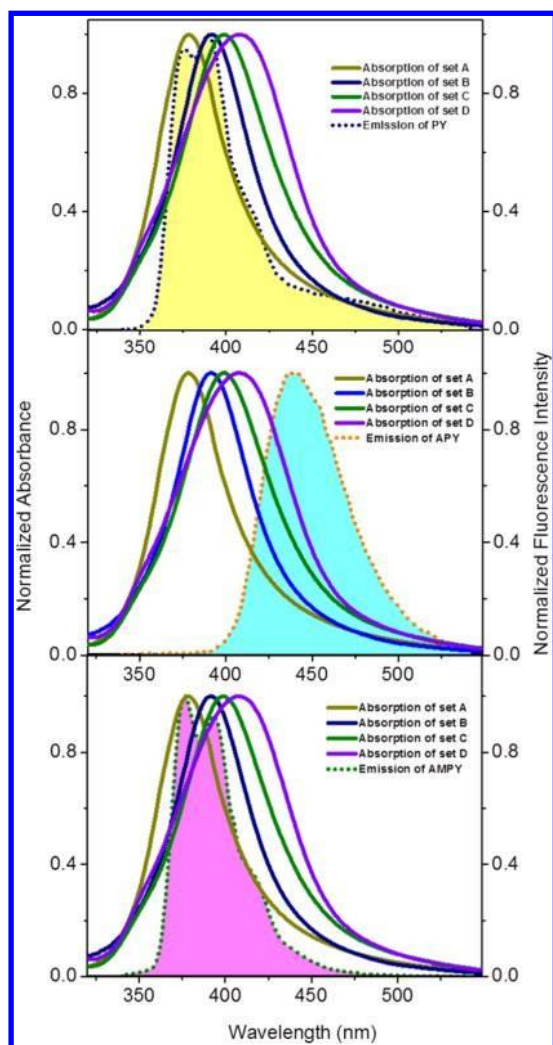
Figure 9. Overlap spectra of the emission spectrum of pyrene (0.3 μM), aminopyrene (0.04 μM), and aminomethylpyrene (0.03 μM) with 2, 6, 9, and 21 nm silver nanoparticles (50 μM).

observed that for smaller nanoparticles (<6 nm), K_{SV} values are very high even for pyrene molecules, although it does not possess the capability of donating a lone pair of electrons. A close inspection of K_{SV} values in Table 3 shows that K_{SV} increases in the sequence of PY < AMPY < APY irrespective of the particle size. Therefore, it is apparent that, although APY has the lower overlap integral values as compared to PY and

AMPY, the K_{SV} values are the highest for APY molecules. This phenomenon could be explicated in a substantial way by introducing a new parameter, differential quenching ($K_{SV}/J(\lambda)$, Stern–Volmer constant per unit overlap integral), to avoid all plausible complications arising from the size of the metal particles, types of the molecular probes, and difference in overlap integral values. On the basis of these perspectives, we have plotted the $K_{SV}/J(\lambda)$ values as a function of particle diameter of the Ag NPs for three different probe molecules as presented in Figure 10. From the graph, two important
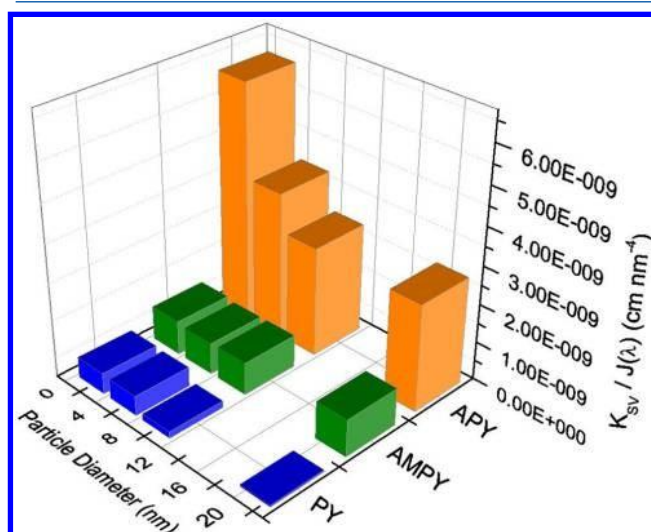

Figure 10. Differential quenching of pyrene moieties as a function of particle size of silver nanostructures.

observations can be made. First, it is seen that, for larger particles (>9 nm), APY and AMPY exhibit 60–20-fold higher $K_{SV}/J(\lambda)$ values, respectively, as compared to PY due to the presence of $-NH_2$ and $-CH_2-NH_2$ functionalities, respectively. Second, for smaller Ag NPs (<6 nm), the $K_{SV}/J(\lambda)$ values of PY are about 10-fold higher as compared to larger particles (>9 nm), which supports the π electron transfer along with FRET to the Ag NPs. Similar results have also been observed for APY molecules, for which $K_{SV}/J(\lambda)$ values are enhanced 2-fold as compared to that of larger silver nanoparticles. Moreover, for smaller silver nanoparticles, the $K_{SV}/J(\lambda)$ value is the highest (11- and 7-fold) for APY as compared to PY and AMPY molecules. Another important observation is that $K_{SV}/J(\lambda)$ values remain the same for AMPY

Table 3. Account of Related Parameters in Silver Nanoparticle-Induced Fluorescence Quenching of Pyrene Moieties

Ag NPs (nm)	molecular probes	overlap integral, $J(\lambda)$	K_{SV} (M^{-1})	K_{SV} (M^{-1})/$J(\lambda)$ (cm nm^{-4})	mode of quenching	observed quenching
2 ± 0.5	PY	2.2243×10^{14}	1.22×10^5	0.548×10^{-9}	FRET and ET	high
	APY	1.0147×10^{14}	6.33×10^5	6.238×10^{-9}	FRET and ET	very high
	AMPY	2.4728×10^{14}	2.21×10^5	0.894×10^{-9}	FRET and ET	high
6 ± 1	PY	1.9952×10^{14}	1.03×10^5	0.516×10^{-9}	FRET and ET	high
	APY	1.3356×10^{14}	5.13×10^5	3.839×10^{-9}	FRET and ET	very high
	AMPY	2.1914×10^{14}	1.82×10^5	0.830×10^{-9}	FRET and ET	high
9 ± 2	PY	1.5882×10^{14}	0.27×10^5	0.169×10^{-9}	FRET	low
	APY	1.2841×10^{14}	3.70×10^5	2.881×10^{-9}	FRET and ET	very high
	AMPY	1.7332×10^{14}	1.47×10^5	0.848×10^{-9}	FRET and ET	high
21 ± 3	PY	1.1052×10^{14}	0.05×10^5	0.0425×10^{-9}	FRET	very low
	APY	1.0492×10^{14}	2.94×10^5	2.802×10^{-9}	FRET and ET	high

| AMPY | 1.1975×10^{14} | 1.17×10^5 | 0.977×10^{-9} | FRET and ET | high |

molecules irrespective of the size of the particles. From this experimental observation, it is apparent that the energy and electron transfer imbue explicit contributions in nanoparticle-induced fluorescence quenching and the extent of electron transfer is prominent for smaller (<6 nm) silver nanoparticles, which is due to the pronounced residual force with decreasing size of the particles. On the basis of these perspectives, a schematic presentation of the possible deactivation pathways in silver–fluoroprobe hybrid assemblies is enunciated in Scheme 1.

Scheme 1. Schematic Presentation of the Possible Deactivation Pathways in Silver–Fluoroprobe Hybrid Assemblies
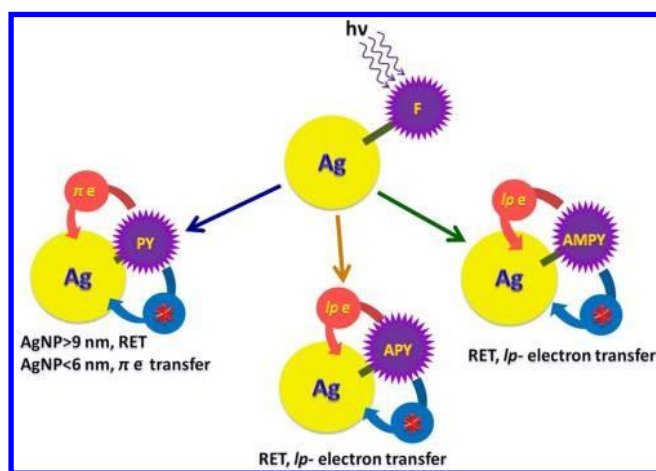
4. CONCLUSIONS

Silver nanoparticles drastically alter the emission characteristics of pyrene and its amine derivatives that result from an invasive integration of the photophysical aspects of the molecular probes as well as the morphology and optical characteristics of the small metallic particulates. Thus, it is observed that fluorophore-bound silver nanostructures provide a convenient way to understand the surface binding properties of photoresponsive molecules and therefore to examine the relative contributions of electron and energy transfer in the quenching processes. The new parameter, "differential quenching", has been introduced that appears to realize individual electron and energy transfer in nanoparticle-induced fluorescence quenching. The consequence of physical interaction of nanoparticle–fluoroprobe assemblies provides strong evidence for the donation of both σ and π electrons to the small metallic particulates. Probing the details of the mechanism can provide concrete empirical guidelines that can be used to more realistically select ideal nanostructure–fluoroprobe quenching pairs for optical molecular rulers and optoelectronic nanodevices. We anticipate that experimental observations in the present investigation would pioneer future theoretical work in separating the electron and energy transfer contributions in nanoparticle-induced fluorescence quenching.

■ ASSOCIATED CONTENT

✱ Supporting Information

The Supporting Information is available free of charge on the ACS Publications website at DOI: 10.1021/acs.jpcc.5b08466.

AUTHOR INFORMATION

Corresponding Author

*E-mail: sujit.kumar.ghosh@aus.ac.in.

Notes

The authors declare no competing financial interest.

REFERENCES

(1) Giannini, V.; Fernández-Domínguez, A. I.; Heck, S. C.; Maier, S. A. Plasmonic Nanoantennas: Fundamentals and their Use in Controlling the Radiative Properties of Nanoemitters. *Chem. Rev.* 2011, *111*, 3888–3912.

(2) Ozbay, E. Plasmonics: Merging Photonics and Electronics at Nanoscale Dimensions. *Science* 2006, *311*, 189–193.

(3) Ghosh, S. K.; Pal, T. Photophysical Aspects of Molecular Probes near Nanostructured Gold Surfaces. *Phys. Chem. Chem. Phys.* 2009, *11*, 3831–3844.

(4) Varnavski, O. P.; Ranasinghe, M.; Yan, X.; Bauer, C. A.; Chung, S.
– J.; Perry, J. W.; Marder, S. R.; Goodson, T., III Ultrafast Energy Migration in Chromophore Shell–Metal Nanoparticle Assemblies. *J. Am. Chem. Soc.* 2006, *128*, 10988–10989.

(5) Alvarez-Puebla, R.; Liz-Marzán, L. M.; F. de Abajo, J. G. Light Concentration at the Nanometer Scale. *J. Phys. Chem. Lett.* 2010, *1*, 2428–2434.

(6) Hobson, P. A.; Wedge, S.; Wasey, J. A. E.; Sage, I.; Barnes, W. L. Surface Plasmon Mediated Emission from Organic Light-Emitting Diodes. *Adv. Mater.* 2002, *14*, 1393–1396.

(7) Kamat, P. V.; Barazzouk, S.; Hotchandani, S. Electrochemical Modulation of Fluorophore Emission on a Nanostructured Gold Film. *Angew. Chem., Int. Ed.* 2002, *41*, 2764–2767.

(8) Link, S.; El-Sayed, M. A. Spectral Properties and Relaxation Dynamics of Surface Plasmon Electronic Oscillations in Gold and Silver Nanodots and Nanorods. *J. Phys. Chem. B* 1999, *103*, 8410–8426.

(9) Ghosh, S. K.; Pal, T. Interparticle Coupling Effect on the Surface Plasmon Resonance of Gold Nanoparticles: From Theory to Applications. *Chem. Rev.* 2007, *107*, 4797–4862.

(10) Stewart, M. E.; Anderton, C. R.; Thompson, L. B.; Maria, J.; Gray, S. K.; Rogers, J. A.; Nuzzo, R. G; Nanostructured Plasmonic Sensors. *Chem. Rev.* 2008, *108*, 494–521.

(11) Lakowicz, J. R. *Principles of Fluorescence Spectroscopy*, 3rd ed.; Plenum Press: New York, 2006.

(12) Dubertret, B.; Calame, M.; Libchaber, A. J. Single-Mismatch Detection using Gold-Quenched Fluorescent Oligonucleotides. *Nat. Biotechnol.* 2001, *19*, 365–370.

(13) George Thomas, K.; Kamat, P. V. Chromophore-Functionalized Gold Nanoparticles. *Acc. Chem. Res.* 2003, *36*, 888–898.

(14) Maier, S. A. *Plasmonics: Fundamentals and Applications*; Springer-Verlag: New York, 2007.

(15) Rahman, D. S.; Ghosh, S. K. Fluorescence Spectroscopy in Probing Spontaneous and Induced Aggregation amongst Size-Selective Gold Nanoclusters. *Chem. Phys.* 2014, *438*, 66–74.

(16) Jensen, T. R.; Malinsky, M. D.; Haynes, C. L.; Van Duyne, R. P. Nanosphere Lithography: Tunable Localized Surface Plasmon Resonance Spectra of Silver Nanoparticles. *J. Phys. Chem. B* 2000, *104*, 10549–10556.

(17) Ni, W.; Ambjörnsson, T.; Apell, S. P.; Chen, H.; Wang, J. Observing Plasmonic-Molecular Resonance Coupling on Single Gold Nanorods. *Nano Lett.* 2010, *10*, 77–84.

Article

(18) Boal, A. K.; Rotello, V. M. Fabrication and Self-Optimization of Multivalent Receptors on Nanoparticle Scaffolds. *J. Am. Chem. Soc.* 2000, *122*, 734–735.

(19) George Thomas, K.; Kamat, P. V. Making Gold Nanoparticles Glow: Enhanced Emission from a Surface-Bound Fluoroprobe. *J. Am. Chem. Soc.* 2000, *122*, 2655–2656.

(20) Wang, T.; Zhang, D.; Xu, W.; Yang, J.; Han, R.; Zhu, D. Preparation, Characterization, and Photophysical Properties of Alkanethiols with Pyrene Units-Capped Gold Nanoparticles: Unusual Fluorescence Enhancement for the Aged Solutions of these Gold Nanoparticles. *Langmuir* 2002, *18*, 1840–1848.

(21) Ipe, B. I.; George Thomas, K.; Barazzouk, S.; Hotchandani, S.; Kamat, P. V. Photoinduced Charge Separation in a Fluorophore-Gold Nanoassembly. *J. Phys. Chem. B* 2002, *106*, 18–21.

(22) Ghosh, S. K.; Pal, A.; Kundu, S.; Nath, S.; Pal, T. Fluorescence Quenching of 1–Methylaminopyrene Near Gold Nanoparticles: Size Regime Dependence of the Small Metallic Particles. *Chem. Phys. Lett.* 2004, *395*, 366–372.

(23) Evanoff, D. D., Jr.; Chumanov, G. Synthesis and Optical Properties of Small Silver Nanoparticles. *ChemPhysChem* 2005, *6*, 1221–1231.

(24) Rahman, D. S.; Chatterjee, H.; Ghosh, S. K. Excess Surface Energy at the Tips of Gold Nanospikes: From Experiment to Modeling. *J. Phys. Chem. C* 2015, *119*, 14326–14337.

(25) Smart, L. E.; Moore, E. A. *Solid State Chemistry: An Introduction*, 3rd ed.; Taylor & Francis, CRC Press: Boca Raton, FL, 2005.

(26) Liang, H.; Wang, W.; Huang, Y.; Zhang, S.; Wei, H.; Xu, H. Controlled Synthesis of Uniform Silver Nanospheres. *J. Phys. Chem. C* 2010, *114*, 7427–7431.

(27) Li, S.; Shen, Y.; Xie, A.; Yu, X.; Qiu, L.; Zhang, L.; Zhang, Q. Green Synthesis of Silver Nanoparticles using *Capsicum Annuum* L. Extract. *Green Chem.* 2007, *9*, 852–858.

(28) Offen, H. W. In *Organic Molecular Photophysics*; Birks, J. B., Ed.; Wiley-Interscience: New York, 1975; Vol. *1*.

(29) Förster, Th.; Kasper, K. Ein Konzentrationsumschlag der Fluoreszenz des Pyrens. *Z. Phys. Chem.* 1955, *59*, 976–980.

(30) Kalyanasundaram, K.; Thomas, J. K. Environmental Effects on Vibronic Band Intensities in Pyrene Monomer Fluorescence and their Application in Studies of Micellar Systems. *J. Am. Chem. Soc.* 1977, *99*, 2039–2044.

(31) Bertolotti, S. G.; Zimmerman, O. E.; Cosa, J. J.; Previtali, C. M. Excimer Emission of Pyrene Derivatives Induced by Ionic Detergents below the Critical Micelle Concentration. *J. Lumin.* 1993, *55*, 105–113.

(32) Kaur, M.; Kaur, P.; Dhuna, V.; Singh, S.; Singh, K. A Ferrocene-Pyrene based 'Turn-On' Chemodosimeter for Cr^{3+} -Application in Bioimaging. *Dalton Trans.* 2014, *43*, 5707–5712.

(33) Weitz, D. A.; Garoff, S.; Gersten, J. I.; Nitzan, A. Roughened Silver Electrodes for Use in Metal-Enhanced Fluorescence. *J. Chem. Phys.* 1983, *78*, 5324–5338.

(34) Kerker, M. The Optics of Colloidal Silver: Something Old and Something New. *J. Colloid Interface Sci.* 1985, *105*, 297–314.

(35) Barnes, W. L. Fluorescence near Interfaces: The Role of Photonic Mode Density. *J. Mod. Opt.* 1998, *45*, 661–699.

(36) Otto, S.; Volmer, M. Uber die Abklingzeit der Fluoreszenz. *Phys. Z.* 1919, *20*, 183–188.

(37) Dulkeith, E.; Morteani, A. C.; Niedereichholz, T.; Klar, T. A.; Feldmann, J.; Levi, S. A.; van Veggel, F. C. J. M.; Reinhoudt, D. N.; M?ller, M.; Gittins, D. I. Fluorescence Quenching of Dye Molecules near Gold Nanoparticles: Radiative and Nonradiative Effects. *Phys. Rev. Lett.* 2002, *89*, 2030021 1–4.

(38) Chance, R. R.; Prock, A.; Silbey, R. Molecular Fluorescence and Energy Transfer near Interfaces. *Adv. Chem. Phys.* 1978, *37*, 1–65.

(39) Makarova, O. V.; Ostafin, A. E.; Miyoshi, H., Jr.; Norris, J. R.; Miesel, D. Adsorption and Encapsulation of Fluorescent Probes in Nanoparticles. *J. Phys. Chem. B* 1999, *103*, 9080–9084.

(40) Kamat, P. V.; Flumiani, M.; Hartland, G. V. Picosecond Dynamics of Silver Nanoclusters. Photoejection of Electrons and Fragmentation. *J. Phys. Chem. B* 1998, *102*, 3123–3128.

(41) Puddephatt, R. J. In *Comprehensive Coordination Chemistry*; Wilkinson, G., Gillard, R. D., McCleverty, J. A., Eds.; Pergamon Press: Oxford, 1987; Vol. *5*, pp 862–891.

(42) Barradas, R. G.; Conaway, B. E. Some Applications of Ultra- Violet Spectrophotometry to Studies of Adsorption at Copper, Nickel and Silver Electrodes. *J. Electroanal. Chem.* 1963, *6*, 314–325.

(43) Mohilur, D. M. In *Electroanalytical Chemistry*; Bard, A. J., Ed.; Marcel Dekker: New York, 1996; Vol. *1*, p 355.

(44) Franzen, S.; Folmer, J. C. W.; Golm, W. R.; O'Neal, R. Optical Properties of Dye Molecules Adsorbed on Single Gold and Silver Nanoparticles. *J. Phys. Chem. A* 2002, *106*, 6533–6540.

(45) Whitmore, P. M.; Robata, H. J.; Harris, C. B. Mechanisms for Electronic Energy Transfer between Molecules and Metal Surfaces: A Comparison of Silver and Nickel. *J. Chem. Phys.* 1982, *77*, 1560–1568.

(46) Henglein, A.; Mulvaney, P.; Linnert, T. Chemistry of Ag_n Aggregates in Aqueous Solution: Non-Metallic Oligomeric Clusters and Metallic Particles. *Faraday Discuss.* 1991, *92*, 31–44.

(47) Wu, Y.; Xu, W.; Wang, Y.; Yuan, Y.; Yuan, R. Silver–Graphene Oxide Nanocomposites as Redox Probes for Electrochemical Determination of 1-Fetoprotein. *Electrochim. Acta* 2013, *88*, 135–140.

(48) Kerman, K.; Kobayashi, M.; Tamiya, E. Recent Trends in Electrochemical DNA Biosensor Technology. *Meas. Sci. Technol.* 2004, *15*, R1–R11.

(49) Kapoor, S. Preparation, Characterization, and Surface Modification of Silver Particles. *Langmuir* 1998, *14*, 1021–1025.

(50) Waldeck, H. J.; Alivisatos, A. P.; Harris, C. B. Nonradiative Damping of Molecular Electronic Excited States by Metal Surfaces. *Surf. Sci.* 1985, *158*, 103–125.

(51) Förster, T. Zwischenmolekulare Energiewanderung und Fluoreszenz. *Ann. Phys.* 1948, *437*, 55–75.

(52) Yun, C. S.; Javier, A.; Jennings, T.; Fisher, M.; Hira, S.; Peterson, S.; Hopkins, B.; Reich, N. O.; Strouse, G. F. Nanometal Surface Energy Transfer in Optical Rulers, Breaking the FRET Barrier. *J. Am. Chem. Soc.* 2005, *127*, 3115–3119.

(53) Hao, E.; Schatz, G. C. Electromagnetic Fields around Silver Nanoparticles and Dimers. *J. Chem. Phys.* 2004, *120*, 357–366.

# Excess Surface Energy at the Tips of Gold Nanospikes: From Experiment to Modeling

Dewan S. Rahman, Hirak Chatterjee, and Sujit Kumar Ghosh*

Department of Chemistry, Assam University, Silchar 788011, India

⚓ *Supporting Information*

ABSTRACT: Physicochemical aspects of anisotropic gold nanostructures have been of considerable interest due to intrinsic shape-dependent phenomena that open up newer perspectives from nanoscale electromagnetism to basic thermodynamics since gold has a highly symmetric face-centered cubic (fcc) structure and usually tends to afford a spherical geometry to reduce surface free energy. The emergence of novel properties of these anisotropic structures could be attributed to the lack of symmetry at the interface or to the confinement of electrons that does not scale linearly with size. Based on these concepts, anisotropic gold nanospike has been chosen as a typical nanostructural system that possesses different surface energy around the nanostructure in comparison to isotropic gold nanosphere to quantify the precise surface energy at the tips of these intricate nanostructures. Cetyltrimethylammonium bromide-stabilized gold nanospheres and nanospikes have been synthesized in aqueous medium under ambient conditions. Since fluorescence spectroscopy is a very sensitive technique, fluorescent dye, alizarin red, has been employed as a local probe to elucidate the detailed spectral characteristics of the metal–probe hybrid assemblies. The influence of morphological anisotropy of these nanostructures has been, further, emphasized by following the temporal changes in the emission characteristics during the photoinduced conversion of gold nanospikes to nanospheres under NIR laser irradiation. Experimental realization of excess surface energy at the tips of the nanospikes has been calculated from theoretical perspectives.
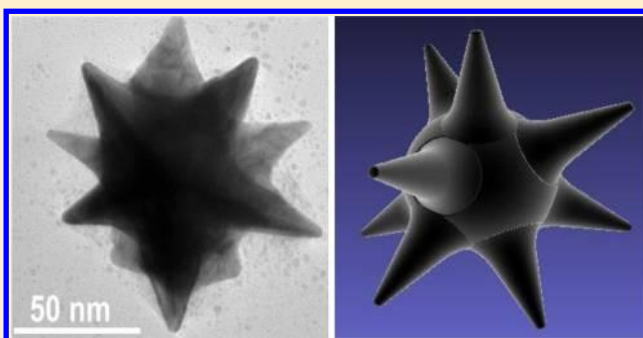
1. INTRODUCTION

Nanoscaled systems have become an active area of research in materials science, condensed matter physics, and chemistry because of their high surface-to-volume ratio and accordingly, the surface or interface energy is becoming the most important attributes in governing the physical and chemical properties of nanoscaled systems that may open new windows in technological applications.[1] As a result, thermodynamics of ultrasmall particles is becoming increasingly important as the dimension of electronic devices approaches the nanoscale. As the shape of the system deviates from isotropic spherical nanostructures, finding effective ways to deal with these systems has been a long-standing challenge. On the other hand, the ability of noble metal colloids to manipulate light at the nanoscale has pioneered an emerging research area called plasmonics.[2] In recent years there has been tremendous progress over the past decade in the investigation of the shape-dependent properties of metallic nanocrystals and realization of their numerous potential applications in various fields, such as, electronics, photonics, or sensing.[3,4] Noble metal particles, namely, copper, silver, and gold, in the nanometer size regime exhibit strong absorption in the visible and NIR region, and this is indeed a small particle effect, since they are absent in the individual atom as well as in the bulk.[5,6] The dispersive electric field of the electromagnetic radiation causes collective oscillation of conduction electrons in metal nanoparticles with a resonance frequency, often coined as localized surface plasmon resonance (LSPR).[7] These collective oscillations of the conduction band electrons enable strong optical absorption and scattering in subwavelength structures, with spectral properties dependent upon the size, shape, interparticle interactions, dielectric properties, and local environment of the nanoparticles.[5,6] While the spectral properties of colloidal nanoparticles are, fundamentally, dependent upon their shape, the LSPR of anisotropic nanostructures could, easily, be tuned by controlling the morphology.[8] Gold nanospikes have been demonstrated to be a highly promising class of shape-engineered nanoparticles, as these multibranched nanoparticles with sharp tips display extremely interesting plasmonic properties with a broad surface plasmon band in the NIR region.[9–11]

The interdisciplinarity of plasmonics and thermodynamics has become a flourishing new field of science and technology offering a tantalizing opportunity to attain unprecedented levels of synergy between optical and electronic pursuances.[12] Organic dye molecules have often been used as local

fluoroprobes to study the optical properties of noble metal nanostructures that are able to manipulate light at the nanometer length scale.[13,14] Theoretical calculations and experimental observations have shown that the main critical parameters that modify the spontaneous rate of emission of organic dyes near metal nanoparticles are the location of the dye molecules around the particles, its separation from the metal surface, and the molecular dipole orientation with respect to the particle surface.[15] It is now well-established in the literature that fluorescence of probe molecules is usually quenched in the vicinity of noble metal nanostructures but enhanced under restricted environments.[16] Beyond these critical experiments on nanospheroids, ingenious investigations have been put forward to study the photophysical aspects of molecular probes near anisotropic nanostructures, for example, nanorods, nanocones, nanoshells, and so on.[17] Although the fundamental physics of the processes involved in metal–probe hybrid assemblies is quite matured, the nonlocal effect of the anomalous surface energy of nanostructures has become the subject of immense investigation.[18] All steps of a surface chemical reaction, sticking, reaction, and desorption, involve energy exchange between the adsorbate and substrate states. Therefore, it is essential to develop new theoretical tools for the understanding and determination of the surface energy distribution of the nanostructures and, therefore, merging plasmonics and thermodynamics at the nanoscale.

In this article, fluorescence spectroscopic technique have been employed in measuring the excess surface energy of the tips of gold nanospikes that play a pivotal role in governing the photophysical aspects of molecular probes near nanostructured metallic surfaces. Multispiked gold nanostructures have been chosen as the model systems as these possess different local environments around the nanostructures. We have employed alizarin red as the local probes to investigate the photophysical properties of the dye molecules near the anisotropic nanospikes in comparison with isotropic spherical nanostructures. It has been found that gold nanospikes are efficient quenchers of molecular fluorescence than the nanospheres due to morphological adversity in these anisotropic nanostructures. This hypothesis has, further, been validated by following the temporal changes of molecular fluorescence during the photoconversion of the nanospikes into nanospheres under NIR laser irradiation. Based on the experimental realization of excess surface energy at the tips of the nanospikes, theoretical tools have been developed by geometrical modeling to calculate the excess surface energy around the nanostructures.

2. EXPERIMENTAL SECTION

Gold nanospheres and nanospikes have been synthesized by following the procedure of Jana et al.[19] and Sau et al.,[20] respectively. Details of the experiment are described in Supporting Information, ESI 1. The as-synthesized gold nanospheres and nanospikes were centrifuged at 10000 rpm for 10 min to remove the excess CTAB from the solution and redispersed into water by sonication. Then, various concentrations (0–40 μM) of gold nanospheres/nanospikes was added in an aliquot of freshly prepared aqueous solution of alizarin red (33 μM), incubated overnight under ambient condition (pH ~ 7.0) to complete the surface complexation process, and the fluorescence spectrum of each solution was

3. RESULTS AND DISCUSSION

Alizarin red or 1,2-dihydroxyanthraquinone, also known as "Turkey Red", is an organic dye belonging to the alizarin family, derived from the roots of plants of the madder genus and has been used as a prominent red dye, especially for dying textile fabrics.[21] Figure 1 shows the absorption and emission spectra of
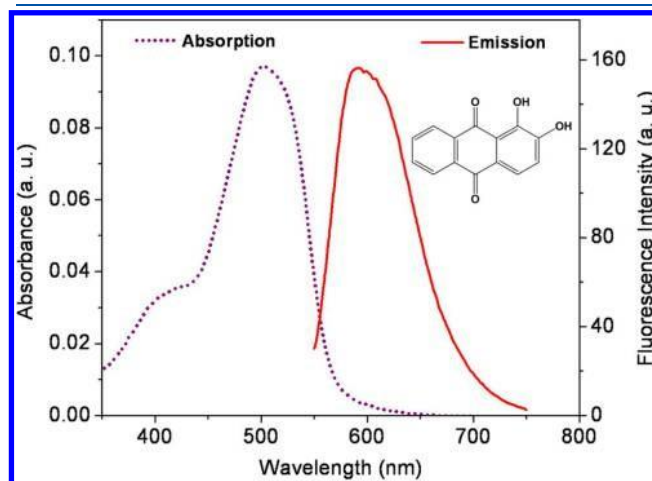
measured in the spectrofluorimeter.

Figure 1. Absorption and emission spectra of alizarin red in aqueous medium. Inset shows the molecular structure of the dye molecule.

alizarin red in aqueous medium. The molecular structure of the dye is shown in the inset. The dye molecules exhibit a very intense absorbance band centered around 503 nm, along with a less intense vibrational shoulder, centered around 307 nm corresponding to $n \rightarrow \pi^*$ and $\pi \rightarrow \pi^*$ transitions and molar extinction coefficient, $\varepsilon \sim 29100$ M^{-1} cm^{-1} corresponding to the monomeric form of the fluorophore.[22] Excitation at 503 nm exhibits a broad emission spectrum with maximum intensity at 593 nm and quantum yield, $\varphi_f \sim 5.1 \times 10^{-4}$ corresponding to the neutral form of the dye molecules.[22] The emission spectra of alizarin red have been examined as a function of dye concentration in the range of 3–33 μM (not shown). It is found that there is no significant perturbation in the band structure and band position of the dye, and fluorescence intensity (at 593 nm) increases linearly with an increase in the concentration of the dye molecules, indicating there is no

significant dimerization or higher order aggregation in this concentration range. These well-suited photophysical aspects have enabled the study of the emission characteristics of the alizarin red molecules with the metallic nanostructures.

The gold nanospheres[19] and nanospikes[20] have been synthesized by the methods described in the Experimental Section. Figure 2 represents the absorption spectra of gold nanospheres and nanospikes, respectively. It is seen that the nanosphere dispersion displays a well-defined optical response with maximum at ca. 540 nm; this absorption band arises due to the localized surface plasmon resonance of spherical gold nanoparticles.[5] The absorption spectrum of gold nanospikes dispersion exhibits a broad absorption band over the range of 500–1100 nm comprising a short-wavelength plasmon band in the midvisible region and a long-wavelength plasmon band in the NIR region with maxima at about 550 and 770 nm, respectively. These two bands could be attributed to the two dipolar resonance modes, which are assigned as localized within the central core and the multiple sharp tips of such particles, respectively. It has been shown that the plasmon of the gold
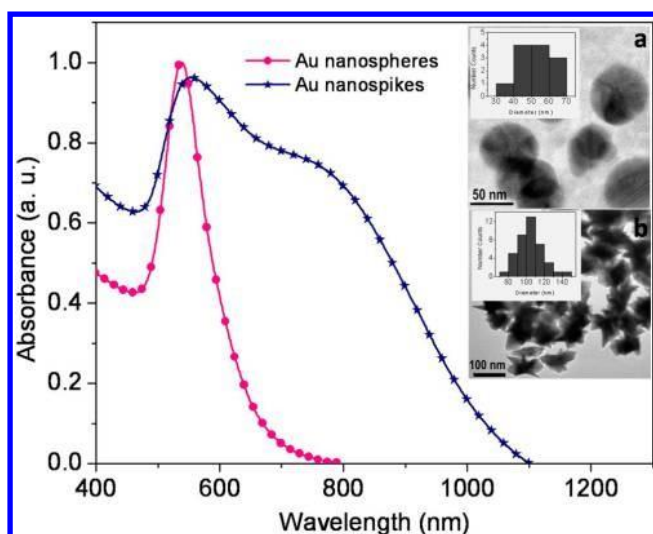
Figure 2. Absorption spectra of CTAB-stabilized gold nanospheres and nanospikes. Inset shows the transmission electron microscopic images (inset shows the corresponding diameter histogram) of gold (a) nanospheres and (b) nanospikes.

nanostars results from the hybridization of plasmons of the core that serves as a nanoscale antenna, dramatically enhancing the excitation cross-section as well as the local electromagnetic field of the protruding prolate tips.[10,11] The plasmon spectrum of

such particles shows a weak absorption around 520 nm that could be attributed to the plasmon resonance of the nanostar's core, and a dominant plasmon band at longer wavelengths due to the resonance supported by the nanostar branches.[11,23] Transmission electron microscopic images (inset shows the corresponding diameter histogram) of gold nanospheres (image a) and nanospikes (image b) are shown in the inset. Transmission electron micrograph of the representative gold nanoparticles shows that the particles are nearly spherical with average diameter in the range of 55 ± 10 nm; the as-synthesized gold nanospikes comprise of quasi-spherical central part with sizes 50 ± 5 nm on the surface of which 8–10 shallow "elliptical cone" shaped protrusions having relatively uniform hemiellipsoidal tips with sizes 40 ± 10 nm in length.

Now, we have performed comparative studies of the emission behavior of alizarin red ($\lambda_{ex} \sim$ 503 nm) in the presence of gold nanospheres and nanospikes as shown in Figure 3. In these experiments, quite dilute solutions (40 μM) have been used so as to minimize the effects of excitation attenuation and solution self-absorption (so-called "trivial effects"). It is seen that the emission of alizarin red showed distinctly different profile in the presence of different concentrations of gold nanospheres (panel a) and nanospikes (panel b) and both the morphology of nanostructures quench the fluorescence emission of the dye molecules. The salient feature of physical significance is that the extent of quenching is greater in case of gold nanospikes as compared to nanospheres, provided that the concentration of
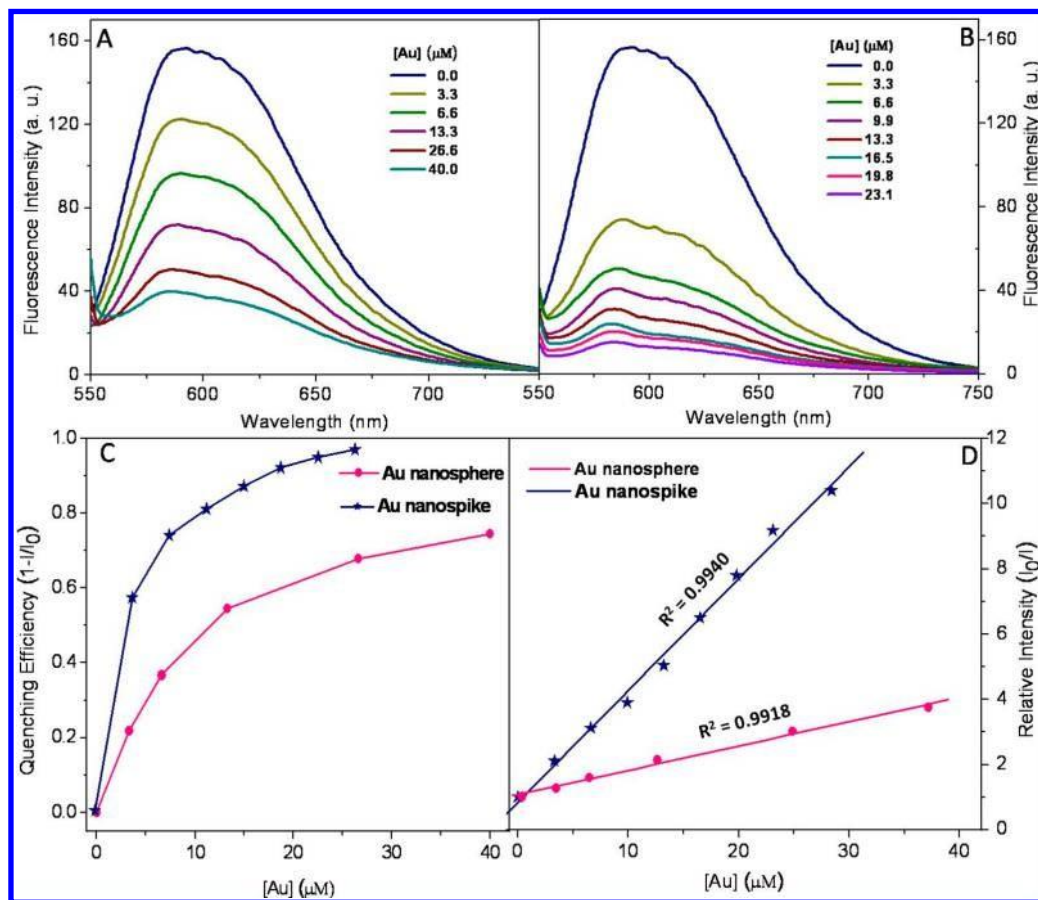

Figure 3. Emission spectra of alizarin red molecules (33 μM) in the presence of different concentrations of gold (A) nanospheres and (B) nanospikes in aqueous medium; (C) Relative efficiency of alizarin red molecules in the presence of gold nanospheres and nanospikes and (D) Stern–Volmer plot showing the quenching efficiency of alizarin red as a function of concentration of gold nanospheres and nanospikes.
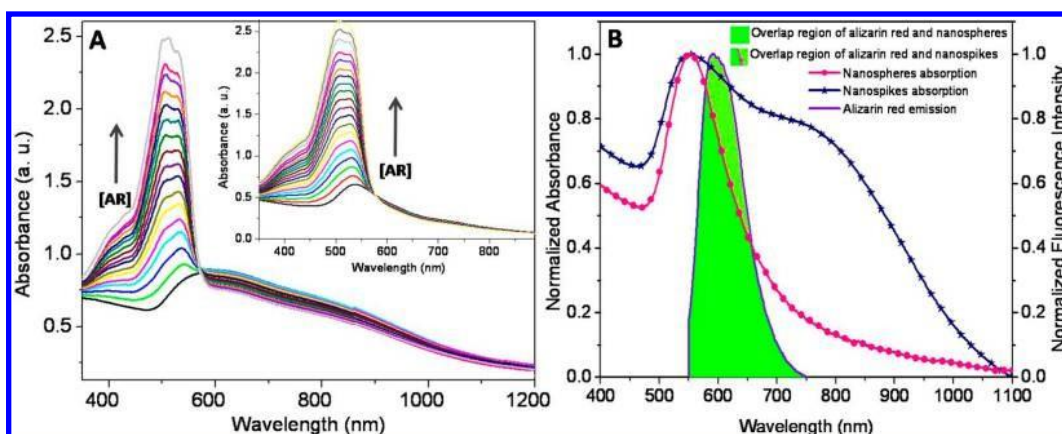
Figure 4. (A) Absorption spectral changes of gold nanospikes (0.25 mM) upon successive addition of alizarin red. Inset shows the corresponding changes of the gold nanospheres upon addition of the dye molecules. (B) Overlap between the emission spectrum of alizarin red (33 μM) with absorption spectra of gold (0.25 mM) nanospheres and nanospikes.

gold remains constant. It is noted that quenching is much sensitive at the low concentration of gold nanostructures; for example, at 4 μM concentration, the quenching efficiency of gold nanospheres is nearly 20%, while for nanospikes, the corresponding value is 50%, and both of these values increases with an increase in concentration of gold nanostructures. About 95% quenching efficiency is observed for gold nanospikes at the concentration of 20 μM but less than 80% quenching observed even at 40 μM of the nanospheres. Panel c shows a plot of relative quenching efficiency, $\theta = 1 - I/I_0$ as a function of gold concentration, where I_0 and I are the intensities of emission spectra of the dye molecules in the absence and presence of the nanostructures as a function of gold concentration of the nanospheres and nanospikes. It is also noted that the relative quenching efficiency exponentially increases with increasing concentration of gold nanostructures. The quenching of molecular fluorescence in the vicinity of metallic nanostructures could be treated by the model proposed by Weitz et al.[24] A fluoroprobe in the vicinity of metallic nanostructures may be influenced by radiative and the nonradiative de-excitation rates involved in the fluorescence emission. Depending on its relative position and orientation with respect to the nanostructures, the fluoroprobe may experience an enhanced or suppressed electric field, leading to a higher or lower excitation rate, respectively, in comparison to a fluorophore in free space. In metal–fluoroprobe hybrid assemblies, the excitation of the electronic plasma resonance leads to an increase in the absorption rate. Again, the molecular emission dipole excites the plasma resonance, leading to an increase in the rate of radiative decay, while the nonradiative branch of the decay provides an additional damping effect. In the present experiment, it is observed that gold nanospikes are efficient quenchers of molecular fluorescence than the nanospheres. It is noted that the gold nanospheres/nanospikes are, themselves, nonfluorescent. When the fluoroprobes are allowed to interact with the nanospheres/nanospikes, a part of the dye molecules are adsorbed on its surface while the rest remain free in solution and thus, the only fluorescing components are the free alizarin red molecules in the solution. The K_{SV} is related to the photoluminescence efficiency via the relationship of the Stern–Volmer equation[25] accounting both static and dynamic

$$\frac{I_o}{I} = 1 + K_{SV}[\text{quencher}] \tag{1}$$

where $K_{SV} = K_S + K_D$. Here, K_S and K_D are the static and dynamic quenching constants, respectively. Panel d shows the profiles of I_0/I versus gold concentration for a fixed concentration of alizarin red (33 μM) for both the morphology of the nanostructures and corresponding K_{SV} values which are determined as 0.7263×10^5 and 3.4297×10^5 M^{-1} for gold (collisional) quenching as

nanospheres ($R^2 = 0.9918$) and nanospikes ($R^2 = 0.9940$), respectively. It is noted that the K_{SV} for gold nanospikes is, surprisingly, about 5-fold higher than the nanospheres, provided that all the other relevant parameters like size of the particles and the structure of the stabilizing ligand shell remain almost invariant.

Metallic nanostructures are known to drastically modify the spontaneous emission of molecular probes placed in their vicinity. The main critical parameters that modify the spontaneous rate of emission of organic fluoroprobes near metallic nanostructures are the location of the fluoroprobes around the particle, its separation from the metal surface, and the molecular dipole orientation with respect to the particle surface.[15] Depending on its relative position and orientation with respect to the nanostructures, the emission of vicinal fluorophores could be drastically changed in several ways: by enhancing the optical intensity incident on the molecule through near field enhancement, by modifying the radiative decay rate of the molecule, and by increasing the coupling efficiency of the fluorescence emission to the far field through nanoparticle scattering. All these processes can be controlled by molecule nanoparticle separation, nanoparticle size, and geometry. The excitation of a localized resonance, by photon absorption, packs the photon energy in a small spatial region and thus increases the local electromagnetic field. A molecule positioned in such a region is polarized by an electric field E, which is enhanced with respect to the incident laser field. The enhancement of the quantity E.E, which is of importance in most spectroscopic measurements, can be as much as 10000, which results in a dramatic increase of the desired spectroscopic signal.[17] In the vicinity of a metal, the fluorescence rate of molecules becomes a function of the distance between the molecule and the metal surface. When a fluorescent probe is placed at an appropriate distance from metallic nanoparticles, there is an effective enhancement of the fluorescence by

transferring the free electrons of the fluorophore to the strong surface plasmon polariton field of the metallic particle. However, the fluorescence of molecules in direct contact with the metal is completely quenched. When fluoroprobe AR molecules are allowed to interact with the nanospheres/nanospikes, since the surface of the nanostructures are positively charged but not robust, the –OH functionality of AR molecules are attached onto the nanostructured surfaces through "place exchange reaction".[26] Moreover, the gold atoms on the surface possess unoccupied orbitals for nucleophiles to donate electrons. Therefore, the AR molecules containing –OH functionality as the strong electron donors displace CTAB molecules from gold nanostructure surfaces without any alteration in the morphology of the particles.[27]

Now, we have tried to elucidate the mechanism of quenching of molecular fluorescence upon interaction with the gold nanostructures. Both electron and energy transfer processes contribute to the major deactivation pathways for excited fluoroprobes on the metal surface as has been elucidated in Figure 4. Panel A shows the absorption spectral changes of gold nanospikes upon successive addition of alizarin red. Inset shows the corresponding changes of the gold nanospheres upon addition of the dye molecules. When alizarin red molecules are added to the gold nanospikes, the broad longitudinal plasmon band of gold nanospikes gradually dampens with increase in concentration of alizarin red while an enhancement of the transverse plasmon band with concomitant blue shift is seen. A closer observation shows that the absorption intensity of alizarin red molecules increases the intensity transverse plasmon band due to sum of the surface plasmon band of gold nanostructures and absorption band of the dye molecules. This effect is observed at the transverse plasmon band region

with increasing concentration of alizarin red at a particular concentration of gold nanostructures; similar change in the plasmonic features of gold nanospheres is seen upon addition of the dye molecules. These results imply electron transfer from the dye to the gold nanostructures and points out that the tips of the nanospikes have different electronic environments than the spherical region.[27] Panel B shows the overlap between the absorption spectrum of gold nanospheres/nanospikes and the emission spectrum of alizarin red molecules ensuring efficient energy transfer. Fluoroprobes placed in the vicinity of gold nanostructures can transfer energy to the nanospheres/nanospikes once it gets excited. The energy transfer is believed to be through the dipole–dipole near-field interaction, where the fluorophores act as dipolar donors and the plasmonic gold nanostructures act as dipolar acceptors. The probability of this Förster resonance energy transfer is proportional to the spectral overlap between the absorption of the metallic nanostructures and the fluorescence emission of the probe molecules. The overlap integral between the donor emission and acceptor absorption could be written as[28]

$$J(\lambda) = \int_0^\infty F_D(\lambda)\varepsilon_A(\lambda)\lambda^4 d\lambda = \frac{\int_0^\infty F_D(\lambda)\varepsilon_A(\lambda)\lambda^4 d\lambda}{\int_0^\infty F_D(\lambda)d\lambda} \quad (2)$$

where $F_D(\lambda)$ is the corrected fluorescence intensity of the donor in the wavelength range λ to $\lambda + \Delta\lambda$, with the total intensity (area under the curve) normalized to unity, $\varepsilon_A(\lambda)$ the extinction coefficient of the acceptor at λ, which is typically in units of $M^{-1}\,cm^{-1}$ and $F_D(\lambda)$ is dimensionless. If $\varepsilon_A(\lambda)$ is

$J(\lambda)$ is in units of $M^{-1}\,cm^{-1}\,nm^4$. In calculating $J(\lambda)$, we could use the corrected emission spectrum with its area normalized to unity or normalize the calculated value of $J(\lambda)$ by the area; in this experiment, we have calculated the overlap integral by correcting the emission spectrum with its area normalized to unity. The calculated overlap integral of donor, alizarin red to acceptor, gold nanospheres and nanospikes have the value of 5.9223×10^{14} and $1.1335 \times 10^{15}\,M^{-1}\,cm^{-1}\,nm^4$, respectively. It is noted that the overlap integral of the gold nanospikes is about 2-fold higher than the nanospheres; therefore, it is apparent that on the viewpoint of energy transfer nanospikes are doubly efficient quenchers of molecular fluorescence than the nanospheres.[29]

Based on the electron transfer mechanism, this apparent difference in the fluorescence quenching efficiency could be anticipated to the enhanced surface area that would allow the excess accommodation of alizarin red molecules on the gold nanospikes. The calculation of total number of particles and hence, the total surface area for a particular gold concentration could provide certain attributes to explain the difference in the fluorescence quenching efficiency due to the presence of anisotropy in the nanostructures. The number concentration (number of particles per milliliter of the solution, N) of gold particles can be calculated by taking the ratio of total volume of the atoms to the effective volume of each particle taken in average. The approximate numbers of nanospheres and nanospikes per milliliter of the solution have been calculated using the formula

$$N = \frac{N_0 C}{1000 f}\left(\frac{r}{R}\right)^3 \quad (3)$$

where N_0 is the Avogadro's number, C is the concentration of the gold precursor, f is the packing fraction of the atoms in the nanostructures, r is the radius of gold atoms, and R is the average radii of the particles. Assuming the packing fraction as 0.74 for fcc gold[30] and a precursor concentration of 1.0 mM, the number concentration of the nanospheres and nanospikes are, approximately, 8.85×10^{10} and $4.91 \times 10^{10}\,mL^{-1}$, respectively. The corresponding surface area per nanostructure is, approximately, 9852.03 and 21855.88 nm^2, respectively, and the total available surface area is 8.71×10^{14} and $10.73 \times 10^{14}\,nm^2\,mL^{-1}$, respectively. Thus, the total available surface area is about $1.2\times$ higher for nanospikes compared to nanospheres. It is, therefore, apparent that the quenching efficiency does not scale linearly with the surface area of the nanostructures; some other factors beyond the surface area are complementary for the fluorescence quenching of the probe molecules in the presence of the anisotropic nanospikes compared to spherically symmetrical gold nanostructures.[16] Thus, it could be conceived that the excess surface energy at the tips of the nanospikes may be responsible for the additional quenching of the molecular probes near the anisotropic nanostructures. To substantiate the additional role of the tips of the nanospikes in fluorescence quenching of the molecular probes, we have observed morphological and spectral changes of the gold nanospikes as a function of heat treatments (Figure 5). In this experiment, expressed in units of $M^{-1}\,cm^{-1}$ and λ is in nanometers, then

gold nanospikes were excited with 785 nm laser that coincides with and, therefore, excites the longitudinal plasmon absorption and photoinduced shape transformation has been monitored in real time by UV–vis-NIR spectroscopy. It can be assumed that the gold nanospikes are uniformly heated since irradiation at 785 nm leads to the collective excitation of all the conduction
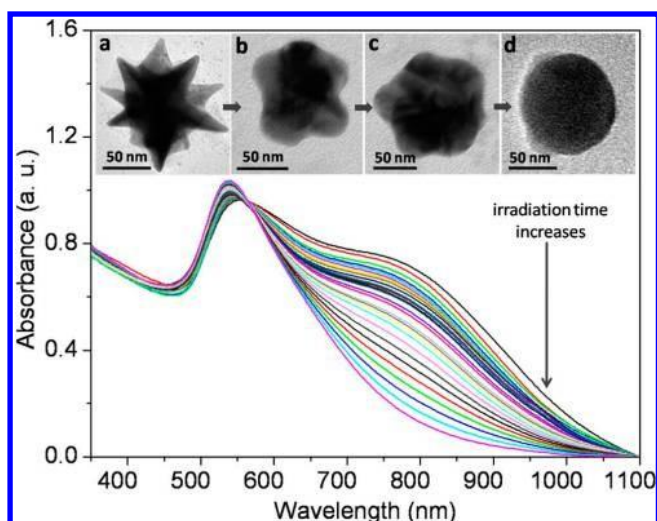
14330

Figure 5. Temporal changes in the absorption spectral features of gold nanospikes upon NIR laser irradiation. Inset shows the transmission electron micrographs during the photoirradiation of gold nanospikes to nanospheres (panels a–d) at different stages of irradiation.

electrons due to the longitudinal surface plasmon resonance. Before irradiation, the spectrum shows two well-resolved bands centered at about 550 and 770 nm, respectively. Upon increase in irradiation time, it is seen that, while the longitudinal plasmon band showed a substantial decrease in its absorbance and a pronounced blue shift, the intensity of the transverse plasmon band consequently increases. A single absorption band at 550 nm was recorded after 24 h of reaction, and no more changes to the spectrum were further seen. The subsequent changes of the nanostructures can be easily visualized by a gradual change in the solution color from deep blue to purplish blue to pink to red with the progress of the irradiation. These spectral changes indicate that the spikes are melting down and this process is continued up to complete the conversion to spheroidal nanostructures.[31] This has resemblance with the work of Lee and Kwak where using discrete dipole approximation (DDA), it has been shown that with decreasing the tip height, the asymmetric LSPR peak converges to that for perfect spheres.[32] It is also noted that the transverse mode of the plasmon absorption of gold nanospikes is less intense than the surface plasmon absorption of spherical gold nanoparticles, and therefore, during the photoconversion, the intensity of the transverse plasmon band of the nanospikes slowly becomes engulfed by the overwhelming intensity of the quasi-spherical to spherical nanostructures.[33] Real-time monitoring of the photoconversion process suggests a strong dependence of the particle spectral response on the specific corner features[34] of the colloidal nanostructures, as shown in the inset. These images have been selected from a group of images to present the most significant changes in the particle shapes. Initially, it is seen that the nanospikes possess numerous well-defined longer and sharper tips relatively uniformly on the gold surface (panel a). Upon irradiation, the branches taper off at the ends and form relatively short and obtuse branches (panel b). Further irradiation shows that the branched corners are more rounded resulting minuscule edge length that could be considered as part of the surface roughness and not as branches (panel c). Finally, spherical nanoparticles are evolved, indicating that gold nanospikes and completely transformed into spheres after exposure to the laser pulses (panel d) as has been observed

during the laser-induced shape transformation of cubic and tetrahedral platinum nanocrystals.[35] The tips of the particles were disappearing because the local atoms have higher energy, and ultimately, the nanospikes undergo a shape transformation to the thermodynamically more stable spherical shape.[36,37] These results suggest that the restructuring of the spikes starts from the top of the tips, indicating high surface energy at the apex of the nanospikes.[38]

In order to precisely obtain the influence of these intricate gold nanostructures, the emission behavior of alizarin red ($\lambda_{ex} \sim$ 503 nm) has been studied in the presence of different gold nanostructures evolved at different times of irradiation, as shown in Figure 6. It is seen that the emission of alizarin red
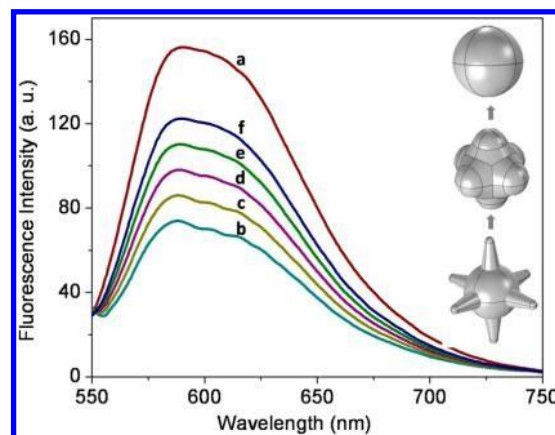

Figure 6. Emission spectra of alizarin red (33 μM) in the (a) absence and (b–f) presence of different morphology of gold nanostructures evolved during the photoconversion of gold nanospikes to nanospheres. Inset shows a schematic presentation of the three-dimensional geometrical modeling of the illustration of the particle shapes evolved during laser irradiation.

showed a distinctly different profile in the presence of gold nanostructures evolved during the morphological transformation of nanospikes to nanospheres. Interestingly enough, it is observed that the quenching efficiency is maximum in the case of gold nanospikes, gradually decreases with decrease in length of the tips and minimum for the ultimate spherical particles. It is seen that the immediate vicinity of the tips of the spikes exhibit regions of high surface energy that is attributable to the lack of symmetry at the interface or to the confinement of electrons that does not scale linearly with size;[39] as a result, with a decrease in the sharpness of the tips, the quenching efficiency decreases. Therefore, it could be authenticated that the excess surface energy near the tips of the spikes plays an important role in adsorption and quenching the fluorescence of molecular probes.

In this context, we have attempted to derive the excess surface energy onto the tip of a nanospike followed by exact determination of the excess surface area. We have employed basic Euclidean geometry to calculate the surface area of nanostructures, highlighting on the solid cone formed by the protruded extension of the spike.[40] A two-dimensional geometrical model (panel A) and the corresponding three-dimensionally rendered structure of a protruded arm (panel B) are shown in Figure 7. Based on the two-dimensional geometrical model (panel A) the nanospike could be assumed to be consisting of a ellipsoidal tip-head (surface area A_e) designed from the real-time TEM image of the tip, and the
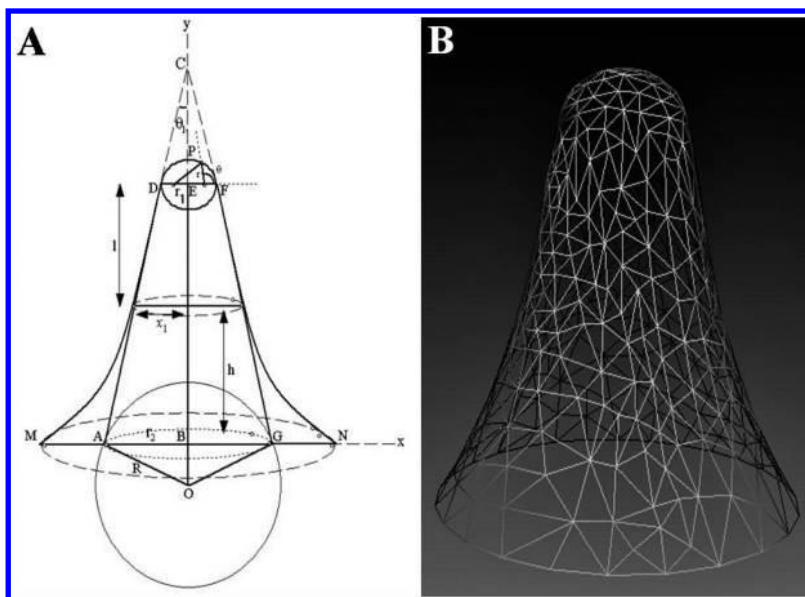
Figure 7. Exponential growth of the protruded arm: (A) two-dimensional geometrical model and (B) corresponding three-dimensionally rendered structure.

prolonged conical arm (surface area A_{cone}) protruded out from a basal spheroidal core (A_{core}), which creates a polynomial surface on protrusion base (surface area A_p). A detailed calculation of the surface area of a nanospike (consisting of a single tip protruded from the spherical core) has been shown in the Appendix. Therefore, the overall surface area could be expressed as

$$dA = dA_p + dA_e + dA_{cone} + dA_{core} \quad (4)$$

For a given particle, the parameters could be measured accurately from a TEM image, and thereby, the surface area could be calculated accordingly. Exploring the geometrical modeling through computational analysis and further modifying the vertices corresponding to the protrusion with Bezier polynomial surface in Meshlab, a three-dimensional model of a protruded arm has been generated (panel B) that replicates the exact geometry and, thereby, could be exploited to determine the surface area of such complex geometrical nanostructures.

Now, excess surface energy at the tips depends on the sharpness of the tip which depends on the ellipticity (e) of the projected segment of the ellipsoidal tip. Hasley[41] derived the corrected form for BET isotherm, depending on the radius of curvature of the surface as

$$\Gamma = \left(\frac{r}{r+1} \right)^{1/r} \quad (5)$$

Menger and Rizvi[42] have shown that, for a rough surface, the change in surface tension depends on the radius of curvature of the surface as

$$\gamma - \gamma_0 = \Gamma_{max} RT \left[\ln\left(1 - \frac{\Gamma}{\Gamma_{max}}\right) - \frac{k}{2}\left(\frac{\Gamma}{\Gamma_{max}}\right)^2 \right] \quad (6)$$

where, $(\gamma - \gamma_0)$ is the difference in surface tension between the

$$\frac{1}{\Gamma_{max}}\frac{d\gamma}{dr} = RT\left[\frac{2r}{r^2+1} + kr\right] \quad (7)$$

Thus, surface energy per unit area of surface coverage at the tip could be defined as

$$\frac{E_{surface}}{\Gamma_{max}} = \frac{1}{\Gamma_{max}} A_e \int d\gamma \quad (8)$$

Now, in this equation, substituting the value from eq 7, the surface energy on tip (E_{tip}) could be expressed as

$$E_{tip} = A_e(\theta, e) \cdot \gamma(r) \quad (9)$$

where $\gamma(r) = RT[\ln(r^2 + 1) + ((kr^2)/2)]$. It is noteworthy that surface energy on the tip could be expressed as the product of two separable functions, of which the first part shows the angular dependence and the later part shows the radial dependence. A profile showing the radial dependence (r) of surface energy (E) and solvent interaction energy parameter (k) is shown in Figure 8. The plot shows exponential increase of surface energy on the increase of the radius of curvature of the ellipsoidal tip, which is dependent on the semimajor and semiminor axis of the ellipse. Equation 9 shows the relationship between surface energy of the tip associated with the radius of curvature (r) of the tip. The surface energy parameter, $\gamma(r)$, consists of quadratic function of the r of the ellipsoidal head, which involves surface tension as a function of eccentricity itself. At the apex, where $r = a/b^2$, it arrives to the maximum. Applying Taylor series expansion for the logarithmic expansion at $x=1$, we get, $\gamma(r) = (a/b^2) + (1 + k)(a^2/b^4)$, which is the maximum value of surface energy at the tip. In the energy expression in eq 9, the surface energy parameter shows linear dependence on co-operativity term, k. In a straightforward manner, it depends on the interfacial tension between the dispersed particles and the solvent medium; specifically, k flat and bent surfaces, the intermolecular interaction coefficient, k,

is negative for cohesive energy.

Considering the polar form of the elliptical tip invoking appropriate boundary conditions, we get

becomes more negative when cohesive energy increases. Hydrophobic effect of the stabilizing ligand shell onto the nanoparticle surface also play a significant role in determining k as has been explained by Menger and Rizvi.[42] With the decrease in nanoparticles/solvent interfacial tension, surface coverage
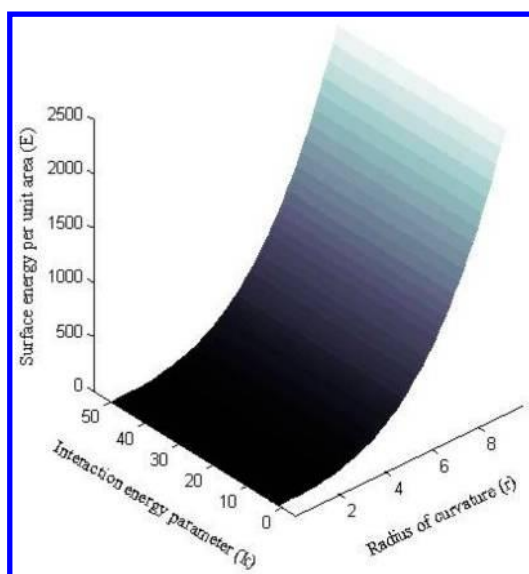
Figure 8. Plot showing relationship between surface energy (E), solvent interaction energy parameter (k), and radius of curvature of the tip (r).

also increases with a more compact placement of the stabilizing ligands, owing to a steep rise in tensiometric curve, as predicted from Gibbs isotherm, leading to more negative values of the k term. Thus, it is dependent on the nature of metal, stabilizing ligand shell and the solvent medium in which the particles are dispersed.

The real-time modeling of tip of a nanospike can be achieved by taking the intersection of a plane with a solid cone.

Depending on the symmetry of the tip, two plausible ways of modeling the nanospike are depicted by pictorial representation as shown in Figure 9. While panel A shows a solid cone with parallel planar intersection, which results in a circular disk, panel B shows an elliptical intersecting disk due to the nonparallel planar intersection with the solid cone. As a compromise, panel C shows the evolution of a conic section, which satisfies all through the points of intersecting planes and passes through the tip point. The spherical womb inside the solid cone is pruned to form a hemispherical tip, which is the most symmetric form of the system and, thus, interpret the deviation from the ideal in each cases. The apex of the conic is slightly tilted from the apex of the parent cone and could, satisfactorily, be employed to devise the three-dimensional structure of the tip of a nanospike by invoking suitable boundary circumference of the conic section.

To employ the aforementioned technique in finding out the surface energy on the tip of a nanospike, two parallel planes were intersect which are perpendicular to apex of the tip (plane MPNQ, red) and basal plane (plane APCQ, blue) owing to form a straight line, PQ. Figure 10 shows the theoretical three-dimensional model (panel A), corresponding anatomy of its two-dimensional projection (panel B) obtained from the TEM image and three-dimensional meshgrid (panel C) of the rendered model of tip. Transmission electron micrograph of a singular tip was scaled with ImageJ software package; it was found that the average length of tip varied from 37 to 47 nm. Then, the tip head of the protruded arm was modeled using the derived theoretical calculations. The major and minor axis of the elliptical fit was found to be about 10 and 15.4 nm, respectively. Based on these measurements, we have employed theoretical perspectives to produce the three-dimensional
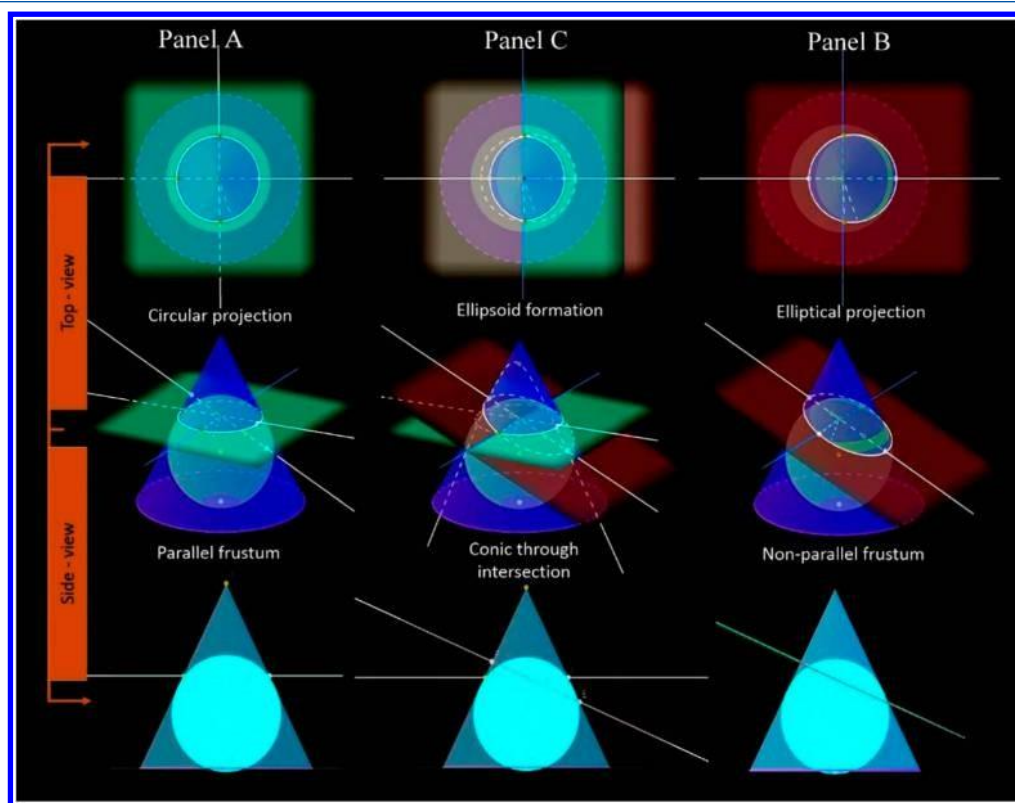

Figure 9. Modeling of the tip of a spike on the basis of intersection with a plane: (panel A) symmetric and (panel B) asymmetrical inclination of the cone; (panel C) the evolution of the conic section describing a general shape of the nonspherical cap.
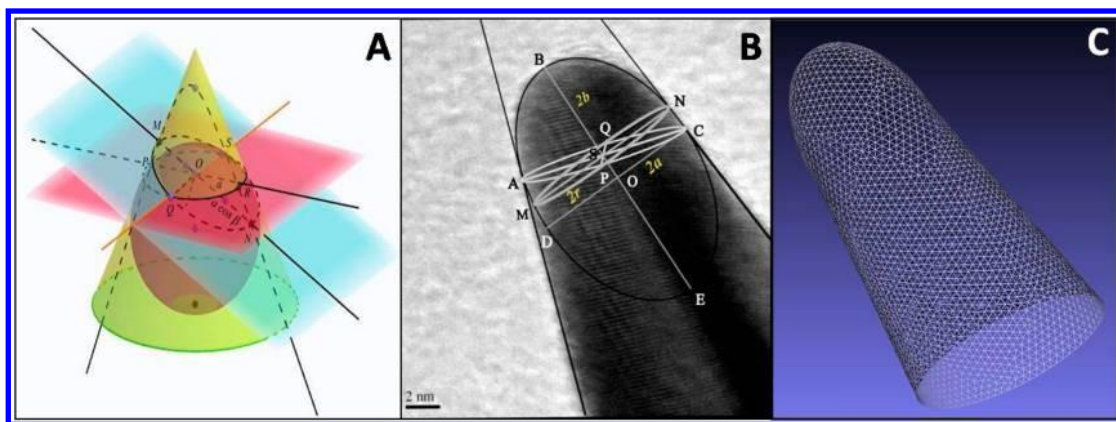
Figure 10. Three-dimensional modeling of the tip of a spike: (A) theoretical model, (B) transmission electron micrograph, and (C) three-dimensional meshgrid of the rendered model of tip.
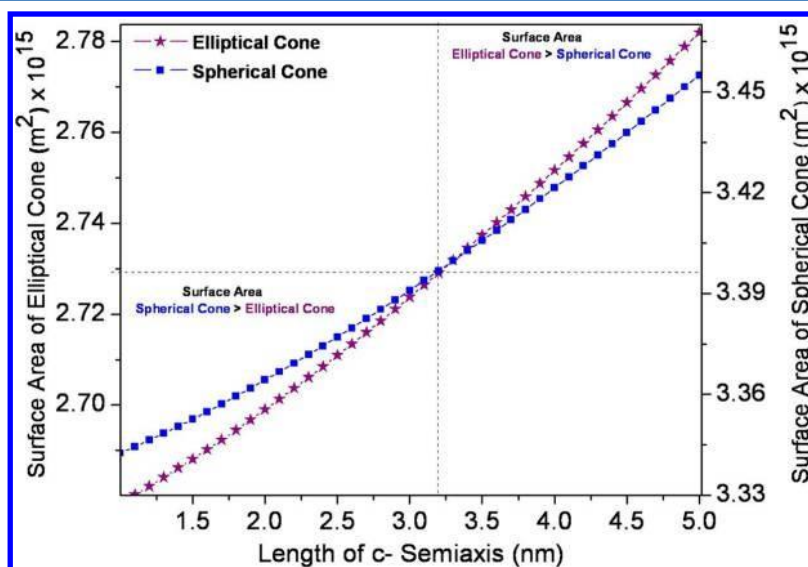

Figure 11. Change in surface energy of a tip ellipsoid as a function of perpendicular semiaxis.

protrusion with FreeCAD and Meshlab software packages. A detailed description of meshgrid of the rendered model of tip is described in Supporting Information, ESI 2. It is seen that the evolved structure has almost equivalent mesh triangulation over the whole surface and the corresponding surface area of about 20700 nm^2, which has ~5% relative error from the value obtained experimentally. The excess surface area with increase in protrusion of the tip has been modeled with respect to the increase in semimajor axis (c) for the tip ellipsoids with elliptical and round cone as shown in Figure 11. From the TEM image, the overall spread of the radius of resultant nanospheres varies in the range between 22.5 to 32.5 nm, having a maximum at 25 nm. We, therefore, calculated the mean difference in surface energy for the overall spread from the modeled nanospike and plotted the function with the increasing particle radius, as shown in Figure 12. Both of the attainable geometries considered in Figure 11 show two feasible ways of atomic aggregation in the nanostructures and pass through a common point of equal surface area when the c semiaxis is ~3.25 nm long. Afterward, the surface area of elliptical cones becomes wider than for conical shaped tips, which provide a measurable account for tip shape with respect to the height of tip head. With the increase in the length, the tip becomes narrower with circular base, which minimizes the extra surface energy that has
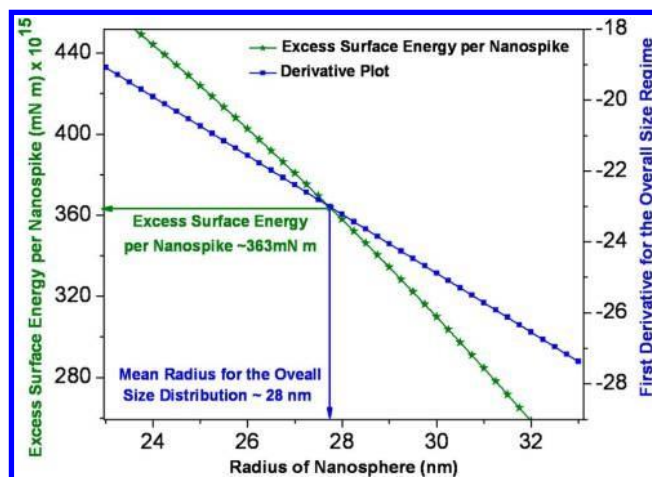

Figure 12. Change in excess surface energy of the nanospikes as a function of radius of the evolved nanospheres.

taken into consideration in the modeling of the nanospike. Assuming the surface tension at the gold−water interface as ~33 mN m^{-1},[43] the surface energy per nanostructure of the nanosphere and nanospike is 3.25 ✖ 10^{-13} and 6.83 ✖ 10^{-13}

mN m, respectively. Thus, the excess surface energy is about 2.1✖ per nanostructure, and as the overall surface are is 1.2-fold higher for nanospike campared to nanospheres, the excess surface energy is 2.5-fold higher for the nanospikes than the nanospheres. Therefore, the 5-fold quenching efficiency of the molecular probes near the nanospikes is contributed 2.5- and 2.0-fold from the electron and energy transfer mechanism, respectively. The theoretical modeling of the nanospikes could act as supplementary to the experimental observation and validates the applicability of the model proposed based on basic Euclidean geometry to calculate the excess surface energy of the anisotropic nanostructures.

4. CONCLUSIONS

In conclusion, this investigation demonstrates that fluorescence quenching of molecular probes near the anisotropic nanostructures does not scale linearly with the surface area; excess surface energy in specific region of the nonspherical particles play a deterministic role in governing the photophysical properties of the molecular probes. This observation has been rationalized by melting experiments while the branched nanostructures have essentially transformed into spherical nanoparticles since sharp tips interact more intensely with NIR laser excitation and probe their role in the modification of the emission characteristics of the dye molecules. The modeling of the tips of the nanospikes based on basic Euclidean geometry and good agreement with the experimentally observed results validates the applicability of the proposed model to calculate the excess surface energy arising from the intriguing anisotropicity of the materials at the nanoscale dimension. The calculation of excess surface energy of the nanospikes, as modeled nanostructures could, thus, be envisioned as potentially seeding to a new paradigm in high throughput investigation of the anisotropic nanostructures.

APPENDIX

Calculation of Surface Area of the Nanospike
Figure A1 shows the hollow bottom protrusion on a spherical core and simplified 2D projection of a protruded cone onto a spherical core. Panel a shows the simplified model, which consists of a spherical core having radius R with a tangential protrusion in a planar projection. For a more simplified view to this problem, let us assume that, for any given blunt cone, the cross-sectional radius of the cone (r_1) is constant, which implies
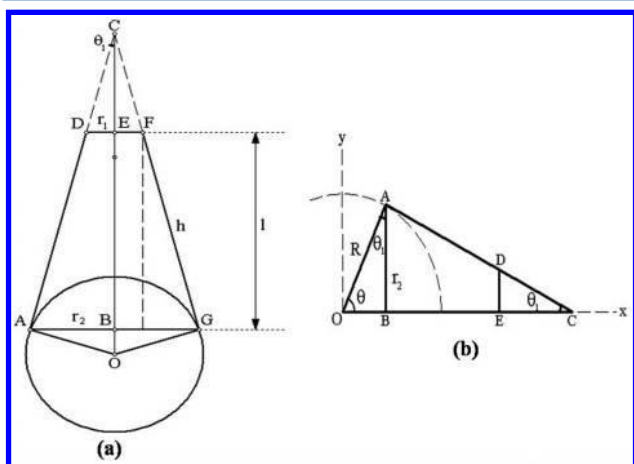
that the points G and H will be fixed, and with the change in angle, θ_1, the top point C moves along the y-axis. In this regard, it is worth mentioning that the maximum limit of angle θ_1 is 45°, which is one of the boundary conditions applied throughout the calculation.

Considering panel b,

$$r_2^2 = R^2 \cos^2 \theta_1 \tag{A1}$$

Now, for the surface area of the spherical core, we have, $dA_{core} = R^2 \sin^2 \theta d\theta d\phi$. Therefore, for spikes having the unchanged spherical core radius, in terms of θ_1, the relationship becomes

$$-dA_{core} = 2\pi r_2^2 d\theta_1 \tag{A2}$$

This equation, thus, depicts the decrease of the surface area of core sphere for each of the cone placed onto the surface of the sphere. The surface area of a hollow bottom cone can be given by $A_{cone} = ((2\pi r_1 l)/(\cos \theta_1))$. Thus, change in surface area of the cone depends on both the half open angle, θ_1 and the difference between top and bottom radii, Δr as

$$dA_{cone} = 2\pi \left(\frac{\Delta r}{\sin \theta_1} dr + \frac{r_1 \Delta r}{\cos \theta_1} d\theta_1 \right) \tag{A3}$$

Therefore, the change in surface area can be estimated if we consider a spherical cross-section of radius r_2 with respect to the tip radius r_1 and inclination angle. But, in practice, a smooth protruded base is found in real spikes when the open angle, θ_1, is narrower than tangential arrangement. The 2-D model of the protruded arm in panel A is based on the consideration that the continuous growth of the arms up to height h as a exponential function to the y-axis as $-x = \exp(sy)$, where s is the steepness factor and could be obtained by taking a tangent at the mid-point of the arc.

The arc length, C, is given by

$$C \quad \frac{(y - z) - (\tan^{-1} y - \tan^{-1} z)}{s} \tag{A4}$$

where $y = (s^2 \exp(2sh) + 1)^{1/2}$ and $z = (s^2 + 1)$. If the top radius of the fulcrum is x_1, the surface area is given by

$$dA_p = x_1 C d\varphi \tag{A5}$$

Again, the surface area of the blunt edge (A_e) at the protrusion end could be modeled by hemi-spheroidal surface cap having a semi-major axis, a, and semi-minor axis, b. The hemi-spheroidal surface can be of two types, namely, prolate and oblate, and the corresponding surface area can be given by

$$A_{prolate} = 2\pi \left(b + a \times \frac{\arcsin}{e} \right)$$

$$A_{oblate} = 2\pi b \left(b + a \times \frac{\sinh^{-1} e}{e} \right) \tag{A6}$$

where $e = 1 - (b^2/a^2)$.

Figure A1. (a) Hollow bottom protrusion on a spherical core and (b)

simplified 2D projection of a protruded cone onto a spherical core.

Therefore, by this anatomical modeling, we have simplified the complex geometry of a nanospike by a combination of basic geometrical counterparts. The present protocol could be applied to imitate any asymmetric nanostructure by fragmentation to the geometrical analogues which inherit the local symmetry among the overall structural asymmetry.

Nanorods. *ACS Nano* 2009, *3*, 744–752.

■ ASSOCIATED CONTENT

⹋ Supporting Information

Experimental details and meshgrid calculations. The Supporting Information is available free of charge on the ACS Publications website at DOI: 10.1021/acs.jpcc.5b03944.

■ AUTHOR INFORMATION

Corresponding Author

*E-mail: sujit.kumar.ghosh@aus.ac.in.

Notes

The authors declare no competing financial interest.

■ ACKNOWLEDGMENTS

■ REFERENCES

(1) Quyang, G.; Wang, C. X.; Yang, G. W. Surface Energy of Nanostructural Materials with Negative Curvature and Related Size Effects. *Chem. Rev.* 2009, *109*, 4221–4247.

(2) Maier, S. A. *Plasmonics: Fundamentals and Applications*; Springer-Verlag: New York, 2007.

(3) Burda, C.; Chen, X. B.; Narayanan, R.; El-Sayed, M. A. Chemistry and Properties of Nanocrystals of Different Shapes. *Chem. Rev.* 2005, *105*, 1025–1102.

(4) Grzelczak, M.; Pérez-Juste, J.; Mulvaney, P.; Liz-Marzán L. M. Shape Control in Gold Nanoparticle Synthesis. *Chem. Soc. Rev.* 2008, *37*, 1783–1791.

(5) Stewart, M. E.; Anderton, C. R.; Thompson, L. B.; Maria, J.; Gray, S. K.; Rogers, J. A.; Nuzzo, R. G. Nanostructured Plasmonic Sensors. *Chem. Rev.* 2008, *108*, 494–521.

(6) Ghosh, S. K.; Pal, T. Interparticle Coupling Effect on the Surface Plasmon Resonance of Gold Nanoparticles: From Theory to Applications. *Chem. Rev.* 2007, *107*, 4797–4862.

(7) Alvarez, M. M.; Khoury, J. T.; Schaaff, T. G.; Shafigullin, M. N.; Vezmar, I.; Whetten, R. L. Optical Absorption Spectra of Nanocrystal Gold Molecules. *J. Phys. Chem. B* 1997, *101*, 3706–3712.

(8) Jin, R.; Cao, Y. C.; Hao, E.; Métraux, G. S.; Schatz, G. C.; Mirkin, C. A. Controlling Anisotropic Nanoparticle Growth Through Plasmon Excitation. *Nature* 2003, *425*, 487–490.

(9) Alvarez-Puebla, R.; Liz-Marzán L. M.; F. de Abajo, J. G. Light Concentration at the Nanometer Scale. *J. Phys. Chem. Lett.* 2010, *1*, 2428–2434.

(10) Hao, E.; Bailey, R. C.; Schatz, G. C.; Hupp, J. T.; Li, S. Synthesis and Optical Properties of "Branched" Gold Nanocrystals. *Nano Lett.* 2004, *4*, 327–330.

(11) Hao, F.; Nehl, C. L.; Hafner, J. H.; Nordlander, P. Plasmon Resonances of a Gold Nanostar. *Nano Lett.* 2007, *7*, 729–732.

(12) Ozbay, E. Plasmonics: Merging Photonics and Electronics at Nanoscale Dimensions. *Science* 2006, *311*, 189–193.

(13) Giannini, V.; Fernández-Domínguez, A. I.; Heck, S. C.; Maier, S. A. Plasmonic Nanoantennas: Fundamentals and Their Use in Controlling the Radiative Properties of Nanoemitters. *Chem. Rev.* 2011, *111*, 3888–3912.

(14) Thomas, K. G.; Kamat, P. V. Chromophore-Functionalized Gold Nanoparticles. *Acc. Chem. Res.* 2003, *36*, 888–898.

(15) Dulkeith, E.; Morteani, A. C.; Niedereichholz, T.; Klar, T. A.; Feldmann, J.; Levi, S. A.; van Veggel, F. C. J. M.; Reinhoudt, D. N.; Möller, M.; Gittins, D. I. Fluorescence Quenching of Dye Molecules near Gold Nanoparticles: Radiative and Nonradiative Effects. *Phys. Rev. Lett.* 2002, *89* (2030021), 1–4.

(16) Ghosh, S. K.; Pal, T. Photophysical Aspects of Molecular Probes Near Nanostructured Gold Surfaces. *Phys. Chem. Chem. Phys.* 2009, *11*, 3831–3844.

(17) Bardhan, R.; Grady, N. K.; Cole, J. R.; Joshi, A.; Halas, N. J. Fluorescence Enhancement by Au Nanostructures: Nanoshells and

(18) Gurkov, T. D.; Kralchevsky, P. A. Surface Tension and Surface Energy of Curved Interfaces and Membranes. *Colloids Surf.* 1990, *41*, 45–68.

(19) Jana, N. R.; Gearheart, L.; Murphy, C. J. Seed-Mediated Growth Approach for Shape-Controlled Synthesis of Spheroidal and Rod-like Gold Nanoparticles Using a Surfactant Template. *Adv. Mater.* 2001, *13*, 1389–1393.

(20) Sau, T. K.; Rogach, A. L.; Döblinger, M.; Feldmann, J. One-Step High-Yield Aqueous Synthesis of Size-Tunable Multispiked Gold Nanoparticles. *Small* 2011, *7*, 2188–2194.

(21) Claro, A.; Melo, M. J.; Schäfer, S.; de Melo, J. S. S.; Pina, F.; van den Berg, K. J.; Burnstock, A. The Use of Microspectrofluorimetry for the Characterization of Lake Pigments. *Talanta* 2008, *74*, 922–929.

(22) Miliani, C.; Romani, A.; Favaro, G. J. Acidichromic Effects in 1,2-Di- and 1,2,4-Tri-hydroxyanthraquinones. A Spectrophotometric and Fluorimetric Study. *Phys. Org. Chem.* 2000, *13*, 141–150.

(23) Prodan, E.; Radloff, C.; Halas, N. J.; Nordlander, P. A Hybridization Model for the Plasmon Response of Complex Nanostructures. *Science* 2003, *302*, 419–422.

(24) Weitz, D. A.; Garoff, S.; Gersten, J. I.; Nitzan, A. Roughened Silver Electrodes for Use in Metal-Enhanced Fluorescence. *J. Chem. Phys.* 1983, *78*, 5324–5338.

(25) Otto, S.; Volmer, M. Uber die Abklingzeit der Fluoreszenz. *Phys. Z.* 1919, *20*, 183–188.

(26) Nikoobakht, B.; El-Sayed, M. A. Evidence for Bilayer Assembly of Cationic Surfactants on the Surface of Gold Nanorods. *Langmuir* 2001, *17*, 6368–6374.

(27) Makarova, O. V.; Ostafin, A. E.; Miyoshi, H., Jr.; Norris, J. R.; Miesel, D. Adsorption and Encapsulation of Fluorescent Probes in Nanoparticles. *J. Phys. Chem. B* 1999, *103*, 9080–9084.

(28) Förster, T. Zwischenmolekulare Energiewanderung und Fluoreszenz. *Ann. Phys.* 1948, *437*, 55–75.

(29) Fan, C.; Wang, S.; Hong, J. W.; Bazan, G. C.; Plaxco, K. W.; Heeger, A. Beyond Superquenching: Hyper-efficient Energy Transfer from Conjugated Polymers to Gold Nanoparticles. *Proc. Natl. Acad. Sci. U.S.A.* 2003, *100*, 6297–6301.

(30) Smart, L. E.; Moore, E. A. In *Solid State Chemistry: An Introduction*, 3rd ed.; Taylor & Francis, CRC Press: Boca Raton, FL.

(31) Smith, B. A.; Zhang, J. Z.; Giebel, U.; Schmid, G. Direct Probe of Size-dependent Electronic Relaxation in Single-sized Au and Nearly Monodisperse Pt Colloidal Nanoparticles. *Chem. Phys. Lett.* 1997, *270*, 139–144.

(32) Lee, T. K.; Kwak, S. K. Effects of LSPR of Gold Nanospheres by Surface Vacancies and Protruding Tips. *J. Phys. Chem. C* 2014, *118*, 5881–5888.

(33) Mafuné, F.; Kohno, J. Y.; Takeda, Y.; Kondow, T.; Schwabe, H. Structure and Stability of Silver Nanoparticles in Aqueous Solution Produced by Laser Ablation. *J. Phys. Chem. B* 2000, *104*, 8333–8337.

(34) Wang, Z. L. Transmission Electron Microscopy of Shape-Controlled Nanocrystals and Their Assemblies. *J. Phys. Chem. B* 2000, *104*, 1153–1175.

(35) Wang, Z. L.; Petroski, J. M.; Green, T. C.; El-Sayed, M. A. Shape Transformation and Surface Melting of Cubic and Tetrahedral Platinum Nanocrystals. *J. Phys. Chem. B* 1998, *102*, 6145–6151.

(36) Link, S.; Wang, Z. L.; El-Sayed, M. A. How Does a Gold Nanorod Melt? *J. Phys. Chem. B* 2000, *104*, 7867–7870.

(37) Wang, Z. L.; Gao, R. P.; Nikoobakht, B.; El-Sayed, M. A. Surface Reconstruction of the Unstable (110) Surface in Gold Nanorods. *J. Phys. Chem. B* 2000, *104*, 5417–5420.

(38) Link, S.; El-Sayed, M. A. Optical Properties and Ultrafast Dynamics of Metallic Nanocrystals. *Annu. Rev. Phys. Chem.* 2003, *54*, 331–366.

(39) Chen, H. M.; Liu, R.-S. Architecture of Metallic Nanostructures: Synthesis Strategy and Specific Applications. *J. Phys. Chem. C* 2011, *115*, 3513–3527.

(40) Weisstein, E. W. Euclid's Postulates. In *CRC Concise Encyclopedia of Mathematics*, 2nd ed.; CRC Press: Boca Raton, FL, 2003; p 942.

(41) Halsey, G. Physical Adsorption on Non-Uniform Surfaces. *J. Chem. Phys.* 1948, *16*, 931–937.

(42) Menger, F. M.; Rizvi, S. A. A. Relationship between Surface Tension and Surface Coverage. *Langmuir* 2011, *27*, 13975–13977.

(43) Nicole, G.; Adams, D. J.; Böker, A.; Krausch, G. Janus Particles at the Liquid–Liquid Interface. *Langmuir* 2006, *16*, 2539–2547.

CrossMark

Fluorescence spectroscopy in probing spontaneous and induced aggregation amongst size-selective gold nanoclusters

Dewan S. Rahman, Sujit Kumar Ghosh [⇑]

Department of Chemistry, Assam University, Silchar 788011, India

a b s t r a c t

Gold nanoparticles have been synthesized by borohydride reduction using poly(N-vinyl 2-pyrrolidone) as the stabilizing agent in aqueous medium in the size regime of 1–5 nm. Aggregation amongst these polymer-stabilized gold nanoparticles has been accomplished by the controlled addition of hydrazine or aggregation may occur spontaneously (devoid of any chemicals) that is ubiquitous to nanoparticulate systems. Now, fluorescencein isothiocyanate (FITC), a prototype molecular probe has been employed in understanding the physical principles of aggregation phenomenon of the size-selective gold nanoparticles undergoing spontaneous and induced-aggregation under stipulated conditions. It is seen that there is enhancement of fluorescence intensity of FITC in the presence of both spontaneously and induced-aggregated gold nanoclusters as compared to free FITC. Interestingly, it is observed that the fluorescence sensitivity is able to distinguish seven different sizes of the gold nanoparticles in the aggregates and maximum enhancement of intensity arises at higher concentration with increase in size of gold particles within the aggregates. With increase in concentration of gold nanoparticle aggregates, the intensity increases, initially, reaches a maximum at a threshold concentration and then, gradually decreases in the presence of both spontaneously and induced-aggregated gold particles. However, the salient feature of physical significance is that the maximum enhancement of intensity with time has remained almost same for induced-aggregated gold while decreases exponentially with spontaneously aggregated gold particles.

© 2014 Elsevier B.V. All rights reserved.

1. Introduction

In recent years, the unique physical and chemical properties of the surfaces of solids have attracted increased attention in scientific parlance [1]. As the size of the particles shrinks into the nanometer regime, there is an increasingly important role of the surface in controlling the overall energy of the particles [2]. Metallic particles at the nanoscale dimension possess high surface-to-volume ratio and therefore, are very prone to rapid and irreversible coalescence. On the other hand, controlled aggregation is of great relevance in colloidal science because of their various technological applications. As a consequence, the aggregation processes in colloids have been the subject of numerous experimental, theoretical and computational studies [3–5].

Metallic particles, *viz.*, copper, silver and gold, in the nanometer size regime exhibit strong absorption in the visible region, often coined as localized surface plasmon resonances (LSPRs) [6]. The physical origin of the light absorption by metal nanoparticles is due to coherent oscillations of the conduction electrons driven by electromagnetic radiation and are dependent upon the metal and host dielectric functions, particle geometry along with light polarization and wavelength [7,8]. The plasmon resonances of the metal nanoparticles aggregated in a close-packed assembly (especially, when the interparticle distance are less than five times of the particle radius, $d \leqslant 5R$) are known to be coupled as a result of electrodynamic interaction between the particles [9]. However, the combination of conjugated organic chromophores and metal nanoparticles has emerged to produce a new class of organic–inorganic hybrid assemblies [10–12] which entice scientists and engineers for numerous potential applications, e.g., in optical emitters [13], nanoscale optical antennas [14], plasmonic integrated circuits [15], surface plasmon enhanced light emitting diodes [16] and so on.[17]. Metallic nanostructures modify the intrinsic photophysical characteristics of fluorophores in a controllable manner governed by nanoparticle morphology, distance between the molecules and nanoparticles and geometry/orientation of the molecules around the nanoparticle surface [18]. While the molecular probes are allowed to interact with plasmon coupled nanoparticle assemblies, it has been found that the majority of the enhancement takes

⇑ Corresponding author. Tel.: +91 348 270848; fax: +91 348 270802.
E-mail address: sujitkchem@gmail.com (S.K. Ghosh).

place at the junction of aggregated particles bringing to light the importance of interparticle interaction [19]. The dependence of the coupled LSPR frequency on the interparticle distance could be used as a "plasmonic ruler" to measure nanometric distances in biological systems [20]. The use of fluorophore-metal interactions in biotechnology has primarily been referred to as metal-enhanced fluorescence or surface-enhanced fluorescence or radiative decay engineering and can be used to develop next-generation biological and chemical sensors [21].

The study of dipolar coupling of radiative molecules to the surface plasmon of metallic surfaces dates back to the beginning of the 20th century with the theoretical work of Zenneck and Sommerfeld among others [22,23]. A great deal of theoretical and experimental studies has been performed over the last few decades in understanding the behavior of probe molecules in which the molecular dipole is damped by the nearby metal surface [18–25]. Therefore, it has become quite obvious to study the influence of the variation of particle size, shape, interparticle coupling and local dielectric environment of the nanoparticles for fluorophores deposited nearby metal nanoparticles under carefully optimized conditions. Geddes and co-workers [26] have reported the first observation of metal-enhanced fluorescence by measuring fluorescence emission of fluorescein isothiocyanate-conjugated human serum albumin on 40 and 200 nm gold colloids deposited onto glass substrates in a homogeneous fashion. It has been found that the fluorescence enhancement is higher with 200 nm gold colloids as compared to 40 nm colloids due to the increased contribution of the scattering portion of the 200 nm gold colloid extinction spectrum. Li and group [27] have shown unusual fluorescence enhancement of a particular carbazolyldiacetylene derivative upon binding onto gold nanoparticles that could be attributed to the effect of restricted intramolecular rotation resulting from nanoparticle aggregation in the organic–inorganic hybrid assemblies. Lv et al. [28] have designed three gold nanoparticle composites protected by perylene bisimide derivatives and it has been seen that the composites render substantial fluorescence enhancement due to the restricted intramolecular rotation/torsion in the packed nanoclusters. The structural effect of the ligands on aggregation-enhanced emission has been studied and temperature-dependent experiments were conducted to demonstrate the mechanism of fluorescence enhancement. Moerner and colleagues [29] observed enhancement of a single molecule's fluorescence up to a factor of 1340 using gold nanobowties. Electromagnetic simulation reveled that this is a result of greatly enhanced absorption and an increased radiative emission rate, leading to enhancement of intrinsic quantum efficiency. Chen et al. [30] have investigated the correlation of the fluorescence intensity of dyes with the localized surface plasmon resonance of the individual DNA-functionalized silver nanoprisms using dark field scattering and fluorescence microscopy. It has been seen that the dye functionalized silver nanoprisms are highly fluorescent and their fluorescence intensity is a sensitive function of the degree of the spectral overlap between nanoparticle LSPR and the absorption and emission spectra of the dye. Mennucci and group [31] have presented a hybrid quantum mechanical/classical mechanical description to study the role of the solvent and plasmon coupling in the metal enhanced fluorescence in a regular array. The self-consistent field character of the model has allowed to show that the number and the location of the 'hot spots' responsible for fluorescence enhancement are strictly related to the solvent-induced effects of both on the optical properties of the fluorophore and plasmon couplings among the nanoparticles in the array.

In this article, we have employed fluorescein isothiocyanate as local probe in elucidating physicochemical aspects of spontaneously and induced-aggregates of gold nanoparticles of seven different sizes. Gold nanoparticles have been chosen for this experiment

as the particles display the most consistent aggregated behavior in the nanostructures. A series of polymer-stabilized spherical gold nanoparticles of variable sizes (<5 nm) have been synthesized by the borohydride reduction method. Aggregation amongst these ultrasmall gold nanoparticles has been accomplished either by controlled addition of hydrazine or aging the colloidal dispersion leading to irreversible coalescence. While the FITC molecules were used as molecular probes, the proximity of the dye to gold nanoparticle aggregates results in an increase in intensity of the fluorophores and markedly varies with the size of the gold nanoparticles in the aggregates. Analysis of the salient features reveals that surface plasmon field is different in case of spontaneous and induced-aggregated gold nanoparticles of different sizes. The effect of different concentration of gold nanoparticle aggregates and time of interaction between the dye molecules and nanoparticle aggregates has been studied explicitly.

2. Experimental

Reagents and instruments

All the reagents used were of analytical reagent grade. Gold chloride trihydrate ($HAuCl_4.3H_2O$) (Aldrich, >99%), poly(N-vinyl-2-pyrrolidone) (PVP K30 40 kDa) (Wako Pure Chemicals, >99%), sodium borohydride (Aldrich, 99.5%) and hydrazine hydrate (Qualigens' Fine Chemicals, India >98%) were used as received. Fluorescein isothiocyanate (Aldrich) was used as molecular probe without any further purification. Double distilled water was used throughout the course of the investigation.

The absorption spectrum of each solution was recorded in a Shimadzu UV 1601 digital spectrophotometer (Shimadzu, Japan) taking the sample in 1 cm well-stoppered quartz cuvette. Fluorescence spectra were recorded with a Shimadzu RF-5301 spectrofluorimeter (Shimadzu, Japan) equipped with a 9.9 W xenon flash lamp and a photomultiplier tube with S-20 spectral response. The spectrofluorimeter was linked to a personal computer and utilized the RF-5301PC software package for data collection and processing. All the samples of FITC and Au-FITC were excited at 490 nm and slit width 5/5 nm were used to record the spectra. Transmission electron microscopic (TEM) measurements were performed on carbon-coated copper grids with a Zeiss CEM 902 operated at 80 kV. The samples were prepared by mounting a drop of the solution on a carbon-coated copper grid and allowing the grids to dry in air.

Synthesis and characterization of PVP-stabilized gold nanoparticles of variable sizes

Monodisperse gold clusters of variable sizes ranging from 1 to 5 nm have been synthesized by following the method reported by Tsukuda and co-workers [32]. In a typical procedure, an aqueous solution of $HAuCl_4$ was mixed with PVP in different molar ratio (R) and reduced with sodium borohydride for the synthesis of different sets of gold nanoparticles. Firstly, an aqueous solution (20 mL) of requisite amount of PVP (5–100 mM) was stirred for 2 h. on an ice-bath maintained at 0 °C. Subsequently, an aliquot of $HAuCl_4.3H_2O$ (0.5 mM) solution was added and the mixture was stirred for 1 h. Then, ice-cold aqueous solution of $NaBH_4$ (0.1 M, 2 mL) was added instantaneously into the mixture under vigorous stirring. The color of the mixture immediately turned from pale yellow to bright brown indicating the formation of small gold nanoparticles. The stirring was continued for another half an hr. The particles are stable for a couple of days while stored in the freeze. The variation in synthetic conditions and sizes for different sets of gold particles are summarized in Table 1.

Table 1
Synthetic conditions and characteristic parameters of the different sets of gold particles.

Set	[HAuCl$_4$] (mM)	[PVP] (mM)	R = [PVP]/[HAuCl$_4$]	Color	Average diameter (nm)
A	0.5	100.0	200	brown	1.0 ± 0.3
B	0.5	75.0	150	brown	1.5 ± 0.3
C	0.5	50.0	100	brown	2.3 ± 0.4
D	0.5	37.5	75	brown	2.9 ± 0.5
E	0.5	25.0	50	brown	3.5 ± 0.6
F	0.5	12.5	25	brown	4.1 ± 0.6
G	0.5	5.0	10	brown	4.9 ± 0.8

For gold nanoparticle synthesis, the total volume of the solution was 25 mL.

Synthesis of gold-probe assembly

In a typical set, requisite amount of spontaneous/induced-aggregated gold (1.0 lM) was added to an aqueous solution of FITC (40 nM) and the final volume of the solution was maintained to 3 mL in well-stoppered quartz cuvettes and the fluorescence of each solution was measured in the spectrofluorimeter.

3. Results and discussion

Photophysical properties of FITC

Fluorescein isothiocyanate ($pK_a \sim$ 6.7) belongs to hydroxyxanthene dyes and is known for their strong absorption (k$_{abs}$ 494 nm; extinction co-efficient >70,000 M^{-1} cm^{-1}) and emission (k$_{em}$ 519 nm; u$_f$ 0.95) in the visible region [33]. It is widely used as a fluorescent tracer in many applications, such as, in microscopy, in a type of dye laser as the gain medium, in forensic and serology to detect latent blood stains and as a bio-tagger to elucidate the cellular transport processes [34]. The molecular structure of FITC is shown in Scheme 1.

Characterization of the gold particles

The as-synthesized PVP-stabilized gold particles have been characterized by UV–vis spectroscopy (Fig. 1). It is seen that the gold particles do not exhibit any prominent surface plasmon band in the visible region rather put a signature at *ca.* 520 nm indicating the formation of ultrasmall gold nanoparticles (<5 nm). It is now well-established in the literature that the surface plasmon band of gold nanoparticles arises only when the particles are larger than 5 nm [35]. The collective oscillation of the conduction electrons on the metal surface with electromagnetic radiation, so called surface plasmon has not been exhibited, due to extremely small sizes of the gold nanoparticles. Moreover, it is noted that absorbance of the surface plasmon band increases with increasing size of the gold nanoparticles.

Transmission electron micrographs of the as-synthesized gold nanoparticles shows that the particles are exclusively spherical with average diameter 1.0 ± 0.3, 1.5 ± 0.3, 2.3 ± 0.4, 2.9 ± 0.5, 3.5 ± 0.6, 4.1 ± 0.6, and 4.9 ± 0.8 nm, respectively. Fig. 2 shows the
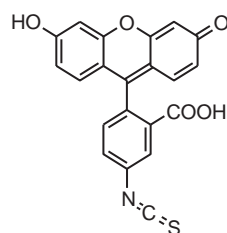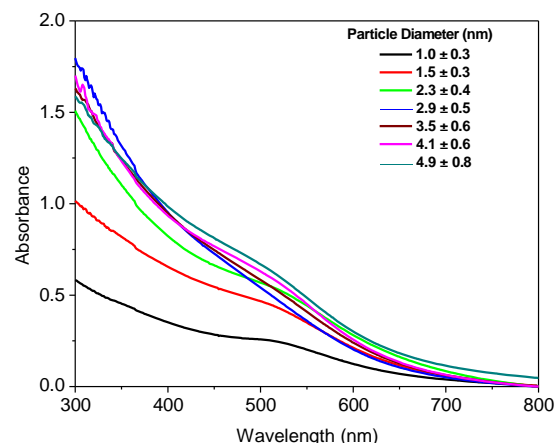

Fig. 1. UV–vis spectra of the as-synthesized colloidal gold of different sizes.

TEM images of the gold clusters showing the formation of monodisperse particles in the specified size regime.

Aggregation amongst the ultrasmall gold nanoparticles

Now, two different methodologies were adopted in pursuing aggregation amongst the as-synthesized gold nanoparticles and the measurement of the UV–vis extinction spectra was performed to enlight the aggregation mechanism.

Spontaneous aggregation

The as-synthesized gold nanoparticles were allowed to aggregate by keeping the colloidal gold (0.5 mM) undisturbed at room temperature (298 ± 5 K) in a closed vial for about 45 h. Fig. 3A represents the evolution of surface plasmon band of the aggregates of gold nanoparticles (set A). It is observed that, although, the monodispersed gold nanoparticles do not exhibit any significant surface plasmon band, upon aging with time, a distinct and broad surface plasmon band evolves at around 520 nm. It is noticeable that there is no red shifting of the plasmon band which is, usually, observed upon aggregation of the large particles. This is, probably, due to the fact that aggregation of the ultrasmall gold particles forms nanoparticle cluster and collectively induce the surface plasmon oscillation that oscillate with a characteristic wavelength of light on coupling with the incident electromagnetic radiation field [36]. Polymer-stabilized gold nanoparticles experience Brownian encounters to cause aggregation of the nanoparticles upon aging [37]. Moreover, in the present experiment, the particle sizes are very small and as a result, the surface energy of the particles is very high. Therefore, due to Brownian encounters of the nanoparticle sols and high surface energy, PVP-stabilized small gold nanoparticles are prone to aggregation under ubiquitous condition. Therefore, a distinct SPR band appears at the wavelength around 520 nm and the absorbance increases with successive increase of
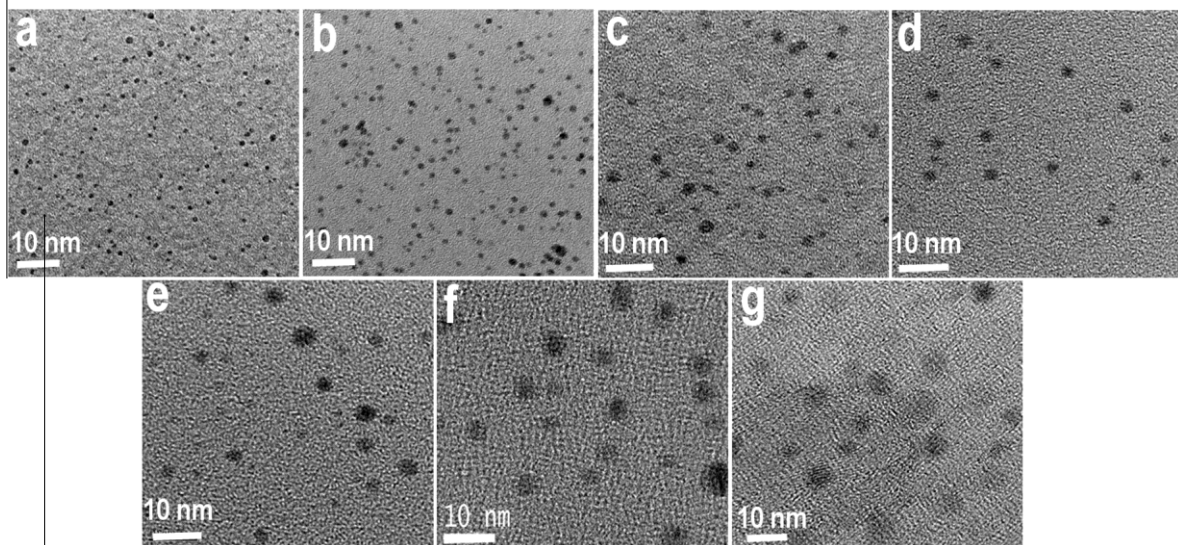

Scheme 1. Molecular structure of FITC.

Fig. 2. (a–g) TEM images of the PVP-stabilized gold nanoparticles corresponding to sets A–G, respectively.
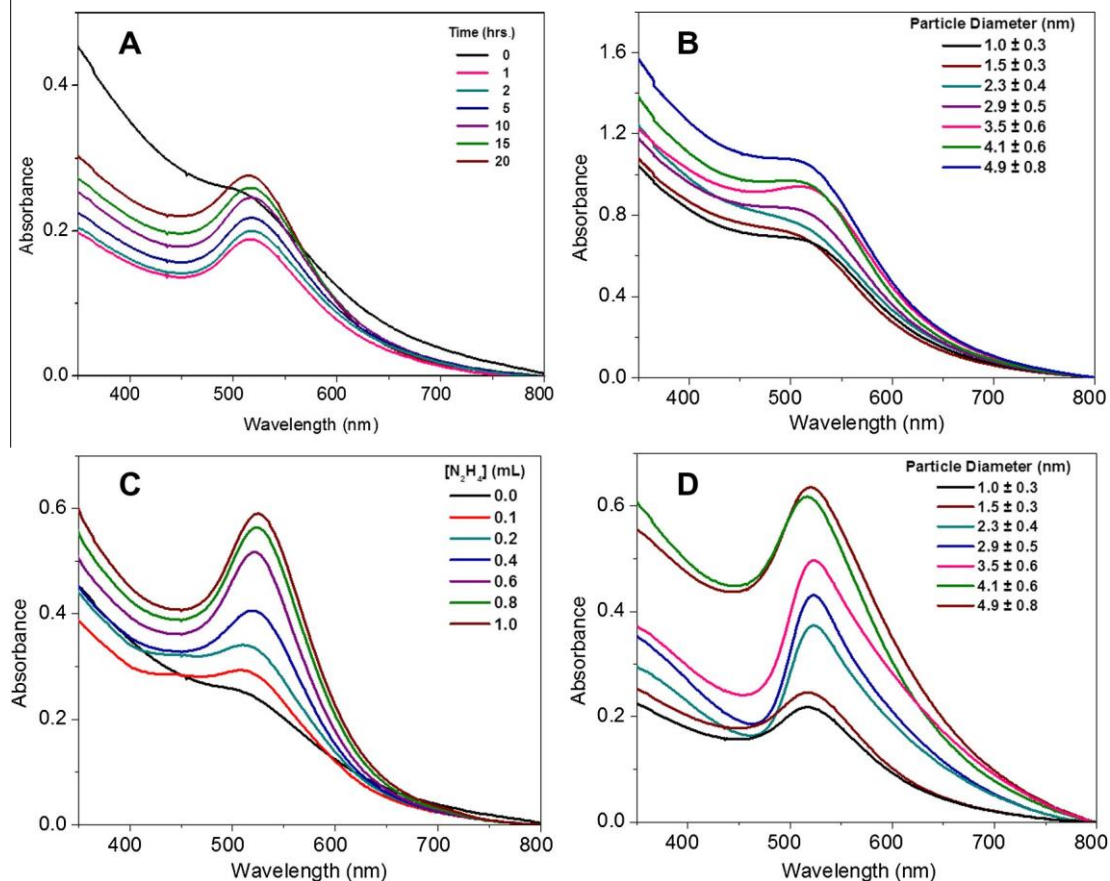

Fig. 3. (A) Evolution of surface plasmon band of gold nanoparticles (set A) upon spontaneous aggregation at different time intervals; and (B) UV−vis spectra of seven different sizes of gold nanoparticles upon spontaneous aggregation followed after 45 h. for each set of gold nanoparticles; (C) Evolution of surface plasmon band of gold nanoparticles (set A) upon induced aggregation at different concentrations of hydrazine; and (D) UV−vis spectra of seven different sizes of gold nanoparticles upon induced aggregation measured after addition of 1.0 mL of hydrazine in each set of gold nanoparticles.

the time of elapse for the gold nanoparticle assemblies. Fig. 3B shows the UV−vis spectra of seven different sizes of gold nanoparticles upon spontaneous aggregation followed after 45 h. of the synthesis of the particles (0.5 mM). It is seen that the absorbance gradually increases without significant red shift of the absorption maximum with increase in size of the individual gold particles in

the aggregate as has been predicted theoretically by Gedanken and co-workers [38].

(Hydrazine)-induced aggregation

The gold nanoparticles were also aggregated induced by hydrazine and the color changes slowly from bright brown to red and
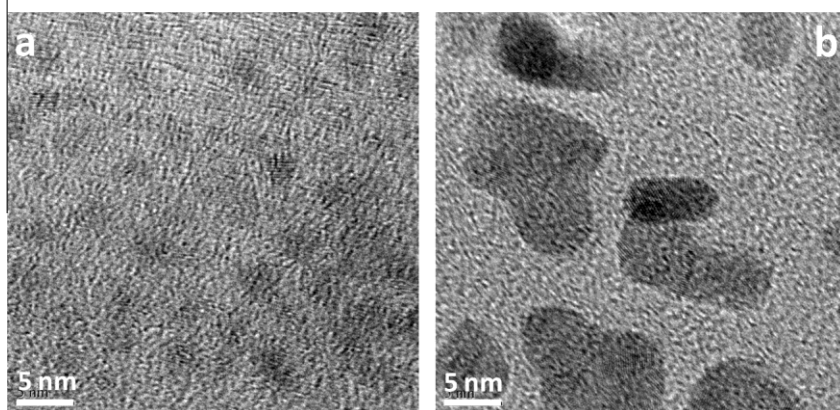
Fig. 4. TEM images of the gold nanoparticle (sets G) aggregates arising due to (a) spontaneous; and (b) induced aggregation.

subsequently to violet. Hydrazine was chosen for aggregation of the gold particles because of its structural simplicity and to avoid any complicacy for further fluorescence experiments. Fig. 3C presents the evolution of surface plasmon band due to aggregation of the gold nanoparticles (0.5 mM, set A) upon addition of different concentrations of hydrazine. It is observed that, although, the monodispersed gold nanoparticles do not exhibit any significant surface plasmon band, upon addition of hydrazine, a distinct and broad surface plasmon band evolves at around 520 nm [39]. It is also seen that SPR band is sharpened with concomitant increase in absorbance when the concentration of hydrazine gradually increases. Upon addition of hydrazine to PVP-stabilized gold nanoparticles, the particles are aggregated due to the screening of electrostatic repulsion (despite the presence of steric repulsion) between the particles and consequently, the absorption spectrum is modified. When the size of the gold nanoparticles decreases, the electronegativity of gold nanoparticles increases and as a result, smaller gold nanoparticles have higher affinity to accept electrons. On the other hand, hydrazine is a Lewis base and can donate lone pair of electrons to the gold nanoparticles. Since each hydrazine molecule has two nitrogen atoms, it can act as a bridge or linker between the two nanoparticles in linear fashion by donating lone pair electrons. We have also tried to induce aggregation of gold nanoparticles by adding other nitrogen containing Lewis bases, ammonia or pyridine, but there is no aggregation between the particles. This observation strongly supports that the hydrazine molecules act as a linker between gold nanoparticles in inducing aggregation and the extent of aggregation become stronger with increasing concentration of hydrazine to the gold nanoparticles. Fig. 3D shows the UV–vis spectra of seven different sizes of gold nanoparticle (0.5 mM) aggregates produced upon addition of 1.0 mL of hydrazine in each set of the particles. It is observed that the absorbance gradually increases without significant red shift of the absorption maximum with increase in size of the individual gold particles in the aggregates.

Comparative overview between spontaneous and induced- aggregation

Now, let us have a comparative overview between the spontaneous and induced-aggregated gold nanoparticles. In the spontaneous aggregation, the absorption spectrum is broad indicating the formation of aggregated structures with 'loose affiliation' of the particles [40]. In this aggregation process, the driving force of aggregation is the high surface energy of the ultrasmall particles. Therefore, it is very difficult to miniature the aggregated state and may be referred to as 'thermodynamically controlled aggregation' [41]. On the other hand, upon hydrazine-induced aggregation,

the spectrum appears at 520 nm and less broadened that arises in case of relatively larger sized nanoparticles, indicating the formation of 'compact association' of the ultrasmall particles [42]. In this aggregation process, control of aggregation could be achieved through addition of hydrazine, a Lewis base, which acts as a linker between the particles. Therefore, the driving force of aggregation is much higher than the spontaneous aggregation leading to compact packing of the nanoparticles and could be assumed as 'kinetically controlled aggregation'. The TEM images of the spontaneously and induced-aggregated gold nanoparticles (set G) are shown in Fig. 4.

Fluorescence spectra of FITC in the presence of spontaneous and induced-aggregated gold nanoparticles

Now, we have employed fluorescein isothiocyanate as a molecular probe to monitor the characteristic features of spontaneously and induced-aggregated gold nanoparticles. It has been seen that the fluorescence spectrum of FITC is not affected, appreciably, by the addition hydrazine in the experimental concentration range. The pH of the spontaneous and induced aggregated gold nanoparticles is, approximately, 7.5 and 10.0; but to measure the fluorescence emission, the pH was adjusted to ~8.0 for all sets including pure FITC. It was noted that, in acidic pH range, fluorescence intensity of FITC molecules is lower as compared to alkaline condition. Fluorescence intensity of FITC, in alkaline condition, almost remains invariant with respect to change of pH. Performing the experiments either in acidic (pH 3.0–6.5) or highly alkaline conditions (pH 10.0–13.0), the binding of FITC molecules on the gold nanoparticle surface decreases that gives rise to additional complexity to the sensitivity of the experiment. Therefore, the pH of the solution, was adjusted to ~8.0 and does not change, considerably, in the different sets of experiments for fluorescence measurements. Fluorescein isothiocyanate molecules have electron enriched isothiocyanate group (—N@C@S) and in particular, containing lone pair of electrons on larger sulfur atom. Therefore, the dye molecules can donate electrons via polarizable sulfur atoms onto the gold nanoparticles and eventually, a fraction of FITC molecules become attached onto the surface of the particles. At this pH, FITC exists in anionic form and the binding occurs through the sulfur atom of reactive isothiocyanate group onto the surface of gold particles [43].

Aggregates containing gold nanoparticles of different sizes

Fig. 5 shows the fluorescence spectra of FITC (40 nM) in the presence of spontaneously and induced-aggregated gold nanoparticles (1 μM) of variable sizes. In the present experiment, quite dilute solutions have been used so as to minimize the effects of
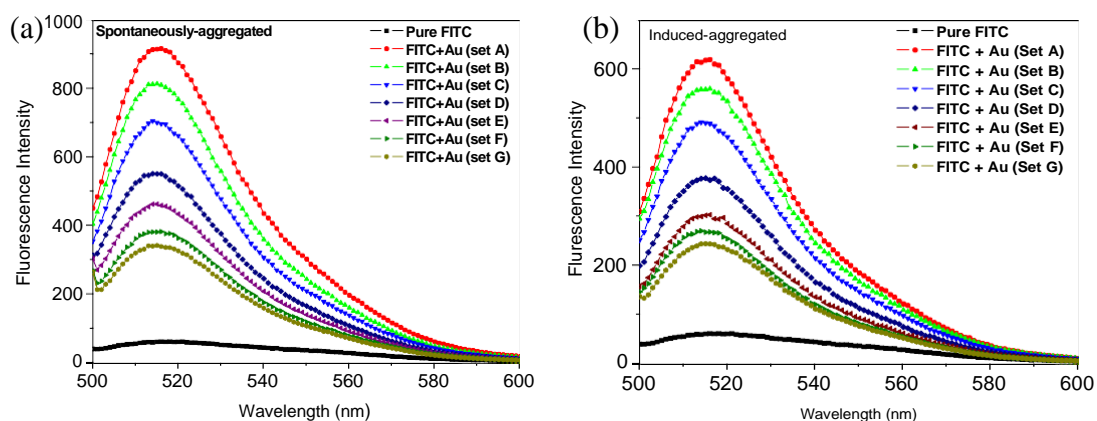
Fig. 5. Fluorescence spectra of FITC molecules in the presence of (a) spontaneously; and (b) induced-aggregated gold aggregates containing different particle sizes after 1 min of the preparation of solution.

the absorption of excitation light and re-absorption of molecular fluorescence light due to the presence of the gold nanoparticles as well as the near field effects on the absorption cross section (so-called "trivial effects"). It is seen that there is enhancement of fluorescence of FITC molecules in the presence of both spontaneous and induced-aggregated gold nanoparticles. It was observed that the aggregates, themselves, as well as the individual gold nanoparticles are non-fluorescent. However, when the individual gold nanoparticles, prior to aggregation, were added to the FITC solution, quenching of fluorescence was observed.

Metallic nanostructures modify the intrinsic photophysical characteristics of fluorophores when the probe molecules are placed near the metal surface. In the presence of isolated metal nanoparticles, fluorescence is quenched due to electron and energy transfer processes from the dye molecules to the nanoparticulate systems [44]. However, in the presence of electromagnetically coupled aggregated metal clusters, the radiative decay rates and the quantum yield of the fluorescent species may increase significantly [45]. According to the model proposed by Weitz et al. [24], the scattering intensity ratio for fluorescence of adsorbed molecules on the metal surface to that of the free ones is given by,

$$R_{fluo} = |A(x_L)|^2 \, |E_L|^2 \, \frac{C_o}{C_o + C_o^s} \tag{1}$$

where, E_L is local electric field at the molecule due to the incident beam. The amplification factor, $A(x_L)$ is increased local field intensity through the excitation of electronic plasmon resonances governed by the morphology and dielectric properties of the nanoparticles. The parameters, C_o denotes the radiative and non-radiative transition rate from excited state to the ground state for free molecules while C_o^s is taken to represent an average value of the surface-induced decay rate for molecules on the gold nanoparticles. The origin of the significant fluorescence enhancement near nanostructured metal can be understood by the consideration of two contributing factors. Firstly, by concentrating the incident light into local density of states, so-called electromagnetic 'hot spots' (i.e., their associated electric fields ($|E|/|E_o|$ where $E = E_o E_L$) are stronger and more localized in the gaps between the particles) [46], surface plasmon excitation of nanostructured metallic surfaces can lead to increase absorption of the surrounding fluorophores by the incident light [47]. Secondly, metal nanostructures alter the radiative and the non-radiative decay rates of the neighboring fluorophores by changing both the fluorescence lifetime and quantum yield of the emitter and hence, plasmonic nanostructures can be used as nanoantenna [48]. The resultant balance of these processes leads to enhancement of molecular fluorescence and the measured enhancement impact important spectroscopic consequences.
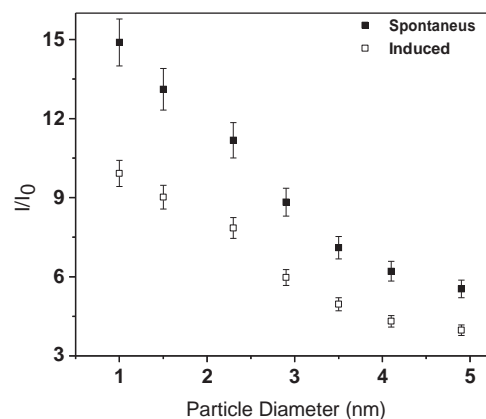

Fig. 6. Relative fluorescence enhancement of FITC molecules in the presence of (a) spontaneously; and (b) induced aggregated gold nanoparticles of different sizes after 1 min of the preparation of solution.

Fig. 6 shows the relative enhancement of fluorescence with increase in size of the gold nanoparticles in the aggregates. It is seen that the enhancement efficiency decreases with increase in size of the gold nanoparticles within the aggregates. However, the salient feature of physical significance is that the relative fluorescence is distinctly different in the two different size regime of the particles. The enhancement efficiency in the presence of different sizes of gold nanoparticles could be treated by considering the effect of nanoparticle size on the aggregates of the particles. It is plausible that with increase in size of the particles, the interstitial space increases and the number of neighboring clusters surrounding the electromagnetic 'hot spot' decreases [48]. Due to decrease in the number of clusters surrounding the electromagnetic 'hot spot', the electromagnetic field enhancement effect on the dye molecules decreases and the enhancement efficiency gradually decreases [49]. The different sizes of the particles in the aggregate produce characteristic patterns and shifts in LSPR resonances, which lead to different wavelength-dependent local field enhancement factors at the absorption and emission frequencies of the dye [50]. However, the dramatic change in the enhancement efficiency in the presence of very small sizes of the nanoparticles could be accounted by considering that is dependent on the core size and there is a transition at 2.3 nm due to the emergence of optical gap between the highest occupied and lowest unoccupied orbitals [51]. When ultrasmall gold particles (those do not possess any surface plasmon band) are coupled together, it is not expected to show significant changes upon aggregation and the clustered

aggregates can exhibit properties similar to the one observed for larger particles (diameter > 5 nm) [36]. The absorption arises from the surface plasmon oscillation modes of conduction electrons in the clustering of these small gold nanoparticles that collectively can induce the surface plasmon resonance. Upon aggregation, the individuality of the clusters is maintained by (arbitrarily) thin separating layers between the neighboring clusters and the clusters remain polarizable individuals even after aggregation [52]. The integrated total extinction due to all clusters hit by the light beam is given by the sum-over all aggregate spectra weighed by the size distribution. After the critical size of 2.3 nm, the individual particles within the aggregate can lead to quenching of fluorescence of the probe molecules vis-a-vis the aggregation leading to enhancement of fluorescence and in consequence, the enhancement is predominating over the quenching of fluorescence of the probe molecules.

Different concentration of the aggregates

Fig. 7 shows the fluorescence spectra of FITC (40 nM) in the presence of spontaneously and induced-aggregated gold nanoparticles (set A) of different concentrations. It is seen that there is enhancement of fluorescence of FITC molecules in the presence of both spontaneous and induced-aggregated gold nanoparticles.

The relative fluorescence intensity of FITC in the presence of different concentrations of spontaneous and induced-aggregated gold nanoparticles (set A) is shown in Fig. 8. It is also observed that, initially, the fluorescence intensity of FITC gradually increases with increase in concentration of aggregated gold nanoparticles; at a particular concentration, it reaches the optimal and then, becomes constant. It has also been noted that the maximum enhancement occurs towards the higher concentration with increase in size of the particles in the aggregate.

In the absence of nanoparticles, the fluorophores radiate into free space. The presence of nearby metallic surfaces or particles can alter the free-space condition. Under this situation, in the definition of fluorescence quantum yield, u_f, a further factor, k appears. According to Parker [53], fluoresence intensity (I) is proportional to the concentration of the fluorophore as given by,

$$I = I_o \epsilon c l u_f k \qquad (2)$$

where, I_o is the intensity of the exciting source beam, ϵ the molar absorption co-efficient of the fluorescent probe, c its concentration, l the path length of the sample, u_f its quantum yield and k a
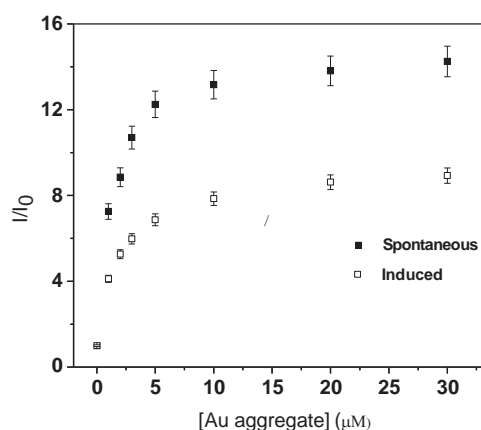

Fig. 8. Relative fluorescence enhancement of FITC molecules in the presence of (a) spontaneously and (b) induced aggregated gold nanoparticles with different concentration after 1 min of the preparation of solution.

geometrical factor that accounts for the geometry of the optical system. The quantities involved within k are the mutual polarization effect among all the components, *viz.*, fluorophore and nanoparticles, fluorophore and solvent, nanoparticles and solvents, and nanoparticles among themselves when the particles are electromagnetically coupled, yielding optical properties that are not the simple sum of those of the individual particles. The metal could be considered as a continuous dielectric characterized by the experimental optical constant [54]. It is well known that the plasmonic properties determining the final enhancement or quenching of the fluorescence depend not only on the characteristics of the nanoparticles (its nature, size, shape, interparticle distance and the local dielectric properties) but also on the position and orientation of the fluorophore with respect to the nanoparticulate systems [55,56]. Coupling of all these environmental and structural parameters does not necessarily present an additive character and the separation of the explicit contribution of each component is extremely difficult [57]. Such an interpretation is very delicate as the final net response of the probe molecules near the nanoparticle surface is determined by the coupling of all these components [58]. In the present experiment, it is seen that with increase in concentration of the gold nanoparticle aggregates, the enhancement efficiency is linear with increase in concentration of the gold
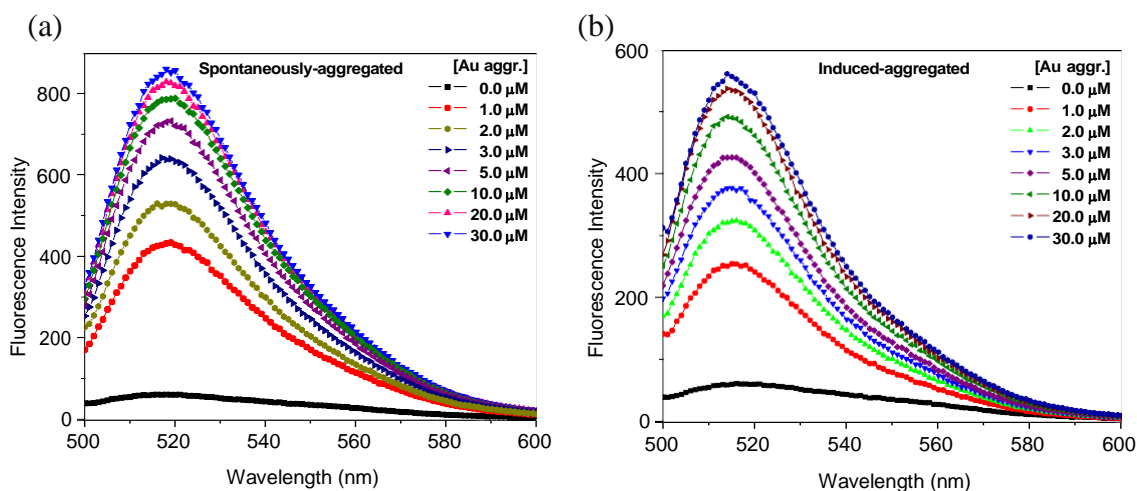

Fig. 7. Fluorescence spectra of FITC molecules in the presence of different concentrations of (a) spontaneously; and (b) induced aggregated gold aggregates containing gold nanoparticles (sets A) after 1 min of the preparation of solution.
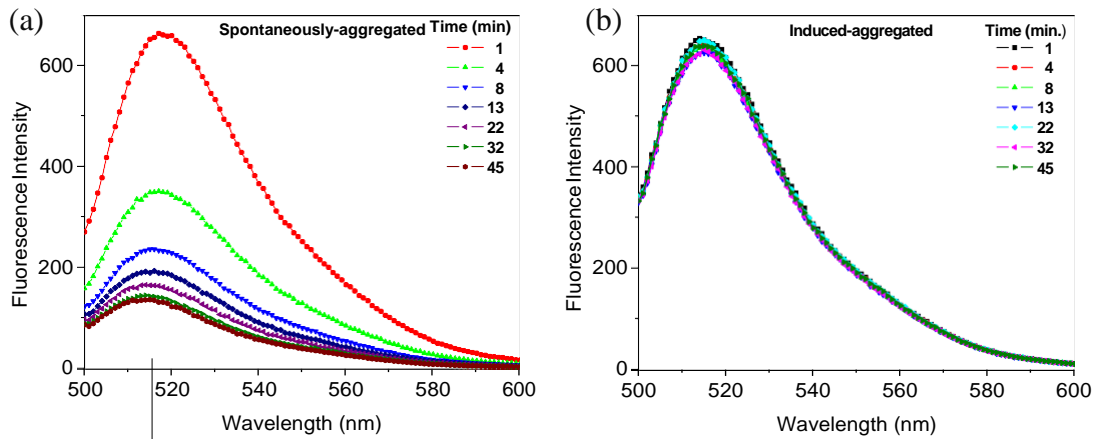
Fig. 9. Fluorescence spectra of FITC molecules in the presence of (a) spontaneously; and (b) induced aggregated gold aggregates containing gold nanoparticles (sets A) at different time intervals.
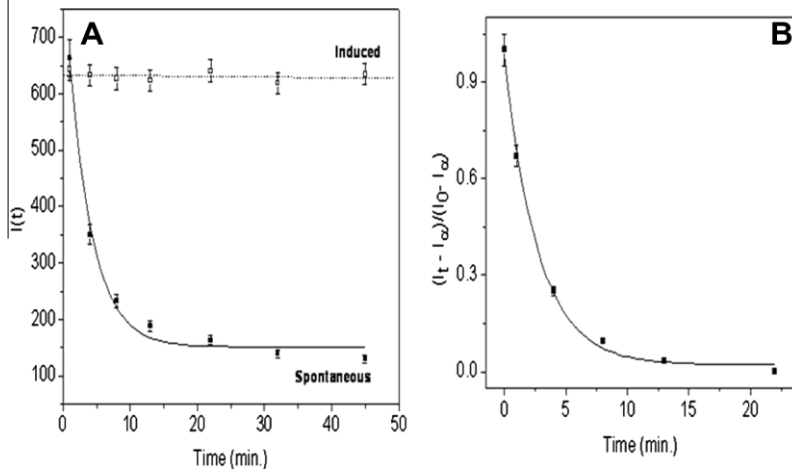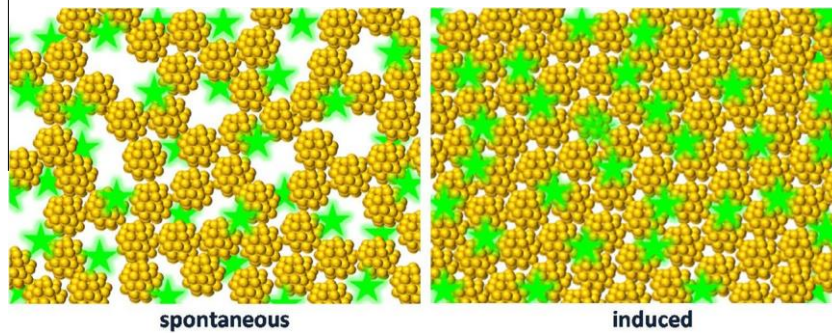

Fig. 10. (a) Fluorescence intensity of FITC molecules at different time intervals in the presence of (a) spontaneously; and (b) induced aggregated gold aggregates containing gold nanoparticles (sets A) and (b) first order analysis of the curve in the presence of spontaneously gold nanoparticles.

Scheme 2. Schematic presentation of the plausible binding modes of the dye molecules to the spontaneous and induced-aggregated gold nanoparticles.

nanoparticle aggregates. Therefore, it can be concluded that the aggregates are isotropic in nature for a particular size of the gold nanoparticles.

3.4.3. Different time of interaction

The fluorescence spectra of FITC molecules (40 nM) in presence of both spontaneous and induced-aggregated gold nanoparticles (1 μM) have been measured as a function of time of aging the

solution (Fig. 9). It is seen that there is a huge enhancement of fluorescence just after addition of the dye to the gold nanoparticle aggregates in case of spontaneous aggregation and then, successively decreases while there is hardly any change in case of induced aggregated gold nanoparticles. Interestingly, it has been observed that the measured fluorescence signal, decreases exponentially with time for spontaneously aggregated gold nanoparticles, while almost remains same for induced-aggregated gold

(set A) as shown in Fig. 10A. This is due to the fact that, during colloid aggregation, the evolution of mean aggregate size as a function of time bears an exponential growth as $P(t) \sim \exp(t/k)$, k is a time constant [59]. Fig. 10B shows that the interaction of the probe molecules with gold nanoparticle aggregates in solution could be fitted, reasonably, well by first order rate equation [60],

$$\frac{I_t - I_{\mathbf{1}}}{I_0 - I_{\mathbf{1}}} = e^{-k_a t} \qquad (3)$$

where, k_a is the association rate of the dye molecules to the nanoparticles, t the time, I_0 the fluorescence signal at time $t = 0$ and $I_{\mathbf{1}}$ the signal when fluorescence no longer changes with time. These phenomena could be accounted by assuming that the packing of the particles in spontaneously aggregated gold nanoparticles are not in ordered arrangement probably for weak interaction force (surface energy) which is the driving force for aggregation. Since the packing as well as particle arrangement are not in proper order, result less enhancement in local field intensity, i.e., the effectiveness of hot spots decreases, which results the less number of molecules in the excited state and therefore, intensity decreases but not less than the pure FITC molecules with time. However, in induced aggregated gold nanoparticles, the hydrazine molecules by kinetically controlled process renders the particles to be organized in proper arrangement. After addition of FITC molecules, the molecules are incorporated inside the electromagnetic 'hot spots' and there is no possibility to change the packing of the nanoparticle aggregates. So, the aggregated particles and therefore, fluorescence enhancement almost remain same for induced-aggregated gold nanoparticles with time. The plausible binding modes of the dye molecules to the spontaneous and induced-aggregated gold nanoparticles are shown in Scheme 2.

4. Conclusion

In conclusion, fluorescence spectroscopy has been employed in realizing the physicochemical insights of aggregation phenomenon of the size-selective gold nanoparticles undergoing spontaneous and induced-aggregation under stipulated conditions. It is seen that there is enhancement of fluorescence intensity of FITC in the presence of both spontaneous and induced-aggregated gold nanoclusters. It is observed that the fluorescence sensitivity is able to distinguish seven different sizes of the gold nanoparticle aggregates and maximum enhancement of intensity arises at higher concentration with increase in size of gold particles within the aggregates. However, the salient feature of physical significance is that the maximum enhancement of intensity with time has remained same for induced-aggregated gold while decreases exponentially with spontaneously aggregated gold particles. The enhancement of the molecular fluorescence increases the molecular detection efficiency by amplifying/tailoring the electromagnetic radiation field of the neighboring fluorophores near metal nanoparticles.

Acknowledgement

References

[1] Y. Harada, S. Masuda, H. Ozaki, Chem. Rev. 97 (1997) 1897.
[2] C.G. Granqvist, R.A. Buhrman, J. Wyns, A.J. Sievers, Phys. Rev. Lett. 37 (1976) 625.
[3] M. Lattuada, H. Wu, J. Sefcik, M. Morbidelli, J. Phys. Chem. B 110 (2006) 6574. and references therein.
[4] M.Z. von Smoluchowski, Phys. Chem. 92 (1917) 129.
[5] T. Jensen, L. Lelly, A. Lazarides, G.C. Schatz, J. Cluster Sci. 10 (1999) 295.
[6] J. Maria, S. Gray, J.A. Rogers, R.G. Nuzzo, Chem. Rev. 108 (2008) 494.
[7] S. Link, M.A. El-Sayed, J. Phys. Chem. B 103 (1999) 4212.
[8] P. Mulvaney, M. Giersig, A. Henglein, J. Phys. Chem. 97 (1993) 7061.
[9] S.K. Ghosh, T. Pal, Chem. Rev. 107 (2007) 4797.
[10] X. Liu, M. Zhu, S. Chen, M. Yuan, Y. Guo, Y. Song, H. Liu, Y. Li, Langmuir 24 (2008) 11967.
[11] H. Liu, J. Xu, Y. Li, Y. Li, Acc. Chem. Res. 43 (2010) 1496.
[12] H. Zheng, Y. Li, H. Liu, X. Yin, Y. Li, Chem. Soc. Rev. 40 (2011) 4506.
[13] S. Kühn, U. Hakanson, L. Rogobete, V. Sandoghdar, Phys. Rev. Lett. 97 (2006) 017402.
[14] P. Mühlschlegel, H.J. Eisler, O.J.F. Martin, B. Hecht, D.W. Pohl, Science 308 (2005) 1607.
[15] S.I. Bozhevolnyi, V.S. Volkov, E. Devaux, J.Y. Laluet, T.W. Ebbesen, Nature 440 (2006) 508.
[16] K. Okamoto, I. Niki, A. Shvartser, Y. Narukawa, T. Mukai, A. Scherer, Nature Mater. 3 (2004) 601.
[17] H.A. Atwater, A. Polman, Nature Mater. 9 (2010) 205.
[18] E. Dulkeith, A.C. Morteani, T. Niedereichholz, T.A. Klar, J. Feldmann, S.A. Levi, F.C.J.M. van Veggel, D.N. Reinhoudt, M. Moller, D.I. Gittins, Phys. Rev. Lett. 89 (2002) 2030021.
[19] N. Mirsaleh-Kohan, V. Iberi, P.D. Simmons Jr., N.W. Bigelow, A. Vaschillo, M.M. Rowland, M.D. Best, S.J. Pennycook, D.J. Masiello, B.S. Guiton, J.P. Camden, J. Phys. Chem. Lett. 3 (2012) 2303.
[20] R.T. Hill, J.J. Mock, A. Hucknall, S.D. Wolter, N.M. Jokerst, D.R. Smith, A. Chilkoti, ACS Nano 6 (2012) 9237.
[21] K. Aslan, I. Gryczynski, J. Malicka, E. Matveeva, J.R. Lakowicz, C.D. Geddes, Curr. Opin. Biotechol. 16 (2005) 55.
[22] J. Zenneck, Ann. Phys. 328 (1907) 846.
[23] A. Sommerfeld, Ann. Phys. 28 (1909) 665.
[24] D.A. Weitz, S. Garoff, J.I. Gersten, A. Nitzan, J. Chem. Phys. 78 (1983) 5324.
[25] J. Gu, G.W. Hacker, Gold and Silver Staining: Techniques in Molecular Morphology, CRC, Boca Raton, Florida, 2002. 107.
[26] K. Aslan, S.N. Malyn, C.D. Geddes, J. Fluoresc. 17 (2007) 7.
[27] C. Li, X. Liu, M. Yuan, J. Li, Y. Guo, J. Xu, M. Zhu, J. Lv, H. Liu, Y. Li, Langmuir 23 (2007) 6754.
[28] J. Lv, Y. Zhao, G. Li, Y. Li, H. Liu, Y. Li, D. Zhu, S. Wang, Langmuir 25 (2009) 11351.
[29] A. Kinkhabwala, Z. Yu, S. Fan, Y. Avlasevich, K. Müllen, W.E. Moerner, Nat. Photonics 3 (2009) 654.
[30] Y. Chen, K. Munechika, D.S. Ginger, Nano Lett. 7 (2007) 690.
[31] Á. Sánchez-González, S. Corni, B. Mennucci, J. Phys. Chem. C 115 (2011) 5450.
[32] H. Tsunoyama, H. Sakurai, N. Ichikuni, Y. Negishi, T. Tsukuda, Langmuir 20 (2004) 11293.
[33] A. Imhof, M. Megens, J.J. Engelberts, D.T.N. de Lang, R. Sprik, W.L. Vos, J. Phys Chem. B 103 (1999) 1408.
[34] N. Thorball, Histochemistry 71 (1981) 209.
[35] T. Linnert, P. Mulvaney, A. Henglein, J. Phys. Chem. 97 (1993) 679.
[36] N. Chandrasekharan, P.V. Kamat, J. Hu, G. Jones II, J. Phys. Chem. B 104 (2000) 11103.
[37] P. Mulvaney, L.M. Liz-Marzan, M. Giersig, T. Ung, J. Mater. Chem. 10 (2000) 1259.
[38] Z. Zhong, S. Patskovskyy, P. Bouvrette, J.H.T. Luong, A. Gedanken, J. Phys. Chem. B 108 (2004) 4046.
[39] A. Guerrero-Martínez, M. Grzelczak, L.M. Liz-Marzán, ACS Nano 6 (2012) 3655.
[40] A.M. Schwartzberg, C.D. Grant, T. van Buuren, J.Z. Zhang, J. Phys. Chem. C 111 (2007) 8892.
[41] A. Albanase, W.C. Chan, ACS Nano 5 (2011) 5478.
[42] Y. Zhang, C. Gu, A.M. Schwartzberg, S. Chen, J.Z. Zhang, Phys. Rev. B 73 (2006) 165405.
[43] O.V. Makarova, A.E. Ostafin, H. Miyoshi, J.R. Norris Jr., D. Meisel, J. Phys. Chem. B 103 (1999) 9080.
[44] S.K. Ghosh, A. Pal, S. Kundu, S. Nath, T. Pal, Chem. Phys. Lett. 395 (2004) 366.
[45] S.K. Ghosh, T. Pal, Phys. Chem. Chem. Phys. 11 (2009) 3831.
[46] L. Novotny, B. Hecht, Principles of Nano-Optics, Cambridge University Press, New York, 2006.
[47] R. Bardhan, N.K. Grady, J.R. Cole, A. Joshi, N.J. Halas, ACS Nano 3 (2009) 744.
[48] V. Giannini, A.I. Fernandez-Domínguez, S.C. Heck, S.A. Maier, Chem. Rev. 111 (2011) 3888.
[49] S. Basu, S. Panigrahi, S. Praharaj, S.K. Ghosh, S. Pande, S. Jana, T. Pal, New J. Chem. 30 (2006) 1333.
[50] I. Kim, S.L. Bender, J. Hrnisavljevic, L.M. Utschig, L. Huang, G.P. Wiederrecht, D.M. Tilde, Nano Lett. 11 (2001) 3091.
[51] O. Varnavski, G. Ramakrishna, J. Kim, D. Lee, T. Goodson, J. Am. Chem. Soc. 132 (2010) 16.
[52] U. Kreibig, M. Vollmer, Optical Properties of Metal Clusters, Springer, Berlin, 1995. Chapter 2, pp. 126.
[53] C.A. Parker, Photoluminescence of Solutions, Elsevier, Amsterdam, The Netherlands, 1981.
[54] J. Zuloaga, E. Prodan, P. Nordlander, Nano Lett. 4 (2010) 5269.
[55] J.C. Maxwell Garnett, Philos. Trans. R. Soc. 203 (1904) 385.
[56] Y. Chen, K. Munechika, D.S. Ginger, Nano Lett. 7 (2007) 1032.
[57] I. Carmeli, I. Lieberman, L. Kraversky, Z.Y. Fan, A.O. Govorov, G. Markonich, S. Richter, Nano Lett. 10 (2010) 2069.
[58] Y. Li, P. Wu, H. Xu, H. Zhang, X. Zhong, Analyst 136 (2011) 196.
[59] F. Zhang, D.G. Dressen, M.W.A. Skoda, R.M.J. Jacobs, S. Zorn, R.A. Martin, C.M. Martin, G.F. Clark, F. Schreiber, Eur. Biophys. J. 37 (2008) 551.
[60] A. Vujačić, V. Vasić, M. Dramićanin, S.P. Sovilj, N. Bibić, J. Hranisavljević, G.P. Wiederrecht, J. Phys. Chem. C 116 (2012) 4655.

Emission behavior of sudan red 7B on dogbone-shaped gold nanorods: Aspect ratio dependence of the metallic nanostructures

Dewan S. Rahman, Debdulal Sharma, Sujit Kumar Ghosh ⇑

Department of Chemistry, Assam University, Silchar 788011, India

a r t i c l e   i n f o

a b s t r a c t

Cetyltrimethylammonium bromide-stabilized 'dogbone-shaped' gold nanorods of aspect ratio varying from 1 to 6 have been synthesized by seed-mediated growth method in aqueous medium. Then, sudan red 7B, an alien molecular probe has been used as local probe to elucidate aspect ratio dependence of the nanorods on the photophysical properties of the dye molecules. It is seen that the relative intensity decreases exponentially with increasing aspect ratio and has been attributed to decrease in overall surface area for a particular concentration of the nanorods. The mechanism of fluorescence quenching has been ascribed to the electron and energy transfer processes in the gold-fluorophore hybrid nanostructures.

© 2013 Elsevier B.V. All rights reserved.

1. Introduction

Studies on the interaction of organic fluorophores with noble metal nanostructures have stimulated research both in basic science and technology [1–3]. Metallic particles *viz.*, copper, silver and gold, in the nanometer size regime exhibit strong absorption in the visible region, often coined as localized surface plasmon resonance (LSPR) [4]. The resonance frequency of this LSPR is strongly dependent upon the size, shape, interparticle interactions, dielectric properties, and local environment of the nanoparticles [5]. Apart from spherical nanoparticles, many anisotropic structures of noble metal nanoparticles with excellent surface plasmon tunability and chemical stability have encouraged their applications in a diverse range of niche applications [6]. Gold nanorods have been demonstrated to be a highly promising class of plasmonic nanostructures as these particles exhibit transverse and longitudinal plasmon resonances that correspond to electron oscillations perpendicular and parallel to the rod length direction, respectively [7]. Organic fluoroprobes have often been used as local probes for the physicochemical characterization of the nanostructures and the resultant organic–inorganic hybrid nanoassemblies could be utilized for the development of plasmonic nanoemitters [8,9].

Recently, gold nanorods have been used to modify intrinsic fluorescence of molecular probes theoretically and experimentally by adjusting the nanorod size and its aspect ratio [10,11]. To date, studies on the interaction of fluorophores with the gold nanorods have predominantly focused on the fluorescence intensity enhancement in the metal-fluoroprobe hybrid nanoassemblies. Halas and colleagues have studied the fluorescence enhancement of the near-infrared fluorophore IR800 by gold nanorods and it was revealed that the quantum yield of IR800 is enhanced ten-fold on the surface of the nanorods [12]. Wang and group have demonstrated direct measurement of the plasmonic-molecular resonance coupling as a function of the nanorod plasmon resonance wavelength [13]. Fu et al. observed a remarkable increase in the fluorescence of a single fluorophore controllably linked to ends of a single gold nanorod [14]. Gong and co-authors have employed FDTD method to investigate single-molecule spontaneous emission that reveals gold nanorod antenna can maintain large field enhancement within the nanorod's longitudinal plasmon resonance band while the emission behavior around the nanorod's short-axis resonance band is similar to that of a spherical particle [15]. Ming et al. reported the strong polarization dependence of the plasmon-enhanced fluorescence where the fluorophores were embedded in a silica shell around an individual gold nanorod [16]. Singamaneni and colleagues have investigated the influence of gold nanorod dimensions on distance-dependent LSPR sensitivity and electromagnetic decay length using electrostatic layer-by-layer assembly of polyelectrolytes and developed plasmonic nanotransducers for label-free biological sensing [17]. Lu et al. have designed a fluorescence resonance energy transfer system containing gold nanorods and fluorescein for the detection of hepatitis B virus DNA sequences [18].

In this article, we have investigated the aspect ratio (length- to-diameter ratio; l/d) dependence of the 'dogbone-shaped gold nanorods' (GDNRs) on the emission behavior of sudan red 7B

⇑ Corresponding author. Tel.: +91 348 270848; fax: +91 348 270802.
E-mail addresses: sujitkchem@gmail.com, sujit.kumar.ghosh@aus.ac.in (S.K. Ghosh).

molecules. Although the fundamental physics of the processes involved is well-known, the effects of several parameters have remained unaddressed in the literature. It is seen that the probe molecules adsorbed onto the surface of GDNRs exhibit strong quenching of their fluorescence and the extent of quenching differs with different aspect ratio of the nanorods. The quenching efficiency in the presence of variable aspect ratio of the rods has been attributed to the surface area dependence arising as a result of cumulative effect of the length and diameter of the nanorods. The mechanism of quenching has been enlightened in the view of electron and energy transfer processes in the metal-fluoroprobe hybrid nanostructures.

2. Experimental

Reagents and instruments

Hydrogen tetrachloroaurate (HAuCl$_4$·3H$_2$O), silver nitrate (AgNO$_3$), sodium borohydride (NaBH$_4$), cetyltrimethylammonium bromide (CTAB), sudan red 7B (SR7B), ascorbic acid were purchased from Sigma−Aldrich and were used as received. Double distilled water was used throughout the course of this investigation. As it is difficult to dissolve SR7B molecules in water but readily in methanol, the stock solution of the fluoroprobe was prepared in 95/5 (v/v) water−methanol mixture at concentration of 0.1 mM.

Absorption spectra were measured in a Shimadzu UV−vis 1610PC spectrophotometer using 1 cm quartz cuvette. Fluorescence spectra were recorded with a Shimadzu 5301PC spectrofluorimeter equipped with a 9.9 W xenon flash lamp and a photomultiplier tube with S-20 spectral response. The spectrofluorimeter was linked to a personal computer and utilized the RF-5301PC software package for data collection and processing. Transmission electron microscopy (TEM) was carried out on a JEOL JEM 2100 microscope with a magnification of 200 kV. Samples were prepared by placing a drop of solution on a carbon coated copper grid.

Synthesis of gold dogbones of variable aspect ratio

Gold dogbones have been synthesized by seed-mediated growth process by following the protocol of Gou and Murphy [19]. In this method, the aspect ratio of the GDNRs has been varied using the different concentration of AgNO$_3$ solution into the reaction mixture. The synthesis of GDNRs has been accomplished in two main steps:

Preparation of gold seeds

Aqueous dispersion of gold seed was prepared by mixing solutions of HAuCl$_4$3H$_2$O (5 mL, 0.5 mM) and CTAB (5 mL, 0.2 M) under stirring, which forms deep yellow color. Then, an aliquot of freshly prepared ice-cold NaBH$_4$ solution (0.6 mL, 10 mM) was added instantaneously into the reaction mixture and stirring was continued for 10 min. The color of the solution changes to deep brown indicating the formation of gold seed and the dispersion was aged, further, for 3–4 h prior to the synthesis of GDNRs.

Preparation of gold dogbones

The growth solution for the synthesis of dogbones (adding onto the ends of the nanorods) consists of HAuCl$_4$·3H$_2$O (5 mL, 1 mM), CTAB (5 mL, 0.2 M) and AgNO$_3$ (4 mM of volume varying from 80 to 300 lL) and freshly prepared ascorbic acid (70 lL, 0.1 M) solution were added to the above mixture, just to make the solution colorless. Then, 10 lL of the dispersion of gold seed was added, mixed by gentle shaking for one second and were kept undisturbed. The red to pink coloration was appeared slowly within 15–20 min indicating the formation of the rods. The synthetic conditions for the preparation of GDNRs with variable aspect ratio are shown in Table 1.

Preparation of nanorod-probe hybrid assembly

In a typical set, an aliquot of GDNRs (20 lM) from different sets was added to a solution of SR7B (0.3 lM) and the final volume of the solution was maintained to 5 mL. The solution was allowed to stand for 12 h to complete the surface complexation process and fluorescence of each solution was measured in the spectrofluorimeter.

3. Results and discussion

Sudan Red 7B [N-ethyl-1-(4-phenylazo)phenylazo-2-naphthyl-amine] (extinction co-efficient 6200 M^{-1}cm^{-1}, quantum yield, u$_f$ 0.01), also called 'oil violet', is a lipid staining dye of the member of Sudan family and is widely used for different scientific and industrial applications [20]. Fig. 1 shows an absorption (0.16 mM) and emission (0.3 lM) profile of SR7B in aqueous solution. It shows a major absorption peak at 535 nm and a vibrational shoulder at 368 nm which might be attributed to the p ? p and n ? p transitions, respectively, corresponding to the monomeric form of the dye [21]. Excitation at 535 nm produces the emission spectrum with maximum at 619 nm. The molecular structure of SR7B is shown in the inset. We have studied the emission spectra of SR7B as a function of dye concentration in the range of 0.1−1 lM (not shown). It is found that there is no significant perturbation in the band structure and band position of the dye and fluorescence intensity (at 619 nm) increases linearly with increase in the concentration of the dye molecules indicating there is no significant dimerization or higher order aggregation in the prescribed concentration range. These characteristics have enabled us to study the emission properties of the SR7B molecules with metallic nanostructures.

Gold nanorods with hemispherical caps looking 'dogbone-like' structures stabilized by cetyltrimethylammonium bromide were grown in aqueous solution using seed-mediated growth method [19]. Fig. 2 shows the absorption spectra (0.25 mM) of spherical gold nanoparticles (SP) and GDNRs of variable aspect ratio. Inset

Table 1
Composition of the growth solutions for the synthesis of 'dogbone-shaped' gold nanorods.

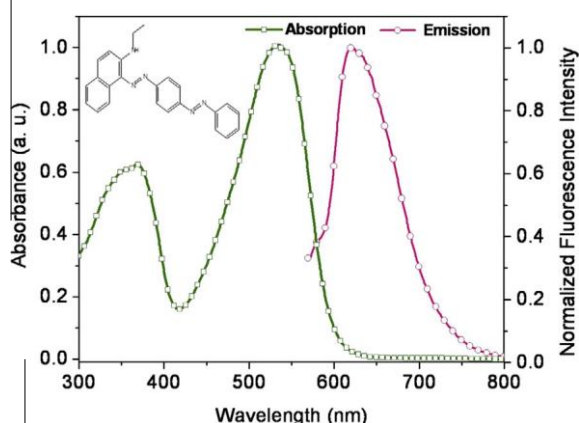| Set	Volume of Au seed (0.25 mM) (lL)	Volume of HAuCl$_4$ (1.0 mM) (mL)	Volume of CTAB (0.2 M) (mL)	Volume of AgNO$_3$ (4.0 mM) (lL)	Volume of ascorbic acid (0.1 M) (lL)	k$_{max}$ at LSPW (nm)	Aspect ratio
SP	–	–	–	–	–	–	1.0 ± 0.2
DNR1	10	5	5	80	70	613	2.0 ± 0.3
DNR2	10	5	5	120	70	635	2.5 ± 0.4
DNR3	10	5	5	140	70	651	3.0 ± 0.5
DNR4	10	5	5	180	70	677	4.0 ± 0.5
DNR5	10	5	5	220	70	700	5.0 ± 0.5
DNR6	10	5	5	240	70	714	5.5 ± 0.6
DNR7	10	5	5	300	70	748	6.0 ± 0.7

Fig. 1. Absorption (0.16 mM) and emission spectrum (0.3 lM) of Sudan Red 7B in aqueous solution. Molecular structure of the dye is shown in the inset.
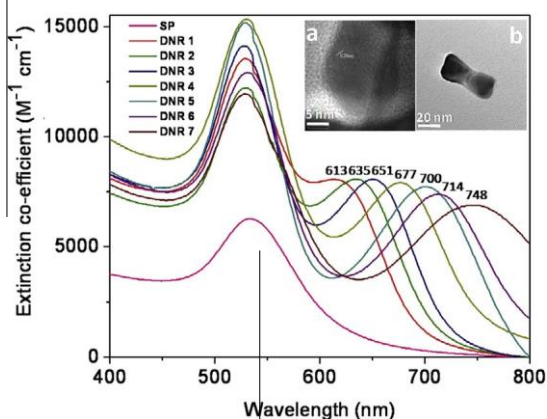

Fig. 2. Absorption spectra of gold dogbones (0.25 mM) of variable aspect ratio. Inset shows TEM images of the (a) end and (b) side view corresponding to transverse and longitudinal plasmon resonances of the dogbones.

shows TEM images of the end and side views corresponding to transverse and longitudinal plasmon resonances of the dogbones, which can be understood within the framework of Gans theory that describes the optical properties of ellipsoid nanoparticles based on dipole approximation [22]. The absorption spectra of the GDNRs exhibit two distinct maxima, a transverse plasmon band arising at around 530 nm that is associated with electron oscillation perpendicular to the length axis of the rods [7] and a longitudinal plasmon band (at >600 nm) that is associated with electron oscillations parallel to the rod length axis [23]. It is seen that the transverse surface plasmon is not influenced much by the aspect ratio of GDNRs, but longitudinal surface plasmons are highly sensitive and could be tuned from visible to the infrared regions by rational control over their aspect ratio.

Transmission electron micrographs of the representative GDNRs of sets SP, DNR 1, DNR 3 and DNR 6 are shown in Fig. 3. It is seen that the nanorods having fatter ends and thinner middle sections are nearly monodisperse and the aspect ratio varies from 1 to 6 (for simplification, the nanospheres are treated as nanorods with aspect ratio 1). The average diameter for the spherical particles is 3–4 nm; average length and diameter of the dogbones are 20 ± 10, 30 ± 10 and 55 ± 10 nm for DNR 1, DNR 3 and DNR 6 respectively. Gou et al. have pointed out that when the unpurified gold nanorods are treated with ascorbic acid, the nanorods act as seeds and subsequently, reduced gold atoms were deposited preferentially onto the ends. With increase in concentration of $AgNO_3$ in the growth solution, the GDNR diameter remains nearly constant, while the length of the dogbones gradually increases.

Now, we have studied the emission behavior ($k_{ex} \sim 535$ nm) of sudan red 7B (0.3 lM) in the presence of GDNRs (20 lM) of variable aspect ratio as shown in Fig. 4. In these experiments, quite dilute solutions have been used so as to minimize the effects of excitation attenuation and solution self-absorption (so-called 'trivial effects'). It is seen that the SR7B emission showed distinctly different emission profile in the presence of different sets of GDNRs and all sets of gold particles quenches the fluorescence of the dye molecules. However, no remarkable difference in the line shape of the emission spectra of SR7B in the presence of the nanostructures was observed.
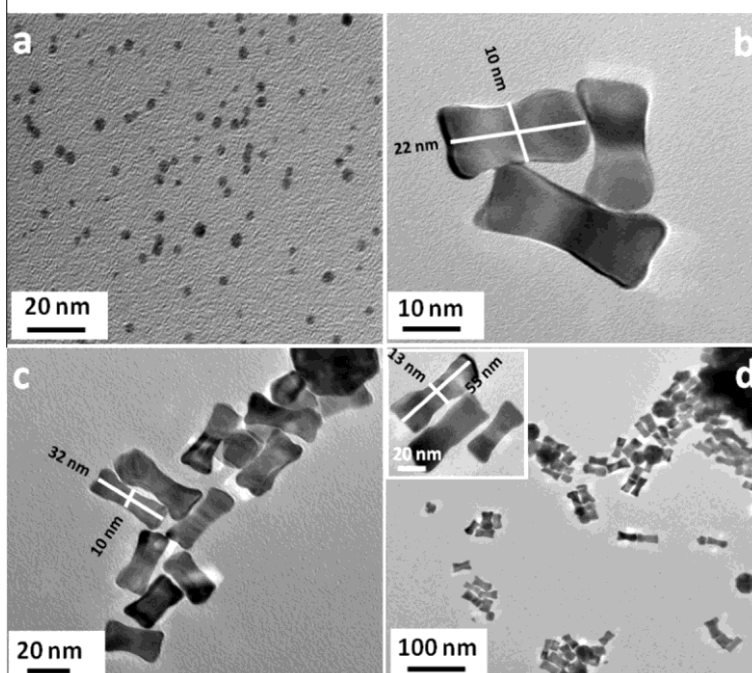

Fig. 3. TEM images of representative gold dogbones of variable aspect ratio: (a) SP, (b) DNR 1, (c) DNR 3 and (d) DNR 6.
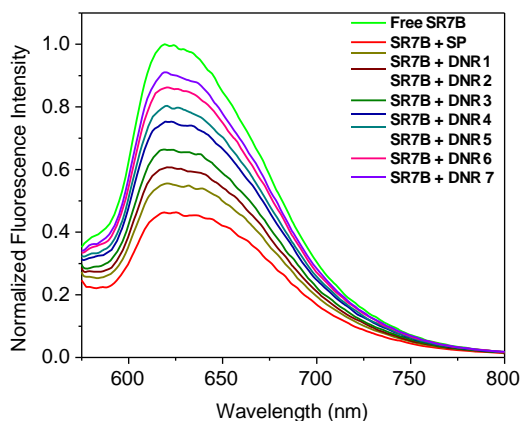
Fig. 4. Emission spectra of SR7B (0.3 lM) in the presence of GDNRs (20 lM) of variable aspect ratio.

A plot of relative efficiency, I_0/I where I_0 and I are the intensities of emission spectrum of the dye molecules in the absence and presence of GDNRs of variable aspect ratio is shown in Fig. 5. The quenching efficiency varied 65% for a set of measurements from same batch of the nanorods and 67.5% from different batches prepared in different times. It is noted that the relative intensity decreases exponentially with increase in aspect ratio of rods, maximum being in case of ultrasmall spherical nanoparticles.

The strongly confined fields near metallic nanostructures can modify the intrinsic fluorescence of nearby fluorophores [24]. The localized plasmon resonances of metal nanoparticles can confine light into nanometer regions and therefore, provide a platform for the control of light-matter interactions at the nanoscale. The quenching of molecular fluorescence near gold nanostructures could be treated within the framework of the model proposed by Weitz et al. [25]. The increased electric field near metal nanostructures modify the fluorescence by increasing optical excitation rates by strengthening the local electric field, lowering the emission efficiency by offering non-radiative decay channels for the molecular dipole, and increasing the fluorescence by coupling radiative molecular emission to a radiative LSPR mode. The variation in intensity of the dye molecules reflects the number of SR7B molecules varies for different GDNRs. Several parameters, *viz.*, shape and size of the nanoparticles, distance between the excited-state molecules and nanoparticle surface, orientation of the molecular dipoles with respect to the nanoparticle surface plane, and overlap

of the molecule's emission spectrum with the absorption spectrum of the nanoparticle are known to influence the radiative and non-radiative decay kinetics of excited states near metal nanoparticles [5]. In the present experimental condition, the separation between nanorod surfaces and fluorophore (upon collision) is constrained by the thickness of the capping monolayer i. e., the molecular chain length of CTAB (~2.57 nm). There is, finally, no designed control over the orientation of the fluorophore molecular dipole relative to the GDNRs core surface and could be anticipated that molecules are statistically oriented at all possible angles onto the surface of the dogbones. Under this situation, the effect of the nanorods on the fluorescence quenching of the dye molecules could be rationalized by considering the interplay of size and shape and therefore, the surface area of the GDNRs. The gold nanorods do not exhibit fluorescence. When the fluoroprobe SR7B is allowed to interact with rods, a part of the dye molecules adsorbed onto the gold nanorods while the rest remain free in solution. Thus, the only fluorescing component is the free SR7B molecules in the solution and the observed emission spectra are due to the presence of unbound probe molecules in the system. As the aspect ratio of the nanorods decreases, the particles become smaller and there is a corresponding overall increase in surface area of the particles for a particular gold concentration. The increased surface area allows accommodation of a greater number of probe molecules around the GDNRs and hence smaller rods become more efficient quenchers of molecular fluorescence than the larger ones [26].

In Fig. 5, it is noted that spherical particles are superior quenchers of molecular fluorescence than the DNRs. This is due to the fact that for a gold spherical nanoparticle, both radiative and nonradiative decay are enhanced around the plasmon resonance, but non-radiative decay clearly dominates, resulting in low quantum efficiency [27]. In the case of GDNRs, the longitudinal plasmon resonance energy of each dogbones is determined by the length-to-diameter aspect ratio, and they exhibit reduced plasmon damping compared to spherical gold nanocrystals [27]. Under the experimental condition, the aspect ratio of the dogbones are changed by keeping the diameter constant but increasing the length of the dogbones and the variation of relative intensity bears an exponential relationship with the aspect ratio of the nanorods. However, this is an empirical relationship under the experimental conditions and could not be generalized as the aspect ratio is the result of interplay of length and diameter of the nanorods. To obtain general relationship, the absolute dimension of GDNRs (i.e., length and diameter) should be taken into account rather than aspect ratio of the rods as the larger nanorods with same aspect ratio may have lesser quenching efficiency than the smaller nanorods.

Now, we have tried to elucidate the mechanism of quenching of molecular fluorescence upon interaction with the GDNRs. The successive changes of the absorption spectrum (0.25 mM) of gold nanorods (DNR 4) upon gradual addition of an aqueous solution of SR7B are illustrated in Fig. 6(A). The consecutive changes of the surface plasmon band upon increase in the concentration of SR7B molecules indicate electron transfer onto the surface of GDNRs. The stabilizer, CTAB molecules exist as bi-layer [28] around the surface of GDNRs, whereby the trimethylammonium head groups of the first monolayer are facing the nanorod surface and the absorbed second layer of CTAB extends outside the groups with positive charges through van der Waals' interactions between the surfactant tails [29]. This formation develops a net positive surface charge due to the presence of adsorbed surfactant layers onto the nanorod surface. This layer is dynamic in nature and a continuous adsorption and desorption takes place in the system with the free CTAB molecules [30]. When fluoroprobe SR7B molecules are allowed to interact with rods, since the surface of the GDNRs are positively charged but not robust, the secondary amine group of the SR7B molecules are attached onto the nanorod surface through 'place ex-
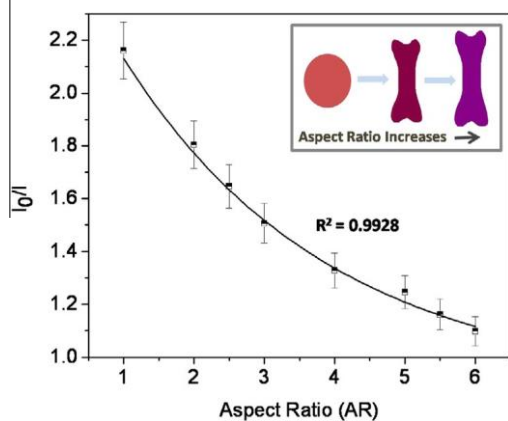

Fig. 5. Profile showing the relative intensity of SR7B as a function of aspect ratio of GDNRs. Inset provides a schematic presentation showing aspect ratio gradually increases from spheres to larger dogbones.
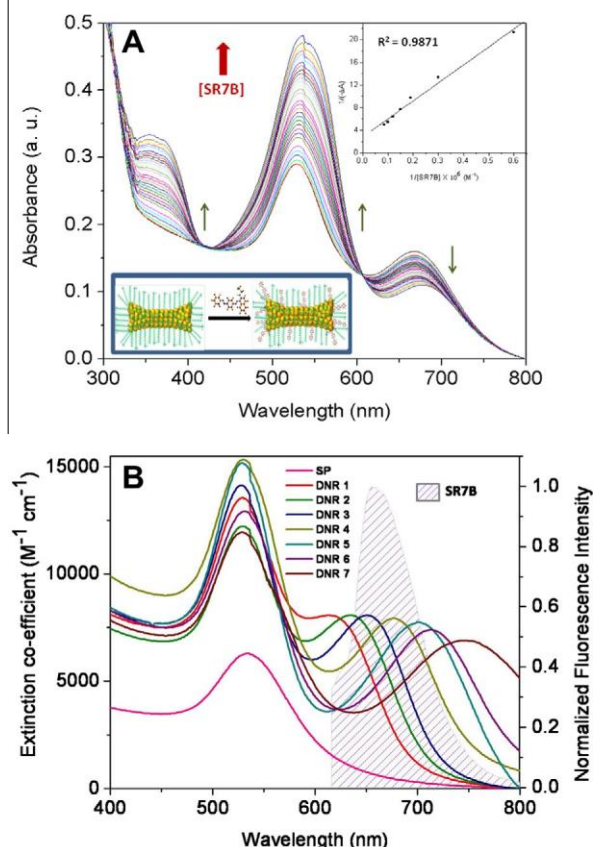
Fig. 6. (A) Surface plasmon band (0.25 mM) of DNR4 upon successive addition of SR7B. (Top) Inset shows the profile showing dependence of $1/(-\Delta A)$ as a function of $1/[SR7B]$. (Bottom) Inset shows a schematic presentation of the attachment of the dye molecules on the surfactant-stabilized of GDNRs. (B) Overlap between the absorption spectra of GDNRs of variable aspect ratio (0.25 mM) and emission spectrum of SR7B molecules (0.3 lM) indicating efficient energy transfer.

change reaction' [31] as shown in the (bottom) inset in Fig. 6(A). Moreover, the gold atoms on the surface possess unoccupied orbitals for nucleophiles to donate electrons. Therefore, the SR7B molecules containing amine functionality as the strong electron donors displace CTAB molecules from gold nanorod surfaces without any alteration in the morphology of the particles. Interestingly, it is observed that an increase in the concentration of SR7B molecules dampens the longitudinal surface plasmon band at 677 nm with successive red-shifting while the absorption at 530 nm increases indicating preferential binding of the dye molecules on the edges of the dogbones. This phenomenon will be accompanied with a change in the refractive index of the medium surrounding the particles which will further determine the preferential shifting of the longitudinal plasmon band [32]. The electron transfer is pronounced for smaller nanorods as they have high surface area/energy and relatively more electronegative and therefore, possess high tendency to accept electrons. Therefore, smaller nanorods are effective quenchers of molecular fluorescence than the larger ones. The presence of an isosbestic point at 600 nm confirms that these absorption changes arise from a complexation equilibrium between the GDNRs and the dye molecules. The spectral changes observed in Fig. 6(A) can be used to assess the apparent association equilibrium under the experimental conditions. The apparent association constant (K_{app}) for the complexation between GDNRs and SR7B was obtained by analyzing the absorption changes similar to a Benesi–Hildebrand approach [33]. The double reciprocal plot of $1/(-\Delta A)$ vs. $1/[SR7B]$ as shown in the (top) inset in Fig. 6(A) gives an apparent association constant of

31.73×10^6 M^{-1}. The high value of K_{app} suggests a strong association between the dogbones and the SR7B molecules.

Quenching may also takes place when a fluorophore molecule is placed in a vicinity of a metal surface. When located near metal nanoparticles, excited fluoroprobes relax rapidly by exciting localized surface plasmons by means of near field coupling. The energy transfer is believed to be through the dipole–dipole near-field interaction which is known as Förster resonance energy transfer [34]. In the energy transfer process, the fluorophore acts as a dipolar donor, and the plasmonic GDNRs core functions as a dipolar acceptor. The probability of this Förster resonance energy transfer depends on the overlap of the emission band of the probe molecules with the absorption spectrum of the nanorods. Fig. 6(B) shows the overlap between the absorption spectra of GDNRs and the emission spectrum of SR7B molecules. It is clear that the absorption of gold nanorods overlaps significantly with the SR7B emission, ensuring efficient energy transfer. In addition, strong plasmonic-molecular resonance coupling occurs between noble metal nanoparticles and organic fluoroprobes when the plasmonic resonance is degenerate with the molecular one. On a metallic surface, the nonradiative decay rate also increases for short fluorophore-metal distances, 4 nm, since the non-radiative energy transfer rate depends on the inverse cube of the molecule-surface separation [35,36]. Due to chemisorption of the SR7B molecules to the gold surface, the molecular orbital of the probe molecules are mixed with metallic band states. Certain orbitals of SR7B interact strongly with the GDNRs and are responsible for chemisorption bond, while others are little affected by adsorption [37]. Thus, the energy transfer quenching is also very sensitive to the density of the electronic state changes.

In view of the above quenching mechanism, the fluorescence quenching of SR7B by GDNRs can be both static and dynamic. The former involves the formation of a non-fluorescent complex between the fluorophore and quencher in their ground states, whereas the latter requires diffusive encounters between the fluorophore and quencher during the lifetime of the excited state of the fluorophore. The Stern–Volmer equation accounting both static and dynamic (collisional) quenching could be written as [38],

$$I_0 = I \, ¼ \, 1 \, þ \, K_{SV} ½Q] \qquad\qquad ð1Þ$$

where, $K_{SV} = K_S + K_D$. Here, K_S and K_D are the static and dynamic quenching constants respectively and Q is the quencher. It has been seen that the fluorescence quantum yield of sudan red 7B does not change appreciably in the presence of experimental concentrations of the surfactant. Therefore, the adsorption onto the metallic surface of the dogbones could be ascribed to be responsible for the quenching of SR7B fluorescence. Fig. 7 shows a plot of I_0/I vs. gold
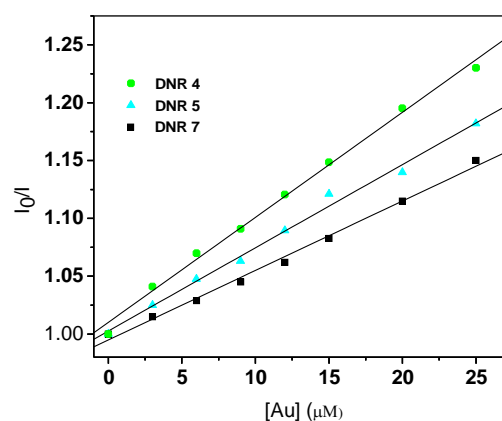

Fig. 7. Stern–Volmer plot of relative intensity as a function of concentration of GDNRs of three different aspect ratio.

concentration at constant SR7B concentration for three different aspect ratio of the GDNRs. It is seen that the relative intensity shows good linear correlation with quencher concentration and corresponding K_{SV} values are determined as 9.08 10², 7.19 10³ and 6.03 ×10³ M⁻¹ with aspect ratio 4 ± 0.5, 5.0 ± 0.5 and 6 ± 0.7, respectively [39]. These results, quantitatively, authenticates that GDNRs with smaller aspect ratio are efficient quenchers of SR7B fluorescence than the larger aspect ratio nanorods.

4. Conclusion

This article directly provides an experimental verification of the effect of aspect ratio of dogbone-shaped gold nanorods on the emission behavior of molecular probe. Upon binding of the probe molecules onto the gold nanorods, the relative emission intensity decays exponentially with increasing aspect ratio of the nanorods. The fact that rods with lower aspect ratio are more efficient quenchers of molecular fluoroscence than higher aspect ratio rods is an important finding and this is due to higher surface-to-volume ratio of the smaller nanorods. Electron and energy transfer are considered to be the two major factors governing the process of deactivation of excited fluorophores onto the metal surface. It is anticipated that these results have significant implications for exploiting dogbone-shaped gold nanorods in a variety of optical and biotechnological applications.

References

[1] C.D. Geddes, Metal-Enhanced Fluorescence, John Wiley & Sons, Inc., 2010.
[2] V.M. Agranovich, Y.N. Gartstein, M. Litinskaya, Chem. Rev. 111 (2011) 5179.
[3] P.V. Kamat, J. Phys. Chem. B 106 (2002) 7729.
[4] J. Zhao, X. Zhang, C.R. Yonzon, A.J. Haes, R.P. Van Duyne, Nanomedicine 1 (2006) 219.
[5] S.K. Ghosh, T. Pal, Chem. Rev. 107 (2007) 4797.
[6] R. Jin, Y.C. Cao, E. Hao, G.S. Métraux, G.C. Schatz, C.A. Mirkin, Nature 425 (2003) 487.
[7] X. Huang, S. Neretina, M.A. El-Sayed, Adv. Mater. 21 (2009) 4880.
[8] V. Giannini, A.I. Fernández-Domínguez, S.C. Heck, S.A. Maier, Chem. Rev. 111 (2011) 3888.
[9] S.K. Ghosh, T. Pal, Phys. Chem. Chem. Phys. 11 (2009) 3831.
[10] J. Duan, D. Nepal, K. Park, J.E. Haley, J.H. Vella, A.M. Urbas, R.A. Vaia, R. Pachter, J. Phys. Chem. C 115 (2011) 13961.
[11] T. Ming, L. Zhao, H. Chen, K.C. Woo, J. Wang, H.-Q. Lin, Nano Lett. 11 (2011) 2296.
[12] R. Bardhan, N.K. Grady, J.R. Cole, A. Joshi, N.J. Halas, ACS Nano 3 (2009) 744.
[13] W. Ni, T. Ambjörnsson, S.P. Apell, H. Chen, J. Wang, Nano Lett. 10 (2010) 77.
[14] Y. Fu, J. Zhang, J.R. Lakowicz, J. Am. Chem. Soc. 132 (2010) 5540.
[15] G. Lu, T. Zhang, W. Li, L. Hou, J. Liu, Q. Gong, J. Phys. Chem. C 115 (2011) 15822.
[16] T. Ming, L. Zhao, Z. Yang, H. Chen, L. Sun, J. Wang, C. Yan, Nano Lett. 9 (2009) 3896.
[17] L. Tian, E. Chen, N. Gandra, A. Abbas, S. Singamaneni, Langmuir 28 (2012) 17435.
[18] X. Lu, X. Dong, K. Zhang, X. Han, X. Fang, Y. Zhang, Analyst 138 (2013) 642.
[19] L. Gou, C.J. Murphy, Chem. Mater. 17 (2005) 3668.
[20] M. Nakazato, Y. Kasuya, H. Matsumoto, K. Yasuda, Tokyo Metropolitan Inst. Public Health Annu. Rep. Jpn. 55 (2004) 107.
[21] H. Yu, L. Qi, Langmuir 25 (2009) 6781.
[22] R. Gans, Ann. Phys. 37 (1912) 881.
[23] J. Perez-Juste, I. Pastoriza-Santos, L.M. Liz-Marźan, P. Mulvaney, Coord. Chem. Rev. 249 (2005) 1870.
[24] L. Novotny, B. Hecht, Principles of Nano-Optics, Cambridge University Press, New York, 2006.
[25] D.A. Weitz, S. Garoff, J.I. Gersten, A. Nitzan, J. Chem. Phys. 78 (1983) 5324.
[26] S.K. Ghosh, A. Pal, S. Kundu, S. Nath, T. Pal, Chem. Phys. Lett. 395 (2004) 366.
[27] K.A. Willets, R.P. Van Duyne, Annu. Rev. Phys. Chem. 58 (2007) 267.
[28] B. Nikoobakht, M.A. El-Sayed, Langmuir 17 (2001) 6368.
[29] J.X. Gao, C.M. Bender, C.J. Murphy, Langmuir 19 (2003) 9065.
[30] J.M. El-Khoury, X. Zhou, L. Qu, L. Dai, A. Urbasc, Q. Li, Chem. Commun. (2009) 2109.
[31] A.C. Templeton, J.J. Pietron, R.W. Murray, P. Mulvaney, J. Phys. Chem. B 104 (2000) 564.
[32] C.J. Orendorff, T.M. Alam, D.Y. Sasaki, B.C. Bunker, J.A. Voigt, ACS Nano 3 (2009) 971.
[33] H.A. Benesi, J.H. Hildebrand, J. Am. Chem. Soc. 71 (1949) 2703.
[34] T. Förster, Ann. Phys. 437 (1948) 55.
[35] D.H. Waldeck, A.P. Alivisatos, C.B. Harris, Surf. Sci. 158 (1985) 103.
[36] E. Dulkeith, A.C. Morteani, T. Niedereichholz, T.A. Klar, J. Feldmann, S.A. Levi, F.C.J.M. van Veggel, D.N. Reinhoudt, M. Moller, D.I. Gittins, Phys. Rev. Lett. 89 (2002) 2030021.
[37] H.-G. Boyen, P. Ziemann, U. Wiedwald, V. Ivanova, D.M. Kolb, S. Sakong, A. Gross, A. Romanyuk, M. Büttner, P. Oelhafen, Nature Mater. 5 (2006) 394.
[38] J.R. Lakowicz, Principles of Fluorescence Spectroscopy, third ed., Plenum Press, New York, 2006.
[39] S. De, A. Pal, N.R. Jana, T. Pal, J. Photochem. Photobiol. A 131 (2000) 111.

Appendix

List of Publications

(Publications Nos. 1, 2, 5 & 6 included in the Thesis)

1. **Dewan S. Rahman,** Sanhita Deb and Sujit Kumar Ghosh *J. Phys. Chem. C* **2015**, *119*, 27145–27155.
    „Relativity of Electron and Energy Transfer Contributions in Nanoparticle-Induced Fluorescence Quenching‟

2. **Dewan S. Rahman**, Hirak Chatterjee, and Sujit Kumar Ghosh *J. Phys. Chem. C* **2015**, *119*, 14326−14337.
    „Excess Surface Energy at the Tips of Gold Nanospikes: From Experiment to Modeling‟

3. Biswajit Chakraborty, Ramkrishna Pal, Mohammed Ali, Leichombam Mohindro Singh, **Dewan S. Rahman**, Sujit Kumar Ghosh and MahuyaSengupta *Cellular & Molecular Immunology* **2015**. DOI:10.1038/cmi.2015.05.
    „Immunomodulatory Properties of Silver Nanoparticles Contribute to Anticancer Strategy for Murine Fibrosarcoma‟

4. Mohammed Ali, Hasimur Rahaman, **Dewan S. Rahman**, Surjatapa Nath and Sujit Kumar Ghosh *Cryst. Eng. Commun*. **2014**, *16*, 7701−7710.
    „Water/n-Heptane Interface as a Viable Platform for Self-assembly of ZnO Nanospheres to Nanorods‟

5. **Dewan S. Rahman** and Sujit Kumar Ghosh *Chem. Phys*. **2014**, *438*, 66–74
    „Fluorescence Spectroscopy in Probing Spontaneous and Induced Aggregation AmongstSize-Selective Gold Nanoclusters‟

6. **Dewan S. Rahman**, Debdulal Sarma and Sujit Kumar Ghosh *Chem. Phys.* **2014**, *429*, 27–32.
    „Emission Behavior of Sudan Red 7B on Dogbone-Shaped Gold Nanorods: Aspect Ratio Dependence of the Metallic Nanostructures‟

7. Sujit Kumar Ghosh, **Dewan S. Rahman**, Abdul Latif Ali and AnamikaKalita *Plasmonics* **2013**, *8*, 1457–1468.
    „Surface Plasmon Tunability and Emission Sensitivity of Ultrasmall Fluorescent Copper Nanoclusters‟

List of Seminar/Conference /Symposium/Workshops Attended

1. Participation in the 9 days GIAN course on „Light Scattering by Different Shaped Particles with Application in Physics" organized by the Department of Physics, Assam University, Silchar from 5 - 13th April, 2016.

2. Oral presentation of paper entitled "Relative Electron Transfer in Nanoparticle Induced Fluorescence Quenching" in the national conference, „Computational Research and its Development in Experimental Sciences" organized by Karimganj College, Karimganj from 12 - 14th March, 2016.

3. Presentation of paper entitled "Measurement of Surface Energy of the Tips of Gold Nanospikes" in the national conference on „Current Perspectives on Research on Chemical Sciences" in Department Chemistry, Assam University on 25 - 26th March, 2015.

4. Presentation of paper entitled "Measurement of Surface Energy of the Tips of Gold Nanospikes" in the national conference organized by CSIR-NEIST, Jorhat in the 8th Mid-Year CRSI National Symposium in Chemistry during 10 - 12th July, 2014.

5. Participants in the three days National Lecture Workshop on „Recent Trends in Synthesis of Chemical Compounds and their Application in Science and Technology" organized by NIT, Silchar, from 5 - 7th May 2014.

6. Presentation of paper in the 5th Asian Conference on Colloid and Interface Science entitled "Band Gap Tuneability in Au-ZnO Nanoscale Hybrid Assemblies" organized by the Department of Chemistry, University of North Bengal, Darjeeling, India during 20 -23rd November, 2013.

7. Oral presentation of paper entitled "Emission Behavior of Sudan Red 7B On Gold Nanorods: Aspect Ratio Dependence" in the national seminar, „Emerging Areas of Research & Development in Chemical and Physical Sciences in North East India" organized by S. S. College, Hailakandi during 16 - 18th September, 2012.

8. Oral presentation of paper entitled „Fluorescence Spectroscopy in Probing Spontaneous and Induced Aggregation amongst Gold Nanoparticles" in the national seminar on „Green Chemistry and Nanosciences: Theory & Applications" organized by MBB College, Agartala during 20 - 21st July, 2012.

- Oral presentation of paper entitled „Fluorescence Quenching of Sudan Red7B by Gold Nanorods of Variable Aspect Ratio" in the „National Workshop on Emerging Trends in Nanochemistry" in St. Anthony's College, Shillong during 20 - 21st September, 2011.